JYU DISSERTATIONS 558

Sami Kinnunen

Hydrogen Incorporation in Al_2O_3 and ZnO Thin Films Grown by Atomic Layer Deposition

UNIVERSITY OF JYVÄSKYLÄ
FACULTY OF MATHEMATICS
AND SCIENCE

JYU DISSERTATIONS 558

Sami Kinnunen

Hydrogen Incorporation in Al_2O_3 and ZnO Thin Films Grown by Atomic Layer Deposition

Esitetään Jyväskylän yliopiston matemaattis-luonnontieteellisen tiedekunnan suostumuksella
julkisesti tarkastettavaksi yliopiston Ylistönrinteen salissa FYS1
syyskuun 16. päivänä 2022 kello 12.

Academic dissertation to be publicly discussed, by permission of
the Faculty of Mathematics and Science of the University of Jyväskylä,
in Ylistönrinne, auditorium FYS1, on September 16, 2022 at 12 o'clock noon.

JYVÄSKYLÄN YLIOPISTO
UNIVERSITY OF JYVÄSKYLÄ

JYVÄSKYLÄ 2022

Editors
Ilari Maasilta
Department of Physics, University of Jyväskylä
Ville Korkiakangas
Open Science Centre, University of Jyväskylä

ISBN 978-951-39-9198-2 (PDF)
URN:ISBN:978-951-39-9198-2
ISSN 2489-9003

Permanent link to this publication: http://urn.fi/URN:ISBN:978-951-39-9198-2

ABSTRACT

Kinnunen, Sami
Hydrogen incorporation in Al_2O_3 and ZnO thin films grown by atomic layer deposition
Jyväskylä: University of Jyväskylä, 2022, 81 p. (+included articles)
(JYU Dissertations
ISSN 2489-9003; 558)
ISBN 978-951-39-9198-2 (PDF)

Atomic layer deposition (ALD) is a novel deposition technique that produces thin and conformal films even on high aspect ratio structures and objects with sub-nanometer thickness precision. Applications of ALD range from semiconductor industry to packaging and medicine. In this thesis, two metal oxides, Al_2O_3 and ZnO, were deposited using both temporal and spatial ALD. While temporal ALD is more established deposition method, spatial ALD offers higher throughput and a possibility to deposit thin films on larger substrates.

In this study Al_2O_3 and ZnO were deposited using trimethylaluminium (TMA) and diethylzinc (DEZ), respectively, and using water as an oxygen source. Both Al_2O_3 and ZnO are common and widely studied ALD materials and the reaction mechanism of these materials are thought to be well understood. However, nonideal conditions such as low deposition temperature or fast deposition can lead to high impurity concentrations. In this thesis precursors containing rare isotopes, namely deuterium (^{2}H) and ^{18}O, were used to study the impurity incorporation with different deposition conditions. It was found out that the impurity hydrogen incorporation depends on the deposition temperature as well as from purging time between the precursor pulses. At low temperatures and when short purges are used, hydrogen in the film originates mainly from metal precursor. The opposite is true for the high temperatures and long purging times. Similar conclusions apply for both temporal and spatial ALD.

Keywords: ALD, Al_2O_3, ZnO, ToF-ERDA, heavy water

TIIVISTELMÄ (ABSTRACT IN FINNISH)

Kinnunen, Sami
Atomikerroskasvatuksella valmistettujen Al_2O_3 ja ZnO ohutkalvojen vetyepäpuhtaudet
Jyväskylä: University of Jyväskylä, 2022, 81 s. (+artikkelit)
(JYU Dissertations
ISSN 2489-9003; 558)
ISBN 978-951-39-9198-2 (PDF)

Atomikerroskasvatus (ALD) on ohutkalvojen valmistamiseen käytetty menetelmä, jolla voidaan tuottaa äärimmäisen ohuita ja tasaisia kalvoja syvienkin kolmiulotteisten rakenteiden pinnalle. ALD-tekniikka mahdollistaa myös kalvojen paksuuden säätämisen halutuksi alle nanometrin tarkkuudella. Atomikerroskasvatuksella valmistettuja kalvoja löytyy nykyisin käytännössä jokaisesta puolijohdeteollisuuden tuotteesta, mutta niitä voidaan käyttää myös niin pakkausmateriaaleissa kuin lääketeollisuudessakin. Tässä väitöskirjassa tutkittiin kahta metallioksidiohutkalvoa, alumiinioksidia (Al_2O_3) ja sinkkioksidia (ZnO), joita valmistettiin sekä temporaalisella että spatiaalisella ALD-menetelmällä. Temporaalinen ALD on menetelmistä vakiintuneempi, kun taas spatiaalisella ALD:llä kasvatusaikoja voidaan lyhentää ja mahdollistaa ohutkalvopinnoitukset myös suurille pinta-aloille.

Al_2O_3- ja ZnO-ohutkalvot valmistettiin käyttäen alumiinin ja sinkin lähdeaineina trimetyylialumiinia (TMA) ja dietyylisinkkiä (DEZ). Hapen lähdeaineena käytettiin vettä. Sekä Al_2O_3 että ZnO ovat tunnettuja ja laajasti tutkittuja ALD-materiaaleja, ja on uskottu että niiden kasvuun liittyvät kemialliset reaktiot tunnetaan varsin hyvin. Jos kasvatus tehdään epäideaaleissa olosuhteissa kuten matalassa lämpötilassa tai nopeasti, ohutkalvoihin kuitenkin jää merkittäviä määriä epäpuhtauksia kuten vetyä. Tässä väitöskirjassa epäpuhtauksien päätymistä kalvoon tutkittiin eri kasvatusolosuhteissa käyttämällä lähdeaineena luonnossa harvinaisia, mutta vakaita isotooppeja sisältävää vettä (raskas vesi, happi-18 rikastettu vesi).

Vetyepäpuhtauden määrä ja lähde molemmissa kalvoissa riippui sekä kasvatuslämpötilasta että huuhteluajasta lähdeainepulssien välissä. Kalvoihin päätyy vetyä lähinnä metallilähdeaineista, kun lämpötila on matala tai huuhteluaika on lyhyt. Jos taas lämpötila on korkea tai huuhtelu pitkä, on suuri osa vedystä peräisin vedestä. Sama johtopäätös pätee sekä temporaaliseen että spatiaaliseen atomikerroskasvatukseen.

Avainsanat: Atomikerroskasvatus, alumiinioksidi, sinkkioksidi, raskas vesi, lentoaikarekyylispektrometria

Author

Sami Kinnunen
Department of Physics
University of Jyväskylä
Finland

Supervisor

Professor Timo Sajavaara
Department of Physics
University of Jyväskylä
Finland

Reviewers

Professor Jolien Dendooven
Department of Solid State Sciences
Ghent University
Belgium

Professor Kaupo Kukli
Institution of Physics
University of Tartu
Estonia

Opponent

Professor Matti Putkonen
Department of Chemistry
University of Helsinki
Finland

PREFACE

The work reported in this thesis was carried out during surprisingly many years at the Accelerator laboratory and Nano Science Center of University of Jyväskylä. I want to thank my supervisor Prof. Timo Sajavaara for finding time to supervise me. As a head of department during the pandemic and war in Europe, there has been more than enough work for you to do in addition to guiding me through my studies.

I want to thank Dr. Jari Malm and Dr. Mari Napari: Jari was the hands-on mentor for me on ALD research and Mari, who started a few years earlier her PhD studies, I looked up to her perseverance. I also want to thank Docent Mikko Laitinen and Dr. Jaakko Julin for the support and help they have provided through the years with ion beam analysis. In addition, I want to thank all the present and previous group members: Mr. Spyridon Korkos, Dr. Marko Käyhkö, Dr. Kai Arstila, Mr. Mikko Kivekäs and Dr. Akbar Hossain. Also, Dr. Kimmo Kinnunen deserves special thanks for helping me tirelessly with broken equipment. In addition, I thank “the-guys-from-JAMK”, Dr. Esa Alakoski and Mr. Timo Laine. Working with you has been delightful.

Two fellow PhD students, Dr. Sami Kaappa and Dr. Vesa-Matti Hiltunen did not spend as many years as I did to finalize their doctoral thesis and left me "alone" to survive in the academic world. However, this is not their fault, and I am grateful for those years we spent having longish lunches discussing all the things that are worth discussing. It was a real pleasure to ponder with the two bright and curious minds whether the subject was scientific, philosophical or something more trivial. Often it was trivial, but not always.

This thesis would never have been finished without the support of the people outside the academia as well. Therefore, I want to thank my brother and my parents. You have always encouraged me to pursue a good education and believed that I can make it. It is also important to know that there is a haven to go to when I need peace and relaxation. I must also thank Slerba, a semi-legendary punk rock band that I have had the pleasure of being part of, that has offered me world class escapism when needed. And finally, I want to thank Alisa for her love and enthusiasm on my PhD journey. I do not know if I would have survived without you the long months writing my thesis in isolation due to pandemic.

Jyväskylä, September 2022,

Sami Kinnunen

LIST OF INCLUDED ARTICLES

PI S. Kinnunen, K. Arstila and T. Sajavaara. Al_2O_3 ALD films grown using TMA + rare isotope $^2H_2^{16}O$ and $^1H_2^{18}O$ precursors. *Applied Surface Science*, 546 (2021), 148909.

PII S. Kinnunen, M. Lahtinen, K. Arstila and T. Sajavaara. Hydrogen and deuterium incorporation in ZnO films grown by atomic layer deposition. *Coatings* 11, (2021), 542.

PIII S. Kinnunen and T. Sajavaara. Spatial ALD of Al_2O_3 and ZnO using heavy water. *Surface & Coatings Technology* 441, (2022), 128456.

The research conducted in this thesis and publications was done at the University of Jyväskylä during 2016–2022. The sample preparation by ALD depositions and elemental analysis was performed by me as well as the original manuscripts in all the publications. In addition, AFM and ellipsometric measurements were conducted by me. Kai Arstila provided HIM imaging in Publication I and II and Manu Lahtinen conducted XRD measurements of thin films in Publication II. Timo Sajavaara helped with planning the research and reviewing and editing the manuscripts.

Author also contributed in the following articles:

API M. Napari, O. Tarvainen, S. Kinnunen, K. Arstila, J. Julin, Ø. S. Fjellvåg, K. Weibye, O. Nilsen and T. Sajavaara. The α and γ plasma modes in plasma-enhanced atomic layer deposition with O_2–N_2 capacitive discharges. *Journal of Physics D: Applied Physics*, 50(9), 095201 (2017)

APII S.A. Kinnunen, J. Malm, K. Arstila, M. Lahtinen and T. Sajavaara. Characterization of ALD grown Ti_xAl_yN and Ti_xAl_yC thin films. *Nuclear Instruments and Methods in Physics Research Section B: Beam Interactions with Materials and Atoms*, 406A, 152–155, (2017)

APIII P. K. Parashar, S.A. Kinnunen, T. Sajavaara, J. Jussi Toppari, V. K. Komarala. Thermal atomic layer deposition of AlO_xN_y thin films for surface passivation of nano-textured flexible silicon. *Solar Energy Materials and Solar Cells*, 193, 231–236 (2019)

APIV M. Napari, T. N. Huq, T. Maity, D. Gomersall, K. M. Niang, A. Barthel, J. E. Thompson, S. Kinnunen, K. Arstila, T. Sajavaara,R. L. Z. Hoye, A. J. Flewitt and J. L. MacManus-Driscoll. Antiferromagnetism and P-Type Conductivity of Nonstoichiometric Nickel Oxide Thin Films. *InfoMat* 2(4), 769-774 (2020)

APV P. K. Parashar, S. A. Kinnunen, T. Sajavaara, J. Toppari and V. K. Komarala. Effective suppression of nanotextured black silicon surface recombination channels by aluminum oxide: comparison from sputtered and ALD grown films. *Semiconductor Science and Technology*, 36(11), 115013 (2021)

APVI S. Korkos, K. Mizohata, S. Kinnunen, T. Sajavaara and K. Arstila. Size dependent swift heavy ion induced Au nanoparticle elongation in SiO_2 matrix. *Journal of Applied Physics* 132, 045901 (2022)

LIST OF ACRONYMS

AFM	Atomic Force Microscopy
ALD	Atomic Layer Deposition
ATR-FTIR	Attenuated Total Reflection Fourier-transform Infrared
BB-SFG	Broadband Sum-frequency Generation
CVD	Chemical Vapor Deposition
DEZ	Diethylzinc, $(C_2H_5)_2Zn$
GPC	Growth Per Cycle
HIM	Helium Ion Microscopy
KIE	Kinetic Isotope Effect
ML	Molecular Layering
MSP	Multiple Short Pulsing
NRA	Nuclear Reaction Analysis
PIXE	Particle Induced X-ray Emission
QMS	Quadruple Mass Spectrometry
RBS	Rutherford Backscattering Spectrometry
RH	Relative Humidity
SALD	Spatial Atomic Layer Deposition
SIMS	Secondary Ion Mass Spectrometry
TMA	Trimethylaluminium, $(CH_3)_3Al$
ToF-ERDA	Time-of-Flight Elastic Recoil Detection Analysis
XPS	X-ray Photoelectron Spectroscopy
XRD	X-ray Diffraction

CONTENTS

1 INTRODUCTION

Atomic layer deposition (ALD) has been an enabling technology for integrated circuits and microelectronics already for two decades [1–3]. Modern day integrated circuits can contain tens of layers of nanometer scale thin films and in many cases ALD is the only possible deposition technique due to its superior conformality and film thickness control even at sub-nanometer precision.

The term "thin film" can mean different things to people from different fields. In this thesis, the term is reserved exclusively to a film that has a macroscopical size in two dimensions, and thickness from few hundred nanometers to a single digit atomic layers corresponding a fraction of a nanometer. In this scale the properties of the material can differ greatly from their macroscopic counterparts. One famous example is gold: it is yellow and very inert in the form used in jewellery and such, but in nanoscale the color of colloidal gold nanoparticles can turn the solution from red to blue depending on the size of the particle and in this form gold can be highly reactive [4].

ALD was patented already in 1977 by Finnish inventor Tuomo Suntola [5] and he received the Finnish Millenium Techonology Prize for his invention in 2018. The first material Dr. Suntola deposited was ZnS from elemental zinc and sulphur. However, Suntola was not the first one to come up with this novel depositing method. Stanislav Koltsov and Valentin Aleskovsky released articles already in the 1960s on technique called molecular layering (ML) which essentially is the same as the atomic layer deposition. These studies were mostly forgotten and were not translated from Russian until recently [6]. Suntola was unaware of this work and he named the new technique atomic layer epitaxy [1]. The name atomic layer epitaxy transformed over time to atomic layer deposition since majority of the films produced with ALD are not epitaxial but rather amorphous or polycrystalline.

The first application of the ALD was in thin film electroluminescent display (TFEL), and one of these displays utilizing ALD was installed to Helsinki-Vantaa airport in 1983. Since then ALD has been used, in addition to aforementioned in-

[1] Not to be confused with atomic layer etching, today also known as ALE. On articles published before early 2000s, ALE usually refers to atomic layer epitaxy, i.e. ALD [7]

tegrated circuits, to deposit gas permeation barriers [8–11], anti-tarnishing coatings for jewellery [12, 13], hydrophobic and hydrophilic coatings [14–17], solar cells [18–20], batteries [21, 22], catalytic particles [23] and much more. More recently ALD has been utilized in more exotic applications, such as drug delivery [24] and vaccines [25]. The number of materials that can be deposited with atomic layer deposition has grown rapidly and there currently are hundreds of different processes available [26–28].

In addition to solid, also liquid and gaseous precursors can be used to deposit films. Plasma assisted or enhanced deposition can be used to make reactions more feasible at lower deposition temperatures. The original design by Tuomo Suntola could be described as spatial atomic layer deposition (SALD). Since then, pulsing precursors and separating them in time has become the conventional ALD method and SALD is gaining popularity as an enabling technique for large scale flexible substrate deposition method.

While ALD processes have been under extensive investigations for the past decades, many of the reaction mechanisms and factors contributing to film growth remain poorly understood. The reaction mechanisms have been previously studied indirectly by detecting the reaction by-products, for example, with quadruple mass spectrometry (QMS) [29–40]. More direct measurements of the film growth include detection of surface species between the precursor pulses with spectroscopic methods [41–44] or using synchrotron radiation for *in operando* X-ray photoelectron spectroscopy (XPS) ALD research [45]. In addition, there are nowadays powerful computational methods that can help to predict and validate the possible reaction mechanisms [46–50].

Hydrogen is a common impurity especially after deposition at low temperatures and it can be harmful in many applications [51–55]. The hydrogen incorporation and its origin at different deposition conditions has not been studied systematically before, especially in relation to purging time. In this thesis, precursors containing rare but stable isotopes were used to probe the impurity incorporation in two well known ALD processes: Al_2O_3 from trimethylaluminium (TMA, $Al(CH_3)_3$) and water, and ZnO from diethylzinc (DEZ, $Zn(CH_2CH_3)_2$) and water. Both Al_2O_3 and ZnO films were deposited with conventional time separated ALD and spatial ALD. Quantification of different isotopes in the films requires the use of ion beam techniques. In addition, only a couple of techniques can detect all the elements down to hydrogen. Time-of-flight elastic recoil detection analysis (ToF-ERDA), which was used in this thesis, can accomplish both. It is also the only method that does not require any reference samples in order to produce quantitative results making it an ideal tool for isotopic tracing of hydrogen in as-deposited films.

2 ATOMIC LAYER DEPOSITION

Conventional atomic layer deposition is a cyclic thin film deposition technique in which at least two gaseous precursors are introduced to the substrate surface one at a time. The precursor then chemically reacts with the surface atoms and molecules and forms new bonds. Between the precursor pulses, reaction chamber (often called a reactor) is purged with an inert gas such as N_2 or Ar. This purging ensures that the unreacted precursor molecules and the reaction by-products are flushed before the next precursor. After the purging, the next precursor is pulsed into the reactor and it reacts with the surface species left on the substrate by the previous precursor. In the ideal case there are no gas phase reactions between the precursors and the reactions are taking place solely on the surfaces.

Precursors used in atomic layer deposition have several key requirements: they must be highly reactive so that reaction times are fast, liquid precursors must be relatively volatile so that they will vaporise easily and the reaction by-products must be gaseous and preferably unreactive so that they can be purged. On the other hand, precursors must not decompose at high temperatures (even over 500 °C) which are often needed for the desired reaction to occur. Due to these requirements, many precursors used to deposit oxides are pyrophoric meaning that they will ignite spontaneously when they are in contact with oxygen and/or moisture in air. This makes the handling of the precursors challenging and it must be done in a glovebox in an inert atmosphere. Precursor itself can be solid, liquid or gas, but in order to be utilized in ALD, precursor must be introduced in a gas phase to the reactor. Solids and low vapour pressure liquids can be heated in order to transform them into usable gas phase.

One cycle which, in theory, produces one atomic layer of material, is called an ALD cycle. A simplistic model of the ALD cycle of a two precursor process is presented in Fig. 1. The film thickness can be accurately controlled simply by the number of cycles, and in principle ALD enables deposition at the accuracy of single atomic layer. Unlike the ideal ALD model would predict, in practice only a fraction of a single atomic layer is deposited in a single cycle.

Ideally the film thickness is linearly proportional to the number of cycles. However, the growth per cycle (GPC) at the beginning of the deposition can

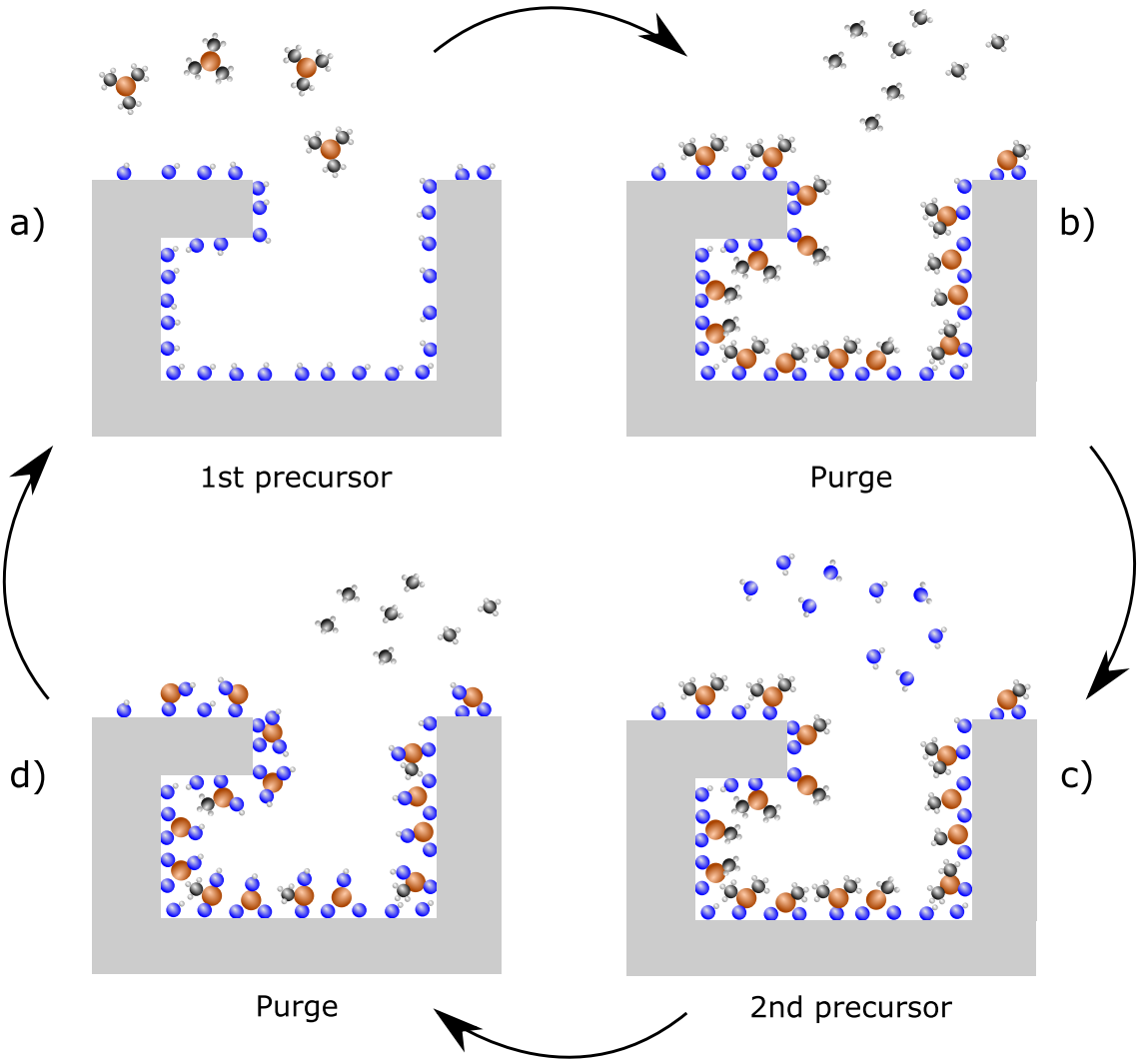

FIGURE 1 In an ideal ALD cycle a) gaseous precursor is first introduced to the substrate. b) After the precursor has formed a monolayer on the substrate, excess precursor and by-products are purged. c) After the purge, second precursor is pulsed and it reacts with a surface saturated by the previous precursor. d) Again, the excess precursor and by-products are purged. After a full cycle the surface is saturated with the same surface species as in a) and the next cycle can begin.

slightly differ from the steady state since the surface reactions on the molecules attached to the substrate surface can differ from the reactions on the already grown film. The period in the beginning of the deposition when the film is not continuous, is called nucleation. This often leads to nonlinear GPC during the first ALD cycles. When the whole substrate is covered with continuous film, the GPC should remain constant [7].

Maybe the most characteristic feature of the ALD is the possibility to deposit conformal films on top of a complex three-dimensional structures. This is enabled due to the self-limiting nature of ALD. In one half-cycle, the precursor reacts with the surface species until the surface is saturated with the precursor or there is no reaction sites available to bind to as presented in Fig. 1. In an ideal case, even prolonged precursor exposure does not have an effect once the saturation is reached. The saturation of the surface is discussed in more detail in section 2.2.

2.1 ALD window

Growth of ALD films is commonly measured with growth per cycle or GPC in units of nanometers or Ångstroms per one ALD cycle. Alternatively the thickness increment can be expressed as deposited atoms per area, often as 1×10^{15} atoms per square centimeter (responding to roughly one atomic layer) per cycle. Both of these units have their merits. While thickness in nanometers gives easily understandable physical measure, it can differ from the picture given by actual number of atoms deposited. The film density can vary with depositing parameters such as temperature and purging time. This can lead to two films with similar thickness in nanometers while the denser film has significantly more material. In addition, GPC should not be mixed with growth rate or throughput of the deposition which are related to the time needed for depositing certain amount of material. While a certain process can have a high GPC, the cycle time required may be long and the actual time needed to deposit a certain thickness can be significantly long. This kind of questions are important when considering industrial applications where the high throughput is necessary.

ALD window, seen in Fig. 2, is a useful concept originally introduced by Suntola [56], which tries to explain how temperature affects the growth per cycle as well as the chemistry of the vapor-solid reactions. If the deposition temperature is low, precursors can condensate (physisorpt) to the substrate surface which can lead to a higher than monolayer adsorption in one half-cycle. This is often called chemical vapour deposition (CVD) like growth, since it resembles more the CVD thin film growth where both precursors are introduced to the substrate simultaneously. On the other hand, low temperature slows down the reactions and even reasonable long reaction times (Equation (3)) can not saturate the substrate surface, which leads to lower than expected growth per cycle. In addition, at low temperatures the activation energy for the reaction can be so high that the energy provided by the temperature can not overcome the barrier.

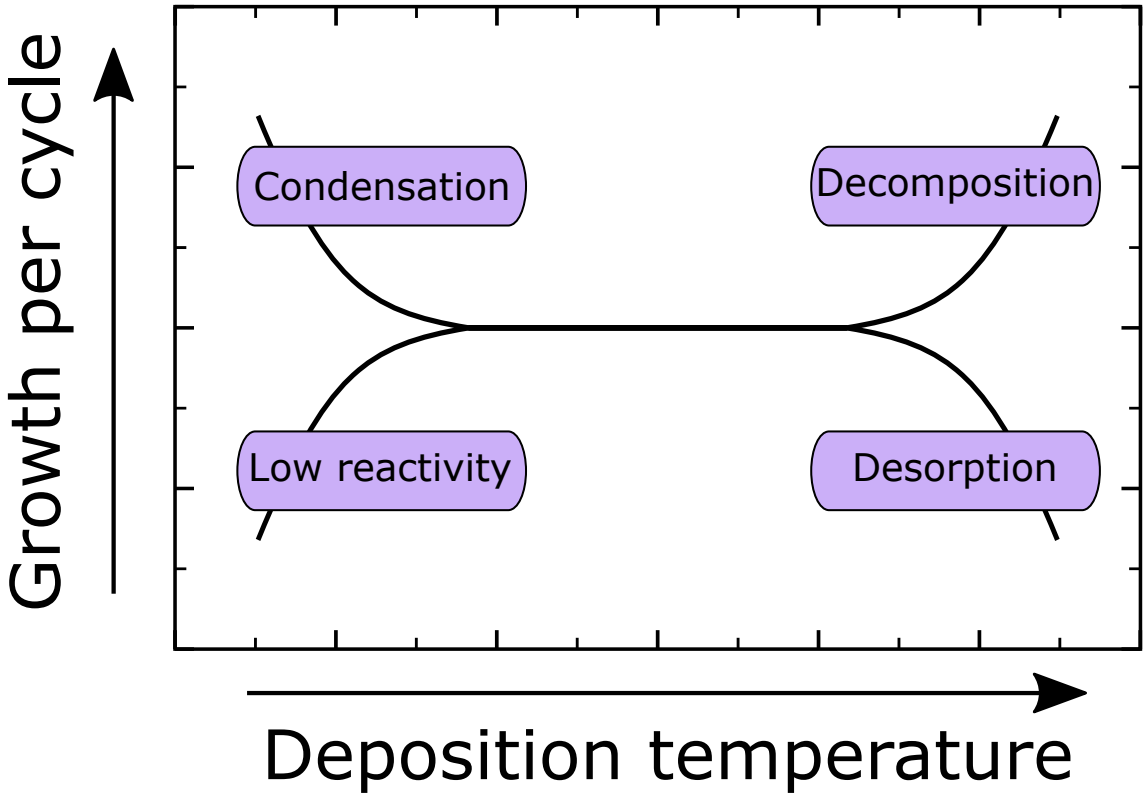

FIGURE 2 Concept of ALD window demonstrates the possible behaviour of GPC as a function of deposition temperature.

At high temperatures the precursors can start to decompose. This leads to a precursor dose dependent growth as the formation of a monolayer does not necessarily terminate the reaction. At high temperatures it is also possible that the desorption of reaction sites during the purging step, such as the hydroxyl groups, can decrease the reaction sites available for the next precursor and therefore saturation of the surface is reached with smaller concentration of adsorbed species.

The ALD window has its merit but it can also lead to misconceptions. For many processes there is not a temperature range where the GPC would be constant as conceptualised in Fig. 2. This does not mean that the reaction would not be a self-limited and well behaving ALD process and particularly not that the process would be unusable.

2.2 Surface chemistry

Atomic layer deposition relies on chemical bonding of precursors onto the substrate surface. Depositing methods, such as evaporation or sputtering, utilize weaker physisorption, which makes them fundamentally different.

Several different chemisorption mechanisms have been identified for the ALD chemistry. Most of them fall into three categories: Ligand exchange, dis-

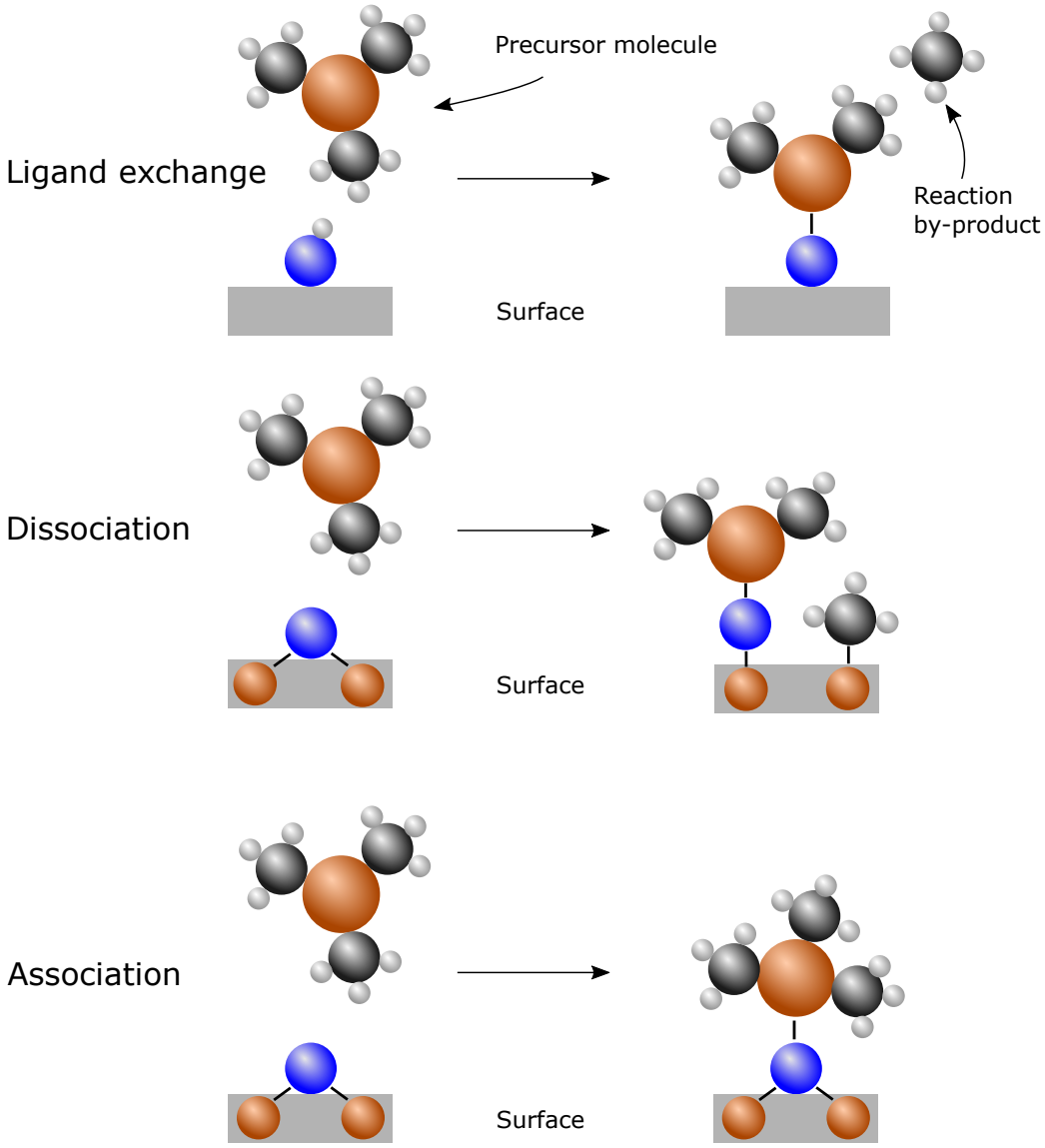

FIGURE 3 Some of the most common ALD surface chemisorption reactions are ligand exchange, dissociation and association.

sociation and association [57] (shown in Fig. 3) and also oxidation [58]. In the ligand exchange reaction a surface species exchanges an atom or a molecule with precursor which in turn binds to the surface. At the same time, a by-product is released. Both main reactions in the TMA + H_2O process are ligand exchange reactions. The same applies for reactions of DEZ and H_2O. In dissociation the precursor molecule splits, a bond in the surface is broken and all the fractions bind to the surface. For example, TMA can dissociate on O-bridge sites as illustrated in Fig. 3 [59]. Association reaction is simply a bonding of the precursor to the surface without breaking any precursor or surface bonds. During both the dissociation and the association, no by-products are released. In addition to these three mechanisms, also oxidation reaction is quite common when strong oxidisers such as O_2 plasma or O_3 are used [58].

Atomic layer deposition relies on self-terminating reactions which come to

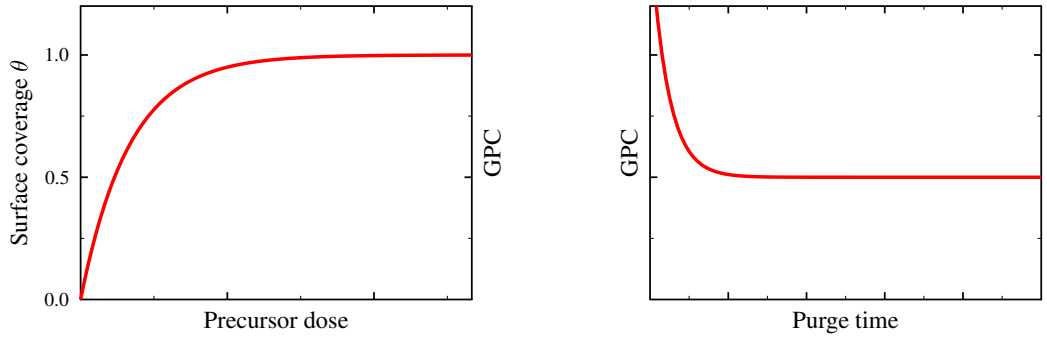

(a) (b)

FIGURE 4 a) Surface coverage saturates with increasing precursor dose according to equation 2. Similarly, the GPC saturates when adequate precursor dose is reached. b) Too short purging time typically leads to CVD-like growth as the multiple layers of physisorpted precursor remains in the surface after the purging.

a stop when the surface is saturated with a precursor or there is no available reaction sites. However, saturation often occurs before all the reaction sites are occupied due to steric hindrance which is discussed in the next section in more detail.

The equation for the rate of the surface saturation can be written as

$$\frac{\mathrm{d}\theta}{\mathrm{d}t} = r_{ads} - r_{des}, \tag{1}$$

where θ is the surface coverage, r_{ads} is the rate of adsorption and r_{des} is the rate of desorption. At equilibrium the net rate is zero.

As the by-products of ALD process are constantly pumped away, the r_{des} can be considered to be close to zero and the reaction to be irreversible. In addition, the precursor surface reaction and the formation of the by-products has ideally a large negative enthalpy, so that the reverse reaction is unlikely. For example, the reaction of TMA with water has a total enthalpy change of -594 kJ/mol [60]. The rate of adsorption is proportional to the adsorption rate constant k_a, precursor partial pressure p, and to the fraction of unoccupied reaction sites $1 - \theta$. Solving the equation (1) with $r_{des} = 0$ we get

$$\theta = 1 - e^{-k_a p t}. \tag{2}$$

Equation (2) indicates that the surface coverage reaches unity when sufficient precursor dose (precursor partial pressure multiplied by time) is provided as shown in Fig. 4a. Both the surface coverage and the GPC increase until a sufficient dose leading to the surface saturation is reached as seen in the Fig 4a. However, this is not always true as there might be persistent surface species that do not react even with long exposure times at given temperature. The persistent surface groups are discussed further in section 2.5.

Furthermore, the reaction (adsorption) rate constant depends on the temperature described by the Arrhenius equation (after Swedish scientist Svante Arrhenius)

$$k = A\, e^{\frac{-E_a}{RT}}, \tag{3}$$

where k is the reaction rate constant, R is the universal gas constant, T is absolute temperature, E_a is activation energy, and A is a pre-exponential prefactor unique for each reaction. This implies that the reaction rate, and therefore the time needed for the saturation of the surface depends on the deposition temperature.

In addition to sufficient precursor dose, adequate purging time between the precursor pulses is also important. In order to keep the growth self-limiting (the increase in the precursor dose not lead to an increase in GPC) the purging time must be long enough in order to remove all the excess precursor. If the purging step is not sufficient, it can lead to a higher than expected growth due to multiple layers of physisorpt precursor. This effect is shown in Fig. 4b.

2.3 Steric hindrance

The key feature of ALD is the self-limiting growth of the film. This means, in theory, that only a single layer of material is deposited in one cycle. In reality, only a fraction of a monolayer is deposited in each cycle for most of the ALD processes [57].

The precursors often contain the target atom surrounded by larger ligands. Good examples of these are the both precursors used in this thesis, TMA and DEZ, which contain metal atom surrounded by alkyl groups. There are also precursors with much larger ligands such as β-diketonate- or cyclopentadienyl-based compounds [26].

As TMA reacts with the surface hydroxyl groups releasing methane (Eq. 5a) it is left with one or two methyl groups. Both, the $AlCH_3$ and $Al(CH_3)_2$, surface species can block a certain area of the surface. As the ligand is larger than the aluminium atom, the ligand(s) can prevent another TMA molecule from reaching the reactive site, namely OH group, at the substrate surface. This is called steric hindrance. Traditionally this has been believed to be the main reason behind the self-limiting growth characteristic of ALD for most processes [57]. Steric hindrance can also explain why the growth per cycle is less than a monolayer: the surface reaches saturation via steric hindrance even though many of the possible reactive sites are physically blocked by the ligands. Therefore the saturation surface coverage of a precursor will be less than the number of reaction sites available and equation (2) does not reach unity. This leads to a less than a monolayer growth per cycle even if the precursor dose would be sufficient to react with all the reactive sites.

Steric hindrance well explains the surface saturation, especially with pre-

cursors with large ligands, but there is a building evidence of more complex mechanisms affecting the saturation and precursor uptake even in the case of TMA + H_2O process which is regarded as the ideal model process for the ALD. At high temperatures the desorption of surface species, which act as the reactive sites for the next precursor, can be the limiting factor for the precursor uptake. It is known, for example, that the surface OH group density decreases in high deposition temperatures [42,57,61]. At high enough temperatures this becomes the limiting factor for precursor uptake in each pulse and therefore for the GPC. Furthermore, there is evidence of persistent surface groups at low deposition temperatures and secondary reaction pathways. These will be discussed more in section 2.5.

2.4 Spatial ALD

In recent years the original design of ALD reactor by Tuomo Suntola has been adopted again as a spatial atomic layer deposition (SALD). In SALD the pulses are separated by space rather than time as in conventional ALD. The spatial ALD can be realized in two different manners: The substrate can be moved in front of the coating head which contains precursor inlets separated by inert gas, or the coating head can be moved on top of the sample surface. The SALD-reactor used in this thesis has a rotating cylinder with stationary inlets for precursors and purging gases as well as stationary suction of gases. A flexible substrate is attached to the rotating cylinder and as the cylinder rotates, the substrate goes through zones of precursor flows and inert gas zones. The reactor design used in the thesis is presented in Fig. 5.

The benefit of SALD is that the reaction space can be kept small and in close proximity to the reaction surface, which eliminates the long purging times needed to remove the excess precursor from reactor space. Not only the purging times are reduced but also the pulse times used with conventional ALD at low pressure can be replaced with shorter but higher precursor partial pressure "pulses". Therefore the precursor dose (pressure multiplied by time, pt in Eq. (2)) can remain the same.

Furthermore, SALD enables roll-to-roll (R2R) operation of flexible substrates as well as deposition on planar large area substrates. ALD is often used for high-end products such as integrated circuits, but SALD can increase the output significantly making ALD processing cheaper and feasible deposition method for new, inexpensive end products such as packaging. In addition, SALD has enabled operation at atmospheric pressures which speeds up the process since long pumping to vacuum conditions is not required. Atmospheric pressure deposition also enables deposition on large substrates which would be impractical or even impossible to be put inside vacuum chamber. On the other hand, continuous precursor flows need to be tuned accordingly in order to minimize precursor waste [62].

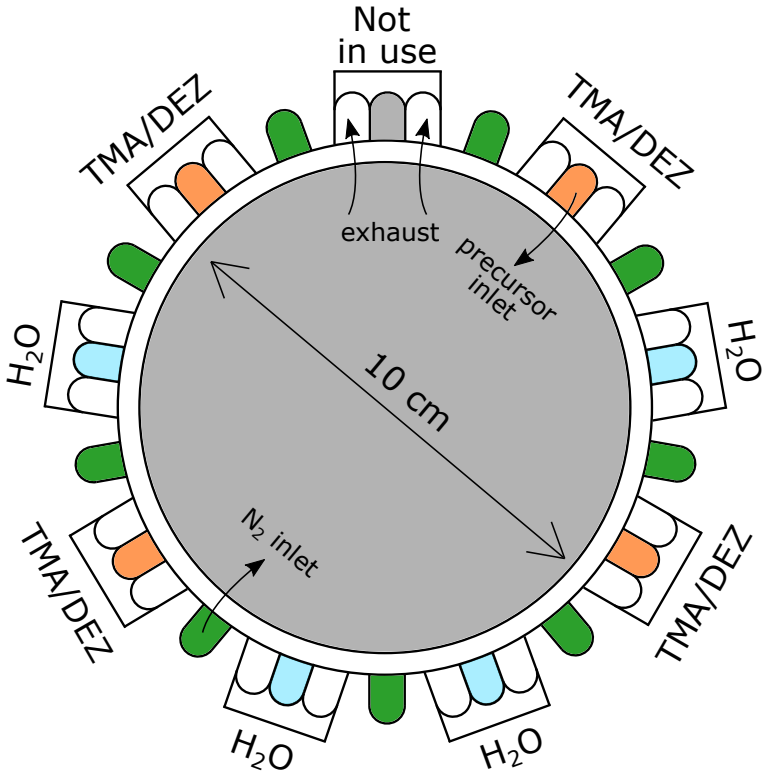

FIGURE 5 Schematic view of the rotating cylinder SALD reactor used in the thesis. The substrate is attached to the cylinder. Reprinted with permission from [PIII], Copyright 2022, Elsevier.

Spatial ALD of many materials is already studied for multiple applications [63–65]. For example in photovoltaics, passivation of solar cells with SALD Al_2O_3 has been shown to produce excellent results [18–20] and Zn(O,S)buffer layers for Cu(In,Ga)Se_2 based solar cells have been deposited with SALD [66].

In addition, SALD has been studied to be used in thin film transistors [67], Li-ion battery technologies [21, 22, 68] and for transparent conducting oxides [64, 69]. Encapsulation of sensitive components such as OLEDs with pinhole free SALD films shows also promising results [10, 11, 70–72]. The higher throughput and therefore lower manufacturing costs has also generated interest of using SALD for packaging [10, 73] and even for surface modification of textiles [74].

2.5 ALD Chemistry of Al_2O_3 and ZnO

The two materials studied in this thesis are metal oxides, aluminium and zinc oxide. Both of them are very stable and non-toxic, so they are suitable for multitude of applications. In addition, the deposition of both materials is possible at relatively low temperature on wide variety of substrates.

2.5.1 ALD of Al_2O_3

Al_2O_3 is a dielectric and it can be used as an insulating high-k layer in several applications [75–77]. The barrier properties of Al_2O_3 are also good as it is basically pinhole free, and thus it can be used as a moisture barrier in packaging [9, 10]. Al_2O_3 is also transparent, so it can be used as oxygen and moisture barrier for OLED displays [8,78,79]. In addition to blocking H_2O and O_2, Al_2O_3 can be used to stop hydrogen induced damage to ceramic capacitor components [51] and thin film transistors [52]. The barrier properties are also good for anti-tarnishing coatings used with jewellery. Aluminium oxide deposited with ALD below 600 °C is practically always amorphous [26] although more recently crystalline Al_2O_3 has been deposited on specific substrates at temperatures as low as 300 °C [80]. In most cases, only post-deposition annealing at 1000 °C or higher transforms amorphous Al_2O_3 to a crystalline form [80].

Atomic layer deposition of Al_2O_3 thin films from trimethylaluminium (TMA) and water was reported already in 1989 by Higashi and Fleming [81]. This process is probably the most studied ALD reaction and can be used as a model reaction for ALD [7,26,57]. The reaction produces high quality films and the reaction is self-limiting in a wide temperature range. The reaction can be simplified as follows [7,57]:

$$2\,(CH_3)_3Al\,(g) + 3\,H_2O\,(g) \longrightarrow Al_2O_3\,(s) + 6\,CH_4\,(g)\,. \tag{4}$$

The total reaction (4) can be divided into two half reactions or half-cycles, one for each precursor pulse:

$$x\,(OH)^* + Al(CH_3)_3\,(g) \longrightarrow O_xAl(CH_3)^*_{3-x} + x\,CH_4\,(g) \tag{5a}$$

$$O_xAl(CH_3)^*_{3-x} + (3-x)\,H_2O\,(g) \longrightarrow O_xAlOH^*_{3-x} + (3-x)\,CH_4\,(g)\,, \tag{5b}$$

where * denotes species bonded to the surface and x is 1 or 2. As a starting situation, the substrate surface is saturated with OH groups. During the TMA pulse, gaseous TMA reacts with one of these hydroxyl surface groups. As a result, a proton from the OH group is transferred to the methyl group and methane is released. The $Al(C_3H)_2$ is now bonded to the surface and it can go through a second ligand exchange reaction with a near OH surface group releasing a second methane molecule. The number of methyl groups per aluminium left on the surface after the TMA pulse should be close to 1.5 in order to produce a stoichiometric film. Experimental work has shown that value of x however seems to vary somewhat with temperature so that at lower temperatures the monomethyl termination dominates (higher x) while at higher temperatures there are more dimethylaluminium surface species [29,41,82]. The surface OH-concentration after the water pulse varies with temperature [42,57] and it has been shown to affect the number of methyl groups per aluminium left on the surface after TMA pulse. Methane is then purged and in the next pulse water is introduced to the surface. The remaining CH_3 groups are removed by the water, again in the form of

methane, and the surface is saturated with hydroxyl groups similar to the starting situation. If the surface has also oxygen bridges (Al-O-Al), TMA can chemisorb on these sites through association and dissociation [59].

Especially at low deposition temperatures, when the conditions for the reactions are not ideal, the factors affecting the deposition can change. Vandalon and Kessels conducted broadband sum-frequency generation (BB-SFG) studies on TMA + H_2O process [41,42] and they observed that when the deposition temperature is low (below 200 °C), persistent CH_3 groups remain in the film surface even after extended H_2O exposure. They concluded that water is not reactive enough towards the CH_3 groups at low temperatures. Therefore, the persistent methyl groups, rather than steric hindrance, are the main reason behind the reduced GPC at low deposition temperatures. They also found out that the reaction cross section of TMA does not depend on the temperature while the cross section of H_2O reaction increases with increasing temperature. However, the absolute value of CH_3 groups at the end of TMA pulse decreased with temperature and it was attributed to the loss of surface OH groups at higher temperatures. Although this is a rather new explanation for surface saturation, something similar was discovered already in 1991 by Soto and Tysoe [83].

Vandalon and Kessels proposed in the follow-up article that the reason behind the persistent CH_3 groups is the coverage dependent activation energy. Some previous computational work by Shirazi and Elliot [46] and Weckmann and Laasonen [47] supported the statement. According to them, this explanation is further amplified by the estimation of CH_3 surface density which is not high enough to cause significant steric hindrance to inhibit growth. Especially at low temperatures the TMA reaction seems to go through a second ligand exchange producing mostly monomethyl $AlCH_3$ surface groups [41]. This further leads to less steric hindrance and more isolated CH_3 groups. They conclude that the loss of under-coordinated oxygen must be the cause for saturation at higher temperatures, while the persistent CH_3 groups decrease the GPC at low temperatures.

Gakis *et al.* [50] proposed that the CH_3 groups, that are bound to aluminium together with an OH group, namely $Al(OH)(CH_3)$, are the source of these persistent methyls reported by Vandalon and Kessels. These groups would have higher activation energy compared to other CH_3 groups and therefore they would be less likely to react with subsequent water pulse. While this is possible, Sperling *et al.* [84] discovered that at low temperatures the surface coverage and finally saturation follows a biexponential function instead of single exponential presented in equation (2). They concluded that the presence of nonreactive $Al(OH)(CH_3)$ surface species would lead to three exponentials which was not detected within the measurement accuracy. They gave a physical meaning to this biexponential function by introducing a coverage dependent E_a as proposed by Vandalon and Kessels. This approach is fundamentally different to the one presented by Gakis *et al.* since in this model every CH_3 group is identical and the reaction probability depends only on the CH_3 surface concentration.

In a recent paper Werbrouck *et al.* [85] found out using time resolved QMS that at the end of the H_2O pulse, when the surface OH concentration is high,

some of the Al can etch away in the form of $HOAl(CH_3)_2$. As the absolute OH concentration is high at low deposition temperatures, this can be one more explanation for the decreased GPC at low temperatures. Furthermore, Werbrouck *et al.* discuss that this secondary reaction can be the source of the second exponential discovered by Sperling *et al.* [84].

2.5.2 ALD of ZnO

ZnO thin films deposited with ALD are polycrystalline even at room temperature [26, 86, 87]. The ZnO films deposited with ALD always show hexagonal wurtzite crystal structure, but the preferred orientation of the crystals depend on the deposition temperature [86], purge time [88], and substrate [26]. ZnO is a wide band gap semiconductor [89] and its electrical properties can be tailored with doping [90]. For example aluminium-doped zinc oxide (AZO) has been studied extensively for photovoltaic and display applications used as transparent conducting oxide (TCO) instead of tin-doped indium oxide [91, 92]. In addition, ZnO has some interesting attributes such as possible antibacterial properties [93] and it has been shown to have tunable wettability that can be controlled with UV-irradiation [16].

The chemistry of ZnO, the second material studied in this work, using diethylzinc (DEZ) and water is very similar to Al_2O_3 even though ZnO films are polycrystalline and Al_2O_3 films are amorphous. Instead of three methyl groups there are two ethyl groups bound to the metal center and the gaseous by-product of the reaction is ethane instead of methane. The idealised mechanism for DEZ and H_2O is [61]:

$$OH + Zn(CH_2CH_3)_2^* \,(g) \longrightarrow O - Zn(CH_2CH_3)^* + CH_3CH_3 \,(g) \tag{6a}$$

$$OH - Zn(CH_2CH_3)^* + H_2O \,(g) \longrightarrow O - Zn - OH^* + CH_3CH_3 \,(g). \tag{6b}$$

In the equation 6a there is a possibility of second ligand exchange reaction similar to TMA + H_2O process. This leaves the surface with bare Zn atoms before the H_2O pulse. Indeed, QCM studies have shown that the mass decrease during the water pulse is smaller than expected and can be due to water reacting with bare zinc atoms [61, 87, 94]. On the other hand, Mackus *et al.* [95] observed that at low deposition temperatures water pulse can not remove all the ethyl groups from the surface. Weckmann and Laasonen [48, 49] found out computationally that persistent ethyl groups inhibit the GPC of ZnO when the deposition temperature is below 100 °C. When the deposition temperature is increased, there is enough energy to remove close to all ethyls and as a result GPC increases. When the deposition temperature is further increased, the desorption of surface species becomes the limiting factor [96] similar to Al_2O_3 deposition and the GPC starts to decline.

Kim *et al.* [97] further concluded that at 150 °C and above the precursor dose needed to saturate the substrate surface increases due to the desorption of DEZ. Weckman and Laasonen predicted that DEZ firstly adsorbs on to the surface

via weak molecular interaction before forming chemical bonds [48]. According to Kim *et al.* desorption of DEZ from this weakly bound state is activated at higher temperatures and leads to lower GPC if the dose is not increased [97]. On the basis of their model they also concluded that steric hindrance is the growth limiting factor below 150 °C. Above that, the number of available surface OH groups sets the limits of the growth.

As pointed out above, the surface reactions of the "ideal" TMA + H_2O or DEZ + H_2O processes seem to be much more complex than previously thought and quite poorly represented by the simplistic ALD window in Fig. 2 or the ideal reactions in equations (5a) and (5b), and in (6a) and (6b).

2.5.3 Impurity incorporation

Even though the reaction mechanism presented in Equations (5a) and (5b) is verified by several different studies [29, 31, 44], it does not give the full picture as discussed above. In addition, the films deposited at low temperatures can contain high concentrations of impurities originating from the precursors, mainly hydrogen and carbon in the case of TMA and DEZ. The ratio of the main components, O/Al in the case of Al_2O_3 and O/Zn in the case of ZnO, is not always stoichiometric [42,50,61,82,86,87,98–101] and the growth per cycle also depends greatly on the deposition temperature [42,50,61,82,86,87,98–101].

Hydrogen is the most notable impurity in the films. It affects the film density and it can have negative effects on other components in some applications. For example, hydrogen can degrade ceramic capacitors [51], thin film transistors [52], create defects in insulators [53] and cause temperature induced degradation in multicrystalline Si used in solar cells [54]. Films deposited at low temperatures contain often significant concentration of hydrogen and the density of the films decreases with increasing hydrogen concentration [98,100]. This goes hand in hand with the barrier properties of the films [55]. However, there are some occasions when hydrogen is even desired, such as passivation of Si-dangling bonds with thin layer of Al_2O_3 [102,103] and doping of ZnO with H in order to increase the carrier mobility [104].

When deposition temperature of TMA + H_2O is decreased to near room temperature, the film can constitute of more than a one fifth of hydrogen. When the deposition temperature is increased to 200 °C the hydrogen concentration drops to only few atomic per cents [82,98,99,102,105,106]. In the case of ZnO, the hydrogen concentration does not climb that high but can be more than 10 at.% and similarly drop to 1 at.% and below [86,107–109].

The persistent methyl and ethyl groups introduced in the previous section would seem like a natural candidate for the source of the hydrogen in the films. It would be possible that these unreacted groups get buried into the film in subsequent pulses. However, only a minor concentration of carbon is found in the films contradicting the assumption. This is true for both ALD Al_2O_3 and ZnO films [41,82,86,109,110].

Guerra-Nuñez *et al.* [82] studied hydrogen incorporation in Al_2O_3 ALD films

using TMA and heavy water. They found out that the total hydrogen concentration increased with decreasing deposition temperature. The carbon concentration followed a similar trend. Furthermore, the main hydrogen isotope found in the film was deuterium in all deposition temperatures between 80 and 220 °C. The impurities left in the film, as well as the surface saturation [57], are often contributed to steric hindrance of methyl groups. If TMA molecule reacts as a monodentate with surface hydroxyl, it is left with two methyl groups which can obstruct TMA molecules from reaching unreacted surface OH groups. Guerra-Nuñez *et al.* concluded that this simple steric hindrance can not explain solely the high concentration of deuterium in the film and proposed two additional mechanisms how these OH groups get buried int the film. According to their results the O/Al ratio increased hand in hand with the deuterium concentration, which they concluded to be an evidence of buried OH groups.

Hiraiwa *et al.* deposited Al_2O_3 with TMA and heavy water at 100 °C and 450 °C [100]. At the higher deposition temperature their findings are in line with Guerra-Nuñez *et al.* but the film deposited at 100 °C contained more ^1H than ^2H. The high concentration of ^1H at 100 °C was attributed to buried CH_3 groups and their explanation resembles the behaviour of the persistent methyl groups presented by Vandalon and Kessels.

In case of ALD ZnO from DEZ and heavy water, Guziewicz *et al.* [107] observed a similar trend at deposition temperature between 100 and 200 °C. The total amount of hydrogen and deuterium decreased with increasing deposition temperature, while heavy water seemed to be the main source of impurity hydrogen as there were more deuterium than hydrogen in the films. These trends seem similar to the ones measured by Guerra-Nuñez *et al.* [82] in the case of Al_2O_3. In a recent study Xia *et al.* also used heavy water in order to study the impurity incorporation. Their results were more complex as the carbon concentration decreased rapidly around 150 °C and increased again when deposition temperature reaches 200 °C. Above 200 °C the carbon concentration started to decrease again. In their study the hydrogen and deuterium incorporation is more simple, but the results are in contradiction with the results obtained by Guziewicz *et al.*. According to Xia *et al.* the main hydrogen isotope found in the film is hydrogen instead of deuterium in all temperatures between 100 and 300 °C.

While many of these studies try to catch the mechanisms at low temperatures, which are not ideal for the discussed processes, most of them use long precursor exposure times and very long purging times between the pulses. This gives a good control over the process, but purging times of tens of seconds are rarely used in real world applications. The incorporation of impurities with two nonideal conditions, the low temperature and short purging times, are not studied properly. Slightly different deposition conditions also seem to affect the results and can lead to big discrepancies. In addition, the results have been somewhat contradictory. In this thesis these matters are addressed.

2.6 Use of rare isotopes in ALD studies

Different isotopes of an element contain the same number of protons and electrons, but the number of neutrons change. Therefore, the isotopes of the same element should be chemically indistinguishable. However, the isotopes can be differentiated based on their mass. This fact can be utilised in ALD research by using precursors that contain stable isotopes, but which are rare in nature. A well known example is heavy water, ^2H_2O, which has two deuterium atoms instead of two hydrogen atoms bonded to the oxygen. The natural abundance of deuterium is only 0.015 % [111], so it is not normally detected in the deposited films.

Reaction mechanisms have been studied by detecting by-products of the ALD reactions using quadrupole mass spectrometry (QMS) together with heavy water as an oxygen source [29–40]. Ion beam methods have also been used to detect hydrogen and deuterium from films deposited with heavy water [82,100,107, 112–114]. In addition to direct measurement of the mass difference between the isotopes, it is also possible to measure the change in bond vibrational frequencies. Utilizing this, surface chemistry of ALD reactions with heavy water have been studied with attenuated total reflection Fourier-transform infrared (ATR-FTIR) [43] and broadband sum-frequency generations (BB-SFG) spectroscopy [41]. In addition to heavy water, precursors containing oxygen-18 enriched O_2 gas [115, 116], oxygen-18 enriched water [43,117,118], deuterated ammonia [119] and deuterated TMA [41] have been used.

In addition to deeper understanding of the reaction mechanisms and impurity incorporation, the use of heavy water has been studied for enhancing the thin film device reliability under electric stress by stabilizing dangling bonds in the interface [120, 121].

While isotopes of the same element are chemically similar, the mass difference between isotopes can affect the reaction kinetics, especially with light elements. Kinetic isotope effect (KIE) was first introduced in 1947 [122] and has been since used in reaction kinetics studies [123]. The simple way to look at the effect is to consider the activation energy and the ground state energy of the bond. Quantum mechanical vibration levels E_n are given by

$$E_n = \left(n + \frac{1}{2}\right) h\nu, \tag{7}$$

where $n = 0, 1, 2...$, h is Planck's constant and ν is the vibration frequency. At ground state $n = 0$ and using simple harmonic oscillator approximation we get for the ground state energy

$$E_0 = \frac{1}{2} h \frac{1}{2\pi} \sqrt{\frac{k}{\mu}}, \tag{8}$$

where k is the force constant and μ is the reduced mass of the system

$$\mu = \frac{m_1 m_2}{m_1 + m_2}. \tag{9}$$

Looking back to Arrhenius equation (3) we can now approximate the ratio of the reaction rates with different isotopes. Both TMA and DEZ react mainly with surface OH groups by ligand exchange. As a proton/deuteron is transferred in the reaction, the OH-bond is important when considering the ALD processes. For example, substitution of hydrogen with deuterium decreases the E_0 approximately by a factor of 0.73 according to equations (8) and (9). On the other hand, we see that the ratio in E_0 between ^{16}O and ^{18}O is only 0.997.

Kinetic isotope effect is sometimes disregarded in ALD studies with heavy water [82] but for example Guziewicz *et al.* [107] and Hiraiwa *et al.* [100] reported reduced GPC and slight changes on other film properties compared to films deposited with normal water.

3 ALD THIN FILM PROCESSING

The deposition of the samples in this thesis was done using temporal Beneq TFS 200 ([PI] and [PII]) and spatial Beneq TFS 200R ([PIII]) ALD reactors.

The TFS 200 reactor is a cross flow reactor with constant inert gas flow across the deposition area. Nitrogen from Inmatec PN 1150 nitrogen generator (99.999 % purity) was used in all deposition with TFS 200 reactor. The base pressure in the reactor during the deposition was 1–2 mbar. All the precursors were delivered to the reactor by their own vapour pressure and the precursors were kept at room temperature.

All the samples prepared with conventional ALD were deposited on n-type (100) oriented silicon substrates which were cut from a bigger wafer. No any specific cleaning of the substrates were performed prior to depositions leaving the native SiO_x on top. The Si-substrates were distributed in all corners the reactor so that the conformality of the deposition could be verified.

For the samples prepared with spatial ALD, a flexible Ti-coated polyethylene terephthalate (PET) (Rowo Coatings) substrate was used. The reflecting Ti-coating allows visual inspection of the conformality of the deposited film. The flexible PET substrate was attached to the rotating cylinder with Kapton tape. For purging in the spatial ALD, 99.999 % purity pressurised nitrogen (Linde AG) was used. The base pressure in the SALD reactor was about 20 mbar.

All the samples were measured with ToF-ERDA immediately after the deposition. If this was not possible, the samples were stored in the load lock of the ALD reactor under vacuum environment ($\sim 1\times10^{-1}$ mbar) and exposed to the air only briefly before the measurements. This was done in order to minimize the ambient hydrogen and moisture exposure to the samples.

3.1 Al_2O_3 processing

In article [PI] the Al_2O_3 films were deposited using TMA from Strem Chemicals, (>98 %). Three waters with different isotopic compositions were used as the sec-

ond precursor: normal water $^1H_2^{16}O$, heavy water $^2H_2^{16}O$ (Medical Isotopes Inc. >99.99 %) and oxygen-18 enriched water $^1H_2^{18}O$ (Medical Isotopes Inc. >97 %). A temperature series of Al_2O_3 films was deposited with normal and heavy water from 70 to 250 °C. For all the samples in the temperature series, both TMA and water pulses were 300 ms and purging time between the pulses was kept at 10 s. Another series of samples was prepared with different purging times at 100 °C. The purging time was varied between 3 and 60 s. In addition to deposition with normal and heavy water, samples with oxygen-18 enriched water were prepared at 100 °C.

Furthermore, Al_2O_3 samples prepared with heavy water and oxygen-18 enriched water were exposed to warm and humid atmosphere in a climate chamber (Weiss WK3-180/40). The heavy water samples were kept 24 h and the oxygen-18 enriched water samples 48 h at 60 °C and 80 % relative humidity (RH).

A set of samples samples was also kept in ambient conditions for several months and measured again with ToF-ERDA after the storage.

3.2 ZnO processing

In article [PII] ZnO films were deposited using DEZ from Strem Chemicals (>95 %) and both normal and heavy water (Medical Isotope Inc. 99.9 %). A temperature series with both waters was deposited from 30 to 200 °C. In all the ZnO depositions the precursor pulse times were 150 ms for DEZ and 500 ms for both waters. The purging time in the temperature series after the DEZ pulse was kept at 10 s while purging time after the water pulse was 20 s. A second series of samples was deposited with varying purging times at 60 °C. The purging times were varied between 3 and 60 s. For the purging times equal to and below 10 s, the purging time after the both precursors was kept the same. For purging times longer than 10 s, only the purging after the water pulse was changed and the purging time after the DEZ pulse was kept at 10 s.

Additional studies with unsymmetric purging times were made at 60 °C with DEZ and heavy water. Purging times of 3-3 s, 3-10 s, 10-3 s and 10-10 s were used after DEZ and water pulses, respectively.

Multiple short pulsing (MSP) scheme was used to deposit ZnO films at 40 °C with DEZ and heavy water in order to study transient steric hindrance. A low temperature was selected for this experiment in order to amplify the effect of slowly desorpting surface species. The DEZ pulse was divided into three 50 ms second pulses and the water pulse into three 167 ms pulses. The pulses of the same precursor were separated from each other by 1 s purging. In order to keep the ALD cycle time the same as in the temperature series, the purging time after the last pulse of each precursor was shortened by 2 s.

Similar to Al_2O_3 samples, all the ZnO samples were measured immediately after the deposition or otherwise stored in the load lock under vacuum before the measurements. In addition, selected samples were measured again after two

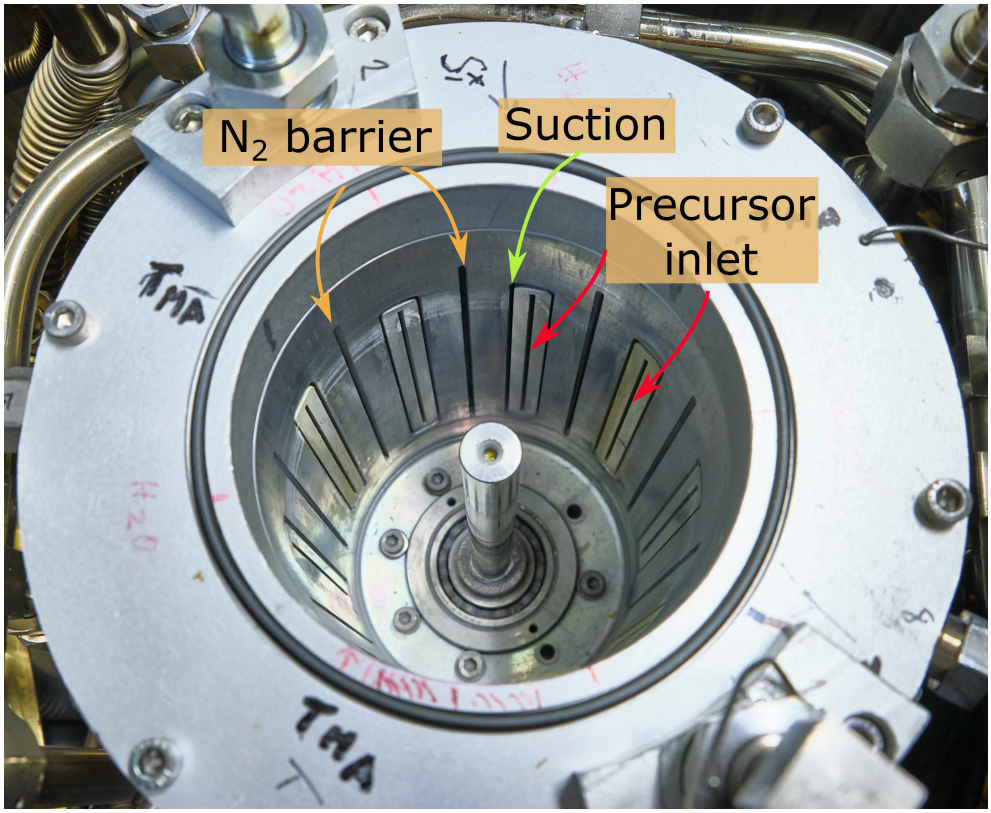

FIGURE 6 The inside of the modified Beneq TFS 200R reactor. The rotating cylinder holding the substrate is removed in order to see the precursor inlets, suction around the precursor inlets and N_2 barrier inlets.

months storage in ambient conditions.

3.3 SALD processing of Al_2O_3 and ZnO

In article [PIII] both Al_2O_3 and ZnO were deposited with TFS 200R (Fig. 6) using TMA and DEZ, respectively. Both normal and heavy water (Medical Isotope Inc. 99.9 %) were used as oxygen source. All the precursors, including normal and heavy water, were heated to 35 °C in order to increase their vapour pressure. Precursors were delivered to the reactor using bubblers with 100 sccm nitrogen carrier flow trough them. The nitrogen barrier between the precursor inlets was realized with total of 4600 sccm nitrogen flow.

Both Al_2O_3 and ZnO films were deposited between 60 and 140 °C with rotation speed of 10 rpm with normal and heavy water. Similarly, at 100 °C, a series of Al_2O_3 and ZnO samples were deposited with varying rotation speeds of 5, 10, 20 and 50 rpm using both normal and heavy water.

4 THIN FILM CHARACTERIZATION

4.1 Elemental composition

4.1.1 Elastic recoil detection analysis

There are several methods to study the elemental composition of thin films including X-ray photoelectron spectroscopy (XPS), secondary ion mass spectrometry (SIMS), Rutherford backscattering spectrometry (RBS) and elastic recoil detection analysis (ERDA). Of these methods ERDA and SIMS are the only ones that can detect the lightest elements including hydrogen. Of these two methods SIMS requires reference samples in order to produce quantitative results while ERDA is the only truly quantitative method [124].

In ERDA an accelerated ion beam is directed to the sample surface at an angle. The incident ion then collides with an atom within the sample and "kicks" out the atom by an elastic collision as shown in Fig. 7. The kinematics of the recoiled atom is given by

$$E_2 = \frac{4m_1m_2}{(m_1+m_2)^2}(\cos^2\phi)\,E_0\,, \tag{10}$$

where E_0 is the energy of the incident ion, E_2 is the energy of the recoiled atom, m_1 and m_2 are the masses of incident and recoiled ions respectively and ϕ is the recoiling angle.

Probability of the scattering to a given solid angle is expressed as a differential scattering cross section and can be written

$$\frac{\mathrm{d}\sigma}{\mathrm{d}\Omega} = \left(\frac{Z_1Z_2e^2}{2E_0}\right)^2\left(\frac{m_1+m_2}{m_2}\right)^2\cos^{-3}\phi\,, \tag{11}$$

where Z_1 and Z_2 are the atomic numbers of incident ion and recoiled atom, respectively, and e is the elementary charge. These two equations give the means to directly measure the elemental ratios in the film.

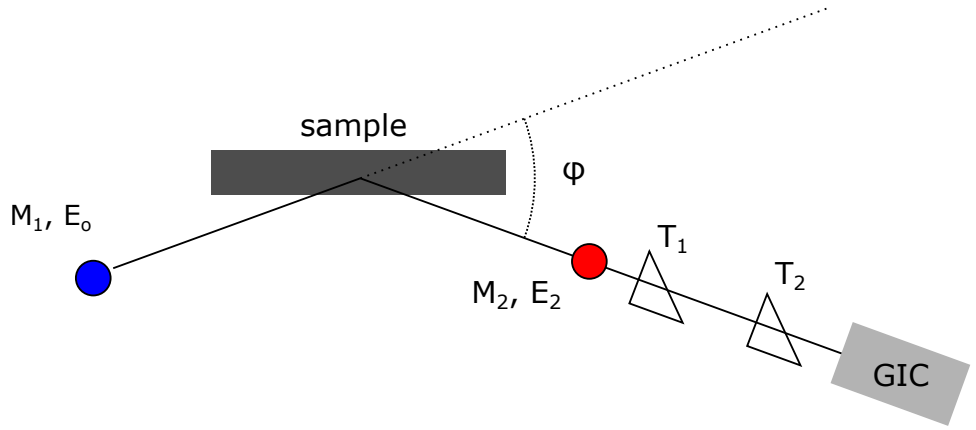

FIGURE 7 The ToF-ERDA measurement consists of an incident ion (blue) kicking out a recoiled sample atom (red) to an angle ϕ. The time of flight of the recoil is measured with two timing gates T_1 and T_2, and finally the energy of the recoil is measured with gas ionization chamber (GIC).

4.1.2 ToF-ERDA

In addition to resolving different elements, ERDA gives information about the elemental depth profile of the sample. Beside the head on collisions between the incident and recoiled nuclei there is also electronic and nuclear interaction between the species. Both incoming and outgoing species lose energy with these interactions while travelling through the film. Together with collision kinematics the energy gives information on which depth the detected recoil originated. This however, adds a new requirement for the measurement setup.

Since the ions and atoms travelling through the sample lose energy, different elements originating from different depth can have the same energy and be therefore indistinguishable. The practical separation of the elements is realized by measuring both the energy and the velocity, or the time-of-flight (ToF), of the recoiled atom. Hence the different masses are separated by simply using the equation for kinetic energy E_k

$$E_k = \frac{1}{2}mv^2 \rightarrow m = \frac{2E_k}{v^2} \tag{12}$$

where v is the velocity. This separation of different masses can be seen in Fig. 8 where the incident time-of-flight and energy events are plotted in a histogram.

4.1.3 Detecting hydrogen and its isotopes

Many elemental analysis techniques exist for thin films but only a few are sensitive to all the elements. Especially the light elements are often hard to detect. Electron binding energies of the light element atoms are so low that detecting them using photon or electron absorption or emission techniques is almost impossible.

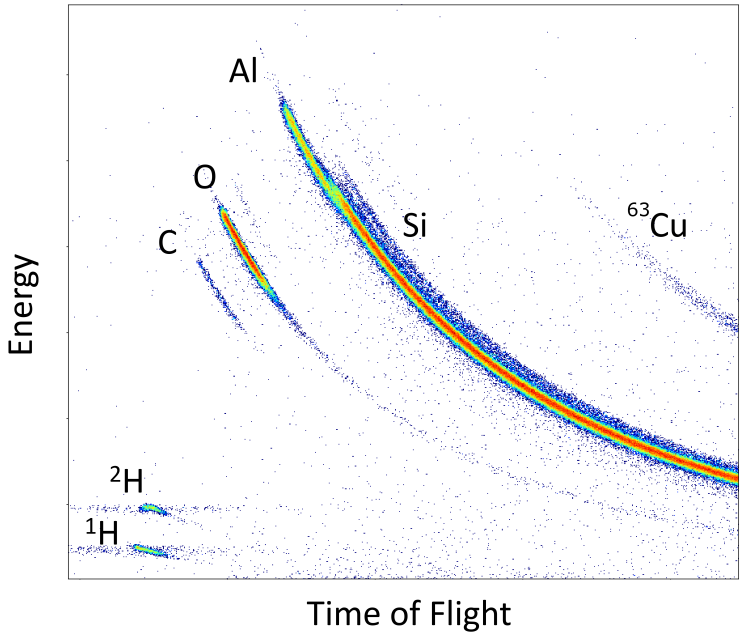

FIGURE 8 Time-of-flight–energy histogram of recoiled atoms of an Al_2O_3 film deposited with ALD on Si substrate. Scattered ^{63}Cu beam is also visible. Species are separated according to their masses. Adapted with permission from [PI], Copyright 2021, Elsevier.

Nuclear reaction analysis (NRA), that relies on nuclear reactions between target atoms and incident beam, can detect hydrogen. However, more straightforward techniques are the two forward recoiling techniques SIMS and ERDA. Especially the adaptation of time-of-flight elastic recoil detection analysis (ToF-ERDA) can easily detect all the elements down to hydrogen. Even more, ToF-ERDA can resolve different isotopes from each other depending on their mass. Different isotopes of the same element act chemically very similarly which makes separating them basically impossible with techniques relying on their electronic properties. Ion beam techniques, excluding particle induced X-ray emission (PIXE), are based on nuclear interaction. As the difference of the isotopes is in the their nuclei, ion beam techniques can be used to separate them in general.

4.1.4 ToF-ERDA measurements

ToF-ERDA measurements were conducted using 1.7 MV Pelletron tandem accelerator [125]. The elemental composition of all the Al_2O_3 samples (both temporal and spatial ALD), were measured using 11.915 MeV $^{63}Cu^{6+}$ beam with detecting angle ϕ of 41 $^\circ$ using mirror geometry. In the case of ZnO samples, incident ion was changed and measurements were done with 13.615 MeV $^{127}I^{7+}$ ion beam in order to avoid having two masses (^{63}Cu and ^{64}Zn) too close to each other. The elemental composition was then calculated with Potku analysis software [126]. The surface and interface regions were disregarded in the analysis and all the concentration values are measured from the bulk of the film. With ZnO samples

and $^{127}I^{7+}$ incident beam, analysis was done just below the surface in order to minimize multiple scattering effects.

Multiple scattering effects can lead to underestimation of heavy elements in the film [127]. The ERD analysis assumes that each detected recoil originates from a single nuclear collision. If the scattering cross section (Eq. 11) is high enough, the probability of an incident ion to scatter multiple times increases. With relatively low energy and high incident and recoil atomic masses, multiple scattering is not negligible. This results in detecting an recoil from a second scattering event to have less energy than expected. Therefore, in the analysis, it is interpreted to originate deeper in the sample than it is in the reality.

The ToF-ERDA system used to measure elemental compositions in this thesis utilizes gas ionization chamber (GIC) to measure the energy of the recoiled atoms. GIC detector has a relatively simple design and it has good energy resolution required to separate also the heavy elements. While gas ionization chamber has its benefits, there are some things that need to considered with lighter elements. In order to minimize multiple scattering, a light incident ion could be used. However, when the films contain deuterium, light incident ions can not be used. As seen in Supplementary Fig. 26, the signal from hydrogen and deuterium overlap if 10.215 MeV ^{35}Cl beam is used. The total energy of the incoming particle is only detected if it stops within the detector volume. Deuterium has a longer range due to higher energy compared to ^{1}H and does not come to the rest within active detector volume. As a result GIC catches only a portion of the actual energy, leading to overlapping TOF-E data as shown in Supplementary Fig. 26. This can be overcome by using lower energy or heavier incident ion which leads to a lower energy of the recoiled atom according to Eq. (10).

ERDA is also regarded as a non-destructive method. However, the incident beam can lead to desorption of volatile species from the sample such as hydrogen during a measurement [124]. This leads to a decrease in the concentration of the desorpted element within the film as the measurement proceeds. In order to get reliable results, the change in relative concentrations of the elements/isotopes must be recorded. If the measured elemental composition has changed during the measurement, it has been taken into account in the analysis.

4.2 Other characterization methods

4.2.1 Atomic force microscopy

Atomic force microscopy (AFM) gives information on surface morphology. A sharp tip at the end of an oscillating cantilever is moved in close proximity of the sample surface. If the surface has topographical changes the cantilever bends as the tip is moved over the surface. Bending of the cantilever is then monitored with a laser reflected from the back of the cantilever. The sample stage is operated by piezo elements so that the tip of the cantilever remains at constant distance

from the surface and the surface morphology is recorded by the piezo elements. By scanning the whole surface it is possible to produce precise topography of the surface. While lateral resolution depends on the sharpness of the tip, fraction of a nanometer vertical resolution can be achieved. The surface morphology of selected ZnO films were investigated with Bruker Dimension Icon atomic force microscope in the peak force tapping mode.

4.2.2 X-ray diffraction

Powder X-ray diffraction (XRD) can also be used to measure the crystallinity of thin films. Monochromatic X-rays, often produced by means of cathode tube such as Cu K_α radiation ($\lambda = 1.54189$ Å), are directed to the sample surface at an angle and the scattered X-rays are detected. Diffraction pattern emerge if the sample contains periodic crystal structure according to Bragg's law

$$2\,d\sin\theta = n\,\lambda \tag{13}$$

where d is the distance between the diffraction planes (i.e. atoms in the crystals), θ is the X-ray incident angle, n is an integer and λ is the the wavelength of the X-rays.

While the position of the diffraction peaks gives information on the crystal structure and orientation, it is possible as well to estimate the average crystal size from the width of the peaks with the Scherrer formula

$$\tau = \frac{K\lambda}{\beta\cos\theta}, \tag{14}$$

where τ is the average crystal size, K is a shape factor (close to 1) and β is the full width half maximum (FWHM) of diffraction peak in radians.

Crystallinity of ZnO films were investigated with Malvern Pananalytical X'pert Pro diffractometer with Cu K_α radiation (λ = 1.54187 Å via Ni β-filter; 45 kV, 40 mA). Data processing and search-match phase analyses were carried out using the program X'pert HighScore Plus v. 4.9 and ICDD-PDF4+ database (version 2020) [128, 129].

4.2.3 Helium ion microscopy

Helium ion microscopy (HIM) shares the basic principles of the scanning electron microscopy (SEM), but instead of electrons, a focused beam of helium ions is accelerated towards the sample surface. Similar to SEM, secondary electrons emitted from the sample are detected and used to produce the final image [130]. Due to the shorter de Broglie wavelength of the He ions compared to electrons, a smaller aperture can be used used resulting in significantly larger depth of field. Compared to electrons He ions also have a smaller excited volume resulting in sharper image. Furthermore, the He beam source is truly point like being in best case a single atom. The best reported resolution of HIM is 0.24 nm [131]. In addition, it is possible to image insulating samples with HIM without metallisation

that is required for the SEM imaging, as the positive charge build up from He ions can be compensated with electron flood gun.

Both Al_2O_3 and ZnO films deposited with temporal ALD were investigated with Carl Zeiss Orion NanoFab helium ion microscope using 30 kV helium ion beam. The samples were cleaved before imaging and tilted in order to see the cross section of the film.

4.2.4 Ellipsometry

Ellipsometry can be used to measure the thickness of transparent thin films. Ellipsometry utilises polarized light that is reflected from the film surface and interface at an angle. The change in polarization and phase is then detected. These two parameters are then converted trough model analysis to film thickness and refractive index. The GPC of both Al_2O_3 and ZnO films deposited with temporal ALD were determined by measuring the thickness of the films with Rudolph AUTO EL III ellipsometer using a 632.8 nm wavelength.

5 RESULTS

5.1 Temporal ALD of Al_2O_3

Aluminium oxide from TMA and H_2O has been considered as a model ALD reaction since the process produces good quality films over a large temperature range. The reactions of this process are thought to be well known as described in chapter 2.5.1. However, recent advancement and more thorough investigations have shown that the reaction between TMA and water is much more complex than what first reaction mechanism studies suggested. Therefore heavy water and oxygen-18 enriched water were used to study the hydrogen impurity incorporation in the films at varying deposition conditions.

Film thicknesses were measured with ellipsometer and the growth per cycle for the Al_2O_3 films as a function of temperature is shown in Fig. 9a. The GPC increases as a function of temperature as expected [32, 42, 50, 100]. The higher the temperature, more energy there is available for the reaction. Changing of the oxygen precursor to heavy water, ^2H_2O, decreases the GPC significantly, especially at low temperatures. This phenomenon is reported earlier for Al_2O_3 by Hiraiwa *et al.* [100] and for ZnO Guziewicz *et al.* [107] and it has been attributed to kinetic isotope effect as described earlier. On the other hand, Guerra-Nuñez *et al.* [82] and Vandalon *et al.* [41], for example, disregarded KIE when using heavy water. If the reaction goes to saturation (or very close to it) after each cycle all the available reactive sites should have been reacted. As the change in zero point energy between ^{1}H-O and ^{2}H-O goes up, the energy barrier increases and the reaction rate goes down according to Eq. 3. Not only are the reactions slower but the higher reaction barrier means that some reactions will not be able to proceed in the given temperature. The evidence of the increase in activation energy is supported by the fact that the GPC difference between the ^1H_2O and ^2H_2O processes decreases as the deposition temperature is increased. At higher temperatures there is more energy available for the reaction to proceed. If the ALD reactions are thought to be virtually irreversible, this means that the density of the O^{2}H-sites increases with temperature as more of the methyl groups are removed during the water

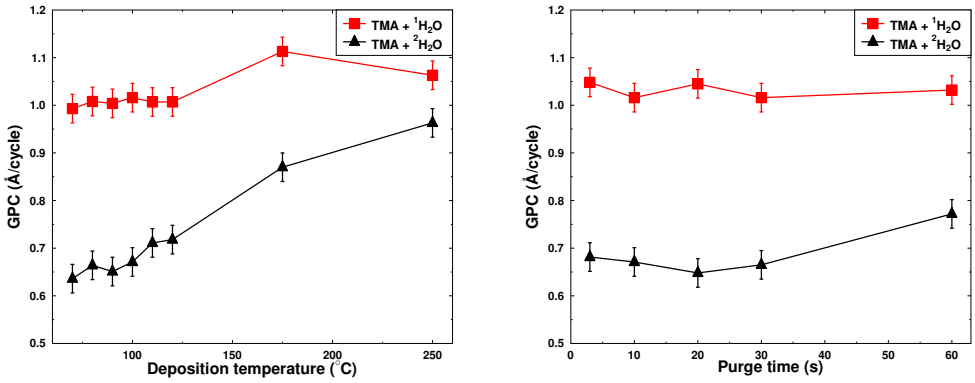

(a) (b)

FIGURE 9 a) Growth per cycle as a function of the deposition temperature. Films were deposited using 300 ms precursor pulses and 10 s N_2 purges between the pulses. b) Growth per cycle of the films deposited at 100 °C. Nitrogen purge was varied between 3 and 60 s. Reprinted with permission from [PI], Copyright 2021, Elsevier.

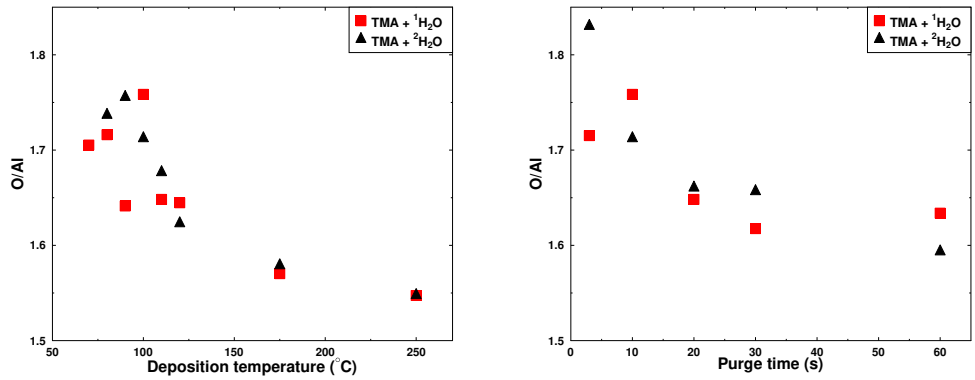

(a) (b)

FIGURE 10 a) O/Al ratio as a function of the deposition temperature. Samples were deposited using 300 ms precursor pulses and 10 s purging. b) O/Al ratio as a function of the purging time. Samples were deposited at 100 °C. Reprinted with permission from [PI], Copyright 2021, Elsevier.

pulse and the GPC increases.

With ^1H_2O the GPC starts to decrease between 175 and 250 °C as shown in Fig. 9a. This is an indication of the decrease of surface OH groups reported by [42, 57, 61]. Interestingly similar behaviour is not seen when heavy water is used. This could be due to the lower reactivity of the heavy water which might still be the growth limiting factor even at 250 °C.

The effect of purging time to GPC at 100 °C is shown in Fig. 9b. The purging time does not seem to affect the GPC significantly. Only when very long purging time of 60 s is used with ^2H_2O, there is a measurable increase in the GPC.

The ratio of the main components in Al_2O_3 is ideally 1.5. At low temperatures ALD-alumina films tend to be oxygen rich [82, 98, 99]. Similar results were obtained in our study. The stoichiometry of the films improve with increasing

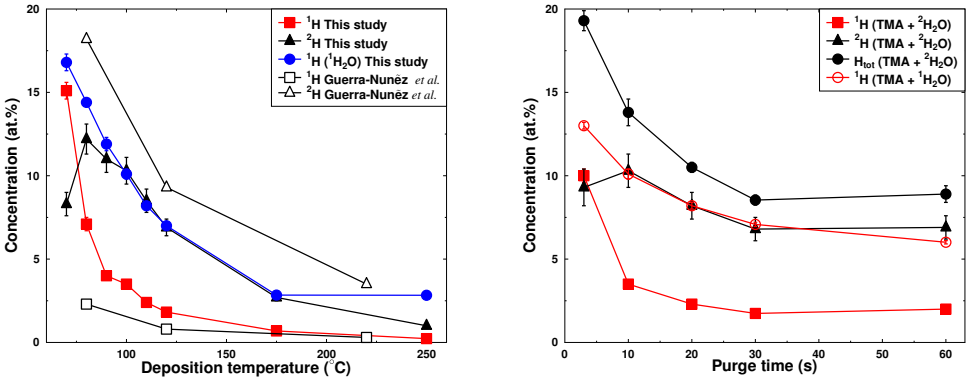

FIGURE 11 a) ^{1}H and ^{2}H impurity concentrations at different deposition temperatures. Films were deposited using 300 ms precursor pulses and 10 s purging times. Comparison to Guerra-Nunëz *et al*. [82] is also shown. b) ^{1}H and ^{2}H concentrations as a function of purge time. Deposited at 100 °C using 300 ms precursor pulses. Reprinted with permission from [PI], Copyright 2021, Elsevier.

deposition temperature and purging time as seen in Figs. 10a and 10b, respectively. Interestingly, the purging time has a significant effect on O/Al ratio while GPC stayed relatively constant. Similar trend is seen in Figs. 11a and 11b in the concentration of hydrogen and deuterium as a function of temperature and purging time, respectively. This shows, that while the films deposited at lower temperature or with short purging time have more impurities and have worse stoichiometry, the GPC remains the same. This will result into films with lower density. Films with O/Al ratio closer to 1.5 and with lower impurity concentration must therefore be denser. This has been measured and reported also by others [98,99].

This can be interpreted so that with longer purging, the reactions have more time to go to completion. Therefore the concentration of the reactive sites is higher after the long purging, which increases the intake of Al and O. In return, the impurity concentration decreases. On the other hand, when purging time is short, some unreacted species or by-products could be embedded in the film. This contributes to the film thickness so that measuring merely the GPC gives an impression that purging time does not have an effect on the film growth.

In Fig. 11a is shown the hydrogen concentration of the TMA + ^1H_2O process as well as the ^{1}H and ^{2}H concentrations of TMA + ^2H_2O process as a function of temperature. For comparison, the concentrations measured by Guerra-Nunëz *et al*. [82] are also included. For both waters the total hydrogen concentration increases with decreasing deposition temperature. These results are in good agreement with earlier research [82,98]. The total hydrogen concentration of the ^2H_2O process (not shown) is somewhat higher than with the ^1H_2O process but the trends are similar. Hiraiwa *et al.* [100] observed an increase in the total hydrogen deuterium concentration at 100 °C when heavy water was used, while Guerra-Nuñez *et al.* did not find any difference [82].

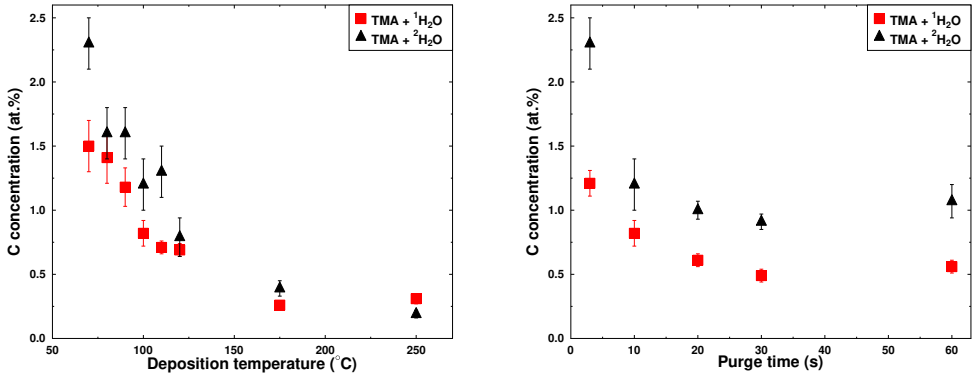

(a) (b)

FIGURE 12 a) Carbon concentration of films deposited at different temperatures using 300 ms pulses and 10 s purging times. b) Carbon concentration as a function of purging times, films were deposited at 100 °C using 300 ms pulses. Reprinted with permission from [PI], Copyright 2021, Elsevier.

When deposition temperature is 80 °C or above, the main hydrogen impurity in the films is ^{2}H originating from water precursor. When the deposition temperature is decreased to 70 °C, the concentration of ^{2}H suddenly starts to decrease and the concentration of ^{1}H to increase rapidly. Similar phenomenon is visible in Fig. 11b in which hydrogen and deuterium concentrations are plotted as a function of purging time. When the purging time is decreased to 3 s the main hydrogen impurity changes from deuterium to hydrogen. This indicates that the change of the major hydrogen isotope in the film relates to the slowness of some reactions. A sufficient purging time is required to produce films with higher deuterium concentration than hydrogen concentration, and this seems to be temperature dependent. Guerra-Nunẽz *et al*. [82] did not see such a change in the major hydrogen isotope seen by us and shown in Fig. 11a. They observed that deuterium is the main impurity hydrogen isotope in all the deposition temperatures. Guerra-Nunẽz *et al*. used very long purging times, 60 s, which might explain the discrepancy between the data. In addition, their process contained a separate 2 s exposure time after the precursor pulses. These remarks clearly show that not only the temperature plays a significant role in impurity incorporation but also the purging time is as important.

When depositing temperature of TMA + ^2H_2O was decreased further to 60 °C (not shown) clear signs of CVD-like growth were detected. This indicates that the purging time of 10 s was not sufficient. This kind of behaviour is often attributed to physisorption or condensation of multiple layers of precursor at low temperatures, as conceptualized in Fig. 2 or if the purging is not sufficient at given temperature as shown in Fig. 4b. While there are two possible precursors that can condensate on the substrate, water is often thought to be the more problematic precursor at low temperatures [98]. This conclusion is supported by the fact that no CVD-like growth was observed for the film deposited at 60 °C with normal water.

The increase of ^{1}H at low deposition temperatures could be due to the per-

sistent methyl groups detected by Vandalon and Kessels [41,42]. They concluded that when the deposition temperature is low, water is not reactive enough to remove all the methyl groups. This could also explain why the total hydrogen concentration is higher when heavy water is used. As heavy water has even lower reactivity than normal water, more persistent methyl groups are left in the film and buried in subsequent pulses. This should also lead to increased carbon concentration.

In Figs. 12a and 12b the carbon concentration in the films is plotted as a function of deposition temperature and purging time, respectively. The carbon concentration follows the trend of the ^{1}H concentration seen in Figs. 11a and 11b. The probable source of C and ^{1}H impurities are methyl groups that are buried in the film. However, if we look at the amount of ^{1}H originating from the TMA and compare it to the carbon concentration, we see that there should be significantly more carbon in the film if all the ^{1}H would be bound to methyl groups. Deposition with ^2H_2O yields to somewhat higher carbon concentration than deposition with normal water. This indicates that at least somewhat more methyl groups are buried in the film due to lower reactivity of heavy water. At low deposition temperatures, in which the ^{1}H is the main hydrogen isotope, there is much more ^{1}H in the film than what would be expected if it was in the form of methyl groups. This, however, changes and above 100 °C the ^{1}H/C ratio is well below 3.

The low amount of carbon at low deposition temperature remains unexplained. This puzzle was addressed by Vandalon and Kessels [41], who suggested that the persistent CH_3 groups could react in the subsequent cycles. According to their results the amount of persistent methyls at low deposition temperature should lead to significant carbon concentration. As discussed in the previous chapter, Sperling *et al.* [84] concluded that the reaction of H_2O with methyl groups has a coverage dependent reaction barrier. They believed that this explains the low carbon concentration as the reaction probability depends purely on the CH_3 coverage, not on if the methyl originates from the previous cycle. Another possible explanation for the low impurity carbon concentration could be etching of $HOAl(CH_3)_2$ during the water pulse phenomenon found by Werbrouck *et al.* [85].

However, none of these possible reactions do not explain the very high concentration of ^{1}H at low deposition temperatures and with short purging times.

5.2 Temporal ALD of ZnO

All the ZnO films were oxygen rich with O/Zn ratio varying between 1.33 and 1.09. The increase of the deposition temperature decreased the ratio, and at 200 °C close to stoichiometric films were deposited. These results suffer, however, from the multiple scattering due to relatively heavy ^{127}I incident beam and Zn recoils ($m_{Zn} = 65.38$). This leads to a small underestimation of Zn concentration [127] and therefore the true O/Zn value is slightly lower than reported. However, oxygen rich films have been reported before [86,101,132–134] and it is possible to tune the electrical properties of the ZnO by manipulating the stoichiometry of the films [132, 135]. The high O/Zn ratio has been attributed to oxygen interstitials [132], Zn vacancies [101] and to hydrogen that occupies Zn-sites [134,135].

The effect of using heavy water to GPC as a function of the deposition temperature is shown in Fig. 13a. At low deposition temperatures the GPC is significantly lower when heavy water is used instead of normal water. As the deposition temperature increases, the gap in GPC between the two processes decreases and at 200 °C the GPC is the same. The difference in GPC between the waters can be again explained by the kinetic isotope effect, which disappears as the temperature provides enough energy to overcome the reaction barrier. Figure 13a also shows that GPC starts to decrease when deposition temperature exceeds 150 °C. The maximum GPC at 150 °C is well documented and it is often contributed to the loss of surface OH groups at higher temperatures [48,61,87,96]. At high temperatures the concentration of surface OH groups starts to decrease during the purging and it becomes the limiting factor of the film growth. The behaviour is similar to the GPC of the Al_2O_3 (Fig. 9a) but it is more pronounced with ZnO.

The effect of purging time to GPC with ^2H_2O was studied at 60 °C. While purging time did not have any significant effect on the GPC in the case of Al_2O_3 at 100 °C, with ZnO there is a small but clear increase in the GPC with increasing purging time. This is quite opposite to the normal behaviour in which GPC is high with short purging times due to the CVD-like growth and then decreases until it reaches constant value with sufficient purging time as illustrated in Fig. 4b. In addition, Park *et al.* [136] observed almost a 30% decrease in GPC by increasing purging time from 20 s to 120 s at 170 °C. These contradictory results are explained by the different deposition temperatures and by the mechanisms that hinder the GPC at different temperatures. At 170 °C the desorption of OH groups decreases the number of reaction sites for DEZ and therefore the GPC as well. As purging time is increased, OH groups will have more time to desorp which leads to lower GPC. Whereas at 60 °C dehydroxylation is not significant and the GPC limiting factor seems to be the low and slow reactivity of precursors. Transient steric hindrance can also play a role as discussed later.

There is no sign of CVD-like growth with neither normal nor heavy water even at 30 °C or at 60 °C with very short purging times. This is in some contradiction with the results from Al_2O_3. The CVD-component in low temperature TMA + H_2O process is believed to be caused by adsorption of multiple layers

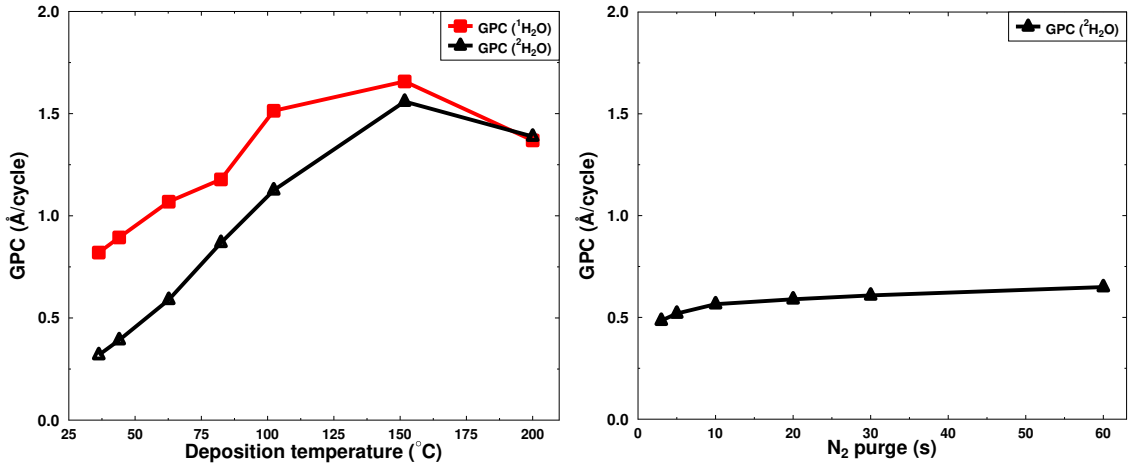

(a) (b)

FIGURE 13 a) Growth per cycle as a function of the deposition temperature. One ALD cycle consisted of 150 ms DEZ pulse, 10 s purge, 500 ms $^1H_2O/^2H_2O$ pulse and 20 s purge. b) Growth per cycle as a function of the purging time using DEZ and ^2H_2O as precursors at 60 °C. The purging times after the both precursors were kept the same when the purging time was 3, 5 or 10 s. For longer purging times only purge after ^2H_2O was increased and purge after DEZ was kept at 10 s. Reprinted with permission from [PII], Copyright 2021, MDPI.

of water. At low temperatures, the desorption rate of water is so slow that very long purging time is needed to remove the excess water. With ZnO this does not seem to be the case. At 60 °C even the 3 s purge times do not cause the GPC to increase rapidly. There are a few possible explanations. Firstly, it is possible that excess water is not the only cause for CVD-like growth, but it also depends on the metal precursor. Secondly, water desorption on ZnO surface is much faster than on Al_2O_3 surface. As DEZ is highly reactive towards water, it is unlikely that DEZ would not react with excess water if it is available.

Al_2O_3 films are amorphous in all deposition temperatures and can usually be crystallized only by post-deposition annealing at very high temperatures [80]. Quite the opposite is true for the ZnO films deposited with DEZ and water. They are polycrystalline even at very low deposition temperatures [26,86,87].

In order to confirm that crystallinity of the films is preserved regardless of the water used, characterization techniques XRD, AFM and HIM were used to study the crystallinity and surface morphology of the films. The XRD patterns of selected films deposited with both normal and heavy water are shown in Fig. 14. The diffraction peaks show that the ZnO films have wurtzite crystal structure in all temperatures but the preferred growth orientation changes. At 40 and 60 °C the preferred orientation is (002) when normal water is used. The preferred orientation changes to (100) when the deposition temperature is increased. The crystallinity e.g. the diffraction peak height is lower for films deposited using ^2H_2O. This is at least partly due to the lower thickness of the films deposited with heavy water. However, similar change in preferred orientation is visible with both waters, although the transformation happens at somewhat higher tem-

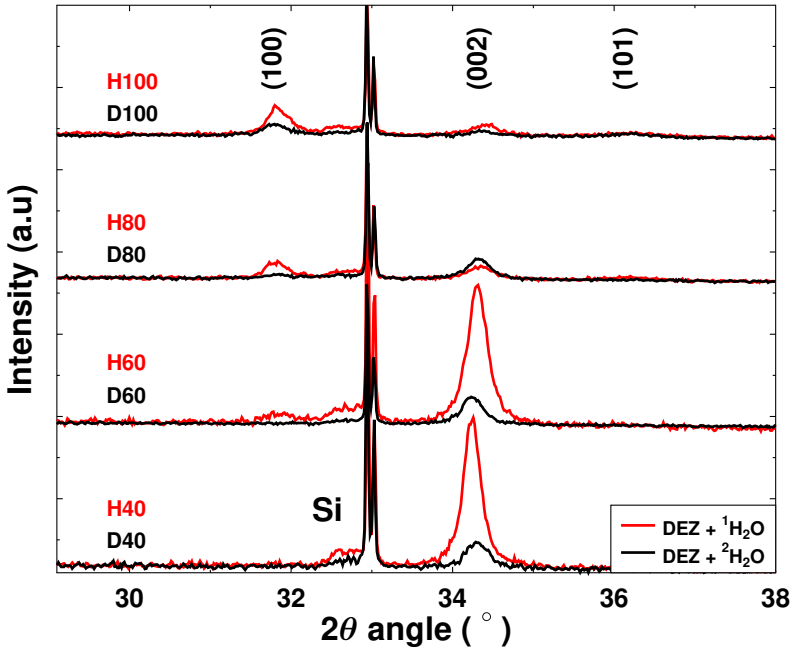

FIGURE 14 XRD patterns of selected ZnO films deposited at different temperatures with both ^1H_2O (red) and ^2H_2O (black). Films deposited with ^2H_2O are thinner than the films deposited with ^1H_2O, which affects the peak intensity. Double peak at 33° originates from the silicon substrate. Reprinted with permission from [PII], Copyright 2021, MDPI.

perature with heavy water. This is in line with the discussion of kinetic isotope effect. The average crystalline size according to Scherrer formula eq. (14) is for (002) oriented crystals 21–34 nm and 27–28 nm for the (100) crystals. The crystalline size of (002) orientation decreases with deposition temperature. There is no significant difference in average crystal size between samples deposited with the two waters.

The AFM micrographs in Fig. 15 confirm the change in crystal orientation. Hints of the transformation are already visible 60 °C when normal water is used. In the case of heavy water, crystals with (100) orientation become visible at 80 °C. In addition, roughness data can be extracted from the AFM micrographs. The films with (100) preferred orientation have higher roughness compared to (002) oriented films. The film deposited with normal water at 100 °C has the highest roughness reaching root-mean-square (RMS) roughness of 9.2 nm The roughness of (002) oriented films varies between 3.6 and 4.6 nm.

In addition to XRD and AFM, HIM was used to image the cross sections of cleaved samples. The change in crystalline orientation is also visible in HIM images (Figs. 16a and 16b). The cross sectional images also confirm that the films are crystalline throughout the film.

The impurity hydrogen concentrations were studied at different deposition temperatures. Fig. 17a shows the ^1H and ^2H concentrations of heavy water process as well as ^1H concentration of normal water process. The hydrogen concentration increases with decreasing deposition temperature. With heavy water, both ^1H and ^2H concentrations increase with decreasing deposition temperature

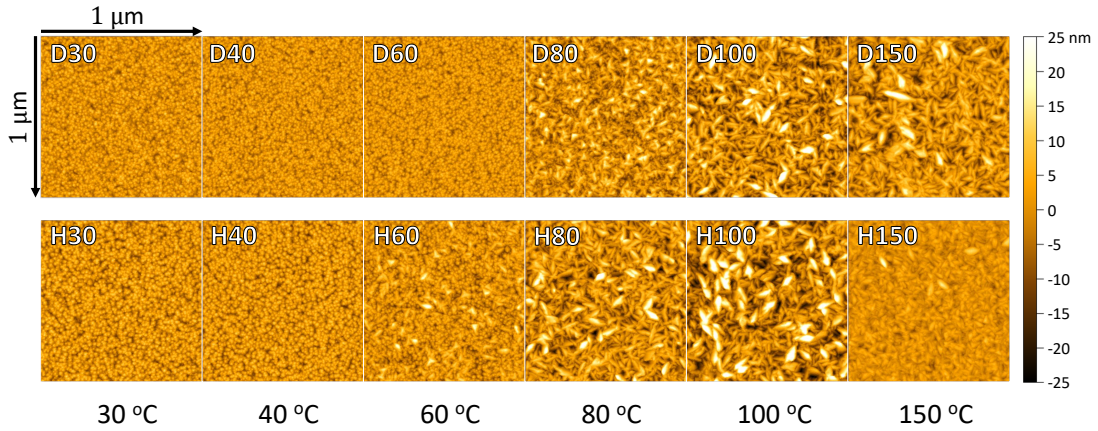

FIGURE 15 AFM micrographs of ZnO films deposited with DEZ and either $^{2}H_2O$ (upper) or $^{1}H_2O$ (lower) at different temperatures. Preferred crystal orientation changes as the temperature is raised. Length of the side in each image is 1 μm. Reprinted with permission from [PII], Copyright 2021, MDPI.

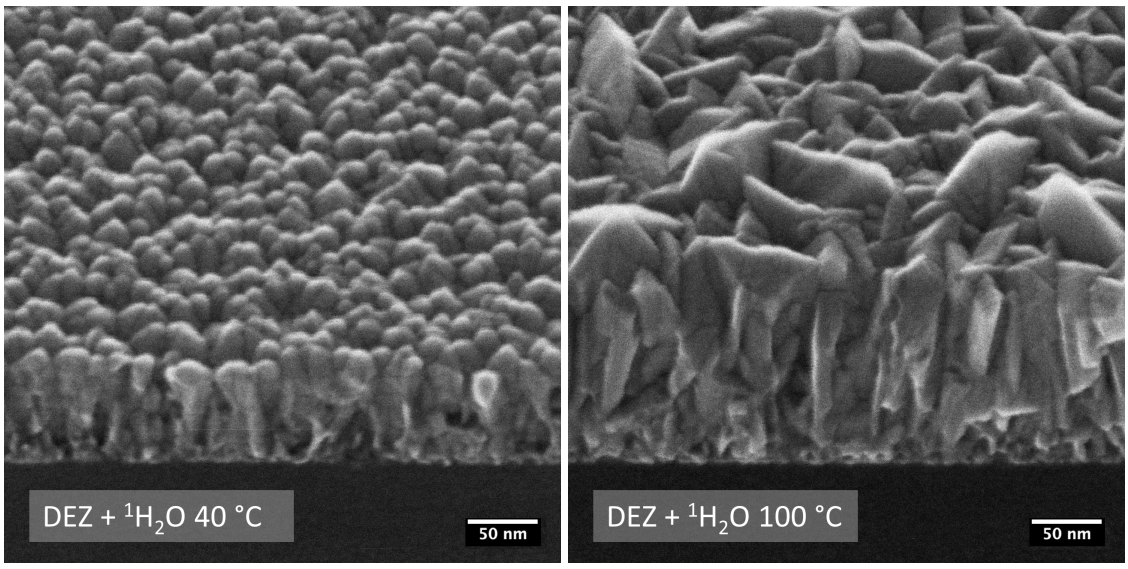

(a) (b)

FIGURE 16 Cross-sectional HIM images of ZnO films deposited with normal water at a) 40 °C and b) 100 °C. The cleaved samples are imaged at a 45° angle relative to the beam. Reprinted with permission from [PII], Copyright 2021, MDPI.

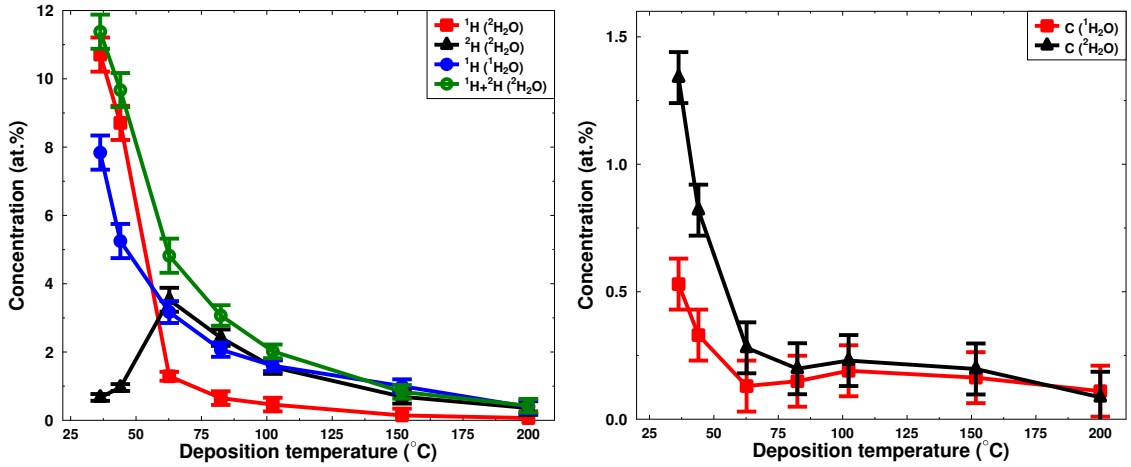

(a) (b)

FIGURE 17 a) Hydrogen isotope and b) carbon concentration of the films deposited at different temperatures using 150 ms DEZ and 500 ms ^1H_2O or ^2H_2O pulses. In a) red and black denote the ^1H and ^2H concentrations when heavy water was used, respectively, and green is the sum of the two isotopes. Blue is the ^1H concentration when normal water was used. Purging times after DEZ and water pulses were 10 and 20 s, respectively. Reprinted with permission from [PII], Copyright 2021, MDPI.

until the the temperature goes below 60 °C. Below 60 °C, the amount of ^2H in the film drops dramatically, while the concentration of the ^1H goes rapidly up. This behaviour looks very similar to Al_2O_3 process in Fig. 11a. However, with Al_2O_3 the change in major hydrogen isotope in the film was quickly followed by the CVD-like growth. As mentioned earlier and shown in Figs. 13a and 13b, there is no CVD-like growth with ZnO. Therefore the change of major impurity hydrogen isotope does not seem to directly relate to the CVD-like growth.

The similarity between the results of the two materials is somewhat surprising even though the precursors and idealised reaction mechanisms are very similar. The fact that Al_2O_3 films are amorphous and ZnO films are polycrystalline does not seem to play any major role in hydrogen incorporation. One possible explanation is that ZnO films contain amorphous regions which are hydrogen rich. There is evidence of this kind of behaviour for In_2O_3 films [113]. The HIM images in Figs. 16a and 16b do not show any clearly amorphous regions but this explanation remains possible. As mentioned earlier, hydrogen might also occupy Zn-sites [134, 135].

Guziewicz *et al.* deposited ZnO from DEZ and ^2H_2O and they reported similar, although somewhat lower ^1H and ^2H concentrations for ZnO films deposited between 100 and 200 °C [107]. In their study they also found out that deuterium is the major isotope in all studied temperatures. Xia *et al.* however report the opposite. They also observed that in all temperatures between 100 and 300 °C the ^1H concentration was higher than ^2H concentration [109]. In our study this was only seen when deposition temperature was low or the purging time was short. Interestingly Xia *et al.* used long 30 s purging times, which contradicts

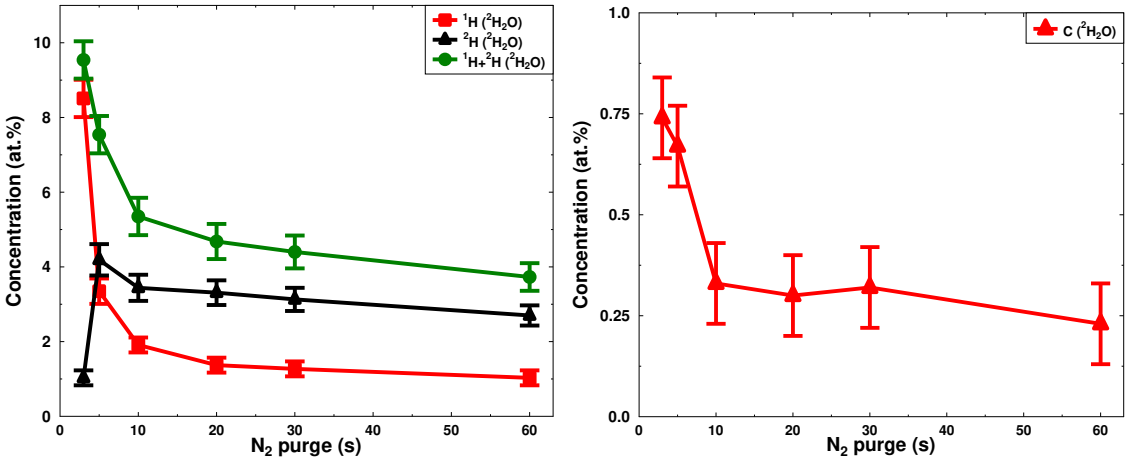

(a) (b)

FIGURE 18 a) Hydrogen and b) carbon concentration as a function of the N_2 purge time. All the samples were deposited at 60 °C using 150 ms DEZ pulses and 500 ms ^2H_2O pulses. Purging time between the pulses was varied. The purging times after both precursors were kept the same if the purging time was 3, 5 or 10 s. For longer purging times only the purge after ^2H_2O was increased and the purge after DEZ was kept at 10 s. Reprinted with permission from [PII], Copyright 2021, MDPI.

with our findings. It must be noted that Xia *et al.* used short (15 ms) DEZ pulses and deposited only few tens of cycles compared to our 150 ms DEZ pulses and 1000–1400 cycles. These differences could possibly explain the discrepancy.

As in the case of Al_2O_3 with the persistent methyls, persistent ethyl groups could explain the high ^1H concentration at low deposition temperatures. Persistent ethyls were experimentally detected by Mackus *et al.* [95] and computationally predicted by Weckman and Laasonen [49]. In Fig. 17b is plotted the carbon concentration of the films as a function of the deposition temperature. The effect of the temperature and the use of heavy water are very similar to the behaviour of the hydrogen incorporation. However, if it is assumed that ^1H impurities would be embedded in the film as an unreacted ethyl groups (C_2H_5), there should be 2.5 ^1H atoms per one carbon atom. If we compare the concentrations of ^1H and carbon at low temperature or with short purging in Figs. 17a and 17b, it is clear that there is much more ^1H than what would be expected. At 100 °C the $^1H/C$ ratio is exactly 2.5 but above that, the ratio is actually below the expected 2.5. This behaviour is very similar to what was observed with Al_2O_3. It is possible that ethyl groups can react with water in subsequent cycles, but again, the definitive explanation behind the relatively high ^1H concentration at low temperature remains unknown.

The effect of purging to impurity hydrogen and carbon concentration is shown in Figs. 18a and 18b, respectively. A low deposition temperature of 60 °C was selected in order to increase the impurity concentrations and emphasize the effect. Longer purging time reduces both hydrogen and carbon incorporation significantly. When the purging time is decreased to 3 s, the main hydrogen isotope changes from deuterium to hydrogen. This resembles the effect of decreasing de-

position temperature and is identical to what was found for Al_2O_3 in Fig 11b. Therefore, this effect must be a result of a slow reaction that goes to a completion only with very long purging times resulting in ^2H rich films. The carbon concentration as a function of purging time follows the ^1H concentration (Fig. 18b). However, independent of the purging time, the ^1H concentration is still higher than what would be expected if the hydrogen would be bound solely to ethyl groups.

As mentioned earlier, the increase of GPC with increasing purging time contradicts with the assumption of steady GPC once sufficient purging time is reached. In order to get more information on the effects of purging, unsymmetric purging test was done. Depositions at 60 °C were made with 3-3 s, 3-10 s, 10-3 s and 10-10 s purging times after DEZ and water pulses, respectively. The hydrogen and deuterium concentrations with different purging schemes are shown in Fig. 19a. Interestingly the change of the purging from 3-10 s to 10-3 s does not have any significant effect on deuterium or hydrogen concentration, although 10-3 s purging produces a little higher ^2H and a little lower ^1H concentrations. A more important factor seems to be the total purging time. It is surprising that longer purging time actually increases the absolute concentration of ^2H, but the reason behind it remains unknown. When it comes to the GPC with different purging times (Fig. 19b), the total purging time seems to be the most significant factor. Similar to our previous results in Fig. 13b, the longer the purging time is, the higher the GPC is.

Longer purging clearly effects the growth of the film as films with long purging times have less impurities and higher GPC. On the other hand, long purges decrease the growth rate even if the growth per cycle is higher. In order to study the possible transient steric hindrance proposed by Wang *et al.* [137], films with multiple short pulsing (MSP) were deposited at 40 °C. Transient steric hindrance can be interpreted as steric hindrance due to slow reactions and desorption of reaction products from the surface which temporarily block reaction sites. Likewise, Muneshwar *et al.* reported an increase of GPC by dividing the metal precursor pulse into multiple short pulses [138]. They contributed the higher GPC to the removal of ligands between the pulsing sequence. As the reaction advances between the short pulses, previously blocked reaction sites are revealed and can react further.

Impurity ^1H and ^2H concentrations of MSP depositions are shown in fig. 19c. The use of the MSP slightly increases the ^1H concentration but did not have significant effect on the ^2H concentration. However, the GPC increased over 35 % when MSP was used with both precursors. Although impurity concentrations slightly increase with MSP, this is a significant increase in throughput, since the total cycle time does not change.

The increase of GPC with MSP indicates that something is blocking reactive sites during precursor pulsing. From our data it is not possible to conclude if it is the physisorpted but unreacted DEZ molecules that desorp later without reacting or the ethane by-products that are not yet desorpted from the surface. Both of these may play a role as the MSP of only one precursor slightly increases the GPC

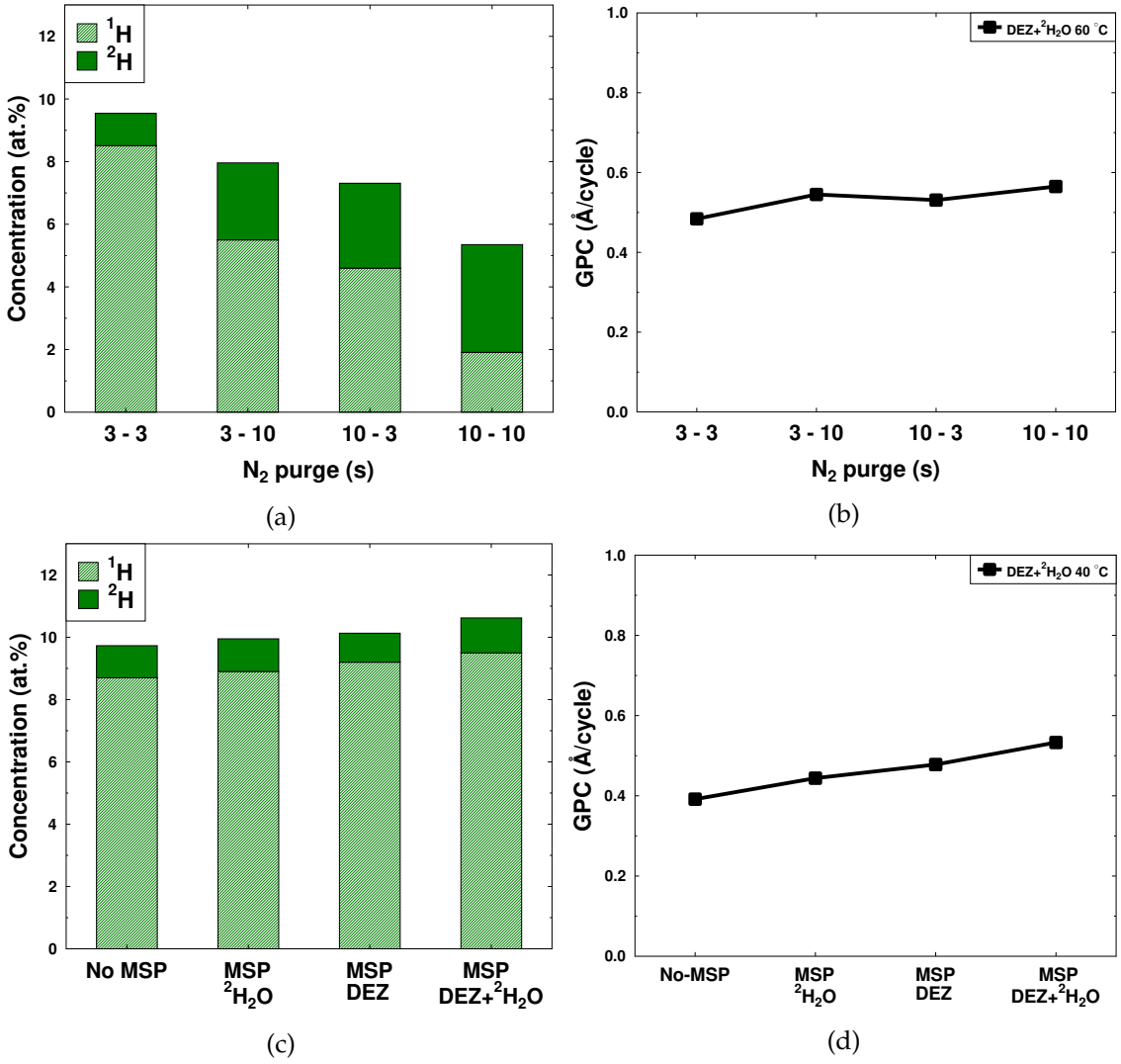

FIGURE 19 a) Hydrogen and deuterium concentration with different N_2 purge schemes deposited at 60 °C. b) Growth per cycle with different N_2 purging schemes deposited at 60 °C. c) Hydrogen and deuterium concentration when multiple short pulsing (see text) was used at 40 °C. d) Growth per cycle using multiple short pulsing at 40 °C. Reprinted with permission from [PII], Copyright 2021, MDPI.

in both cases.

5.3 Spatial ALD of Al_2O_3 and ZnO

The merit of SALD is the speed of depositing the films. As demonstrated earlier in the thesis, shortening the purging time often change the film composition with conventional ALD. The short purging time of the SALD is often justified by the lack of large reactor space that needs to be purged properly before the next precursor pulse and is of no concern. The effect of fast deposition speed to GPC and impurity corporation was studied with both normal and heavy water. The film quality must reflected to the throughput of the process which in the case of spatial ALD is even more important than actual GPC.

The film thickness of SALD Al_2O_3 and ZnO films as a function of deposition temperature are shown in Figs. 20a and 20b respectively. The films were deposited using a substrate rotation speed of 10 rpm. The thickness is estimated from ToF-ERDA depth profiles since the flexible substrate prevented thickness measurements with ellipsometry. Therefore the thicknesses of SALD samples are given as 1×10^{15} at./cm^2 which roughly corresponds to 1 Å in the case of Al_2O_3 and 1.2 Å in the case of ZnO if literature values for densities are assumed. Due to the surface roughness and multiple scattering effects, especially with ZnO films measured with ^{127}I ion beam, the thickness measurement of the films suffers from inaccuracy. However, the results are comparative.

The GPC of the Al_2O_3 stays mostly unchanged from 80 to 140 °C. This is in good agreement with the results with conventional ALD in Fig. 9a. When deposition temperature is decreased to 60 °C the GPC of TMA+^1H_2O quickly doubles and the TMA+^2H_2O did not produce a proper film at all. This is due to CVD-like growth, similar to conventional ALD Al_2O_3. The GPC of Al_2O_3 follows the effect of short purging time presented in Fig. 4b and increases with decreasing purging time as the the CVD-like growth becomes viable. The thickness of Al_2O_3 film at 60 °C was also far from uniform. Very high GPC of Al_2O_3 can also be a result of TMA underdosing reported by Salami *et al.* [139]. However, the behaviour of the GPC is very similar to what was detected with conventional ALD and is most probably due to CVD-like growth. In the case of ZnO, there is an increase in the GPC with increasing temperature until 120 °C. At 140 °C the GPC starts to decrease. The GPC decreased also with the conventional ALD once the temperature was increased enough, but that happened only after 150 °C. If the decreasing of the GPC is due to desorping OH groups, as reported in several studies [42, 57, 61, 96], the relatively high nitrogen flow of SALD reactor may reduce the hydroxyl concentration leading to a lower than expected GPC. In addition, Nelson *et al.* reported that the exposure/purge time can change the temperature of maximum GPC [140].

Increasing the rotation speed of SALD reactor with fixed precursor and purging inlets decreases both the precursor exposure time and inert gas purg-

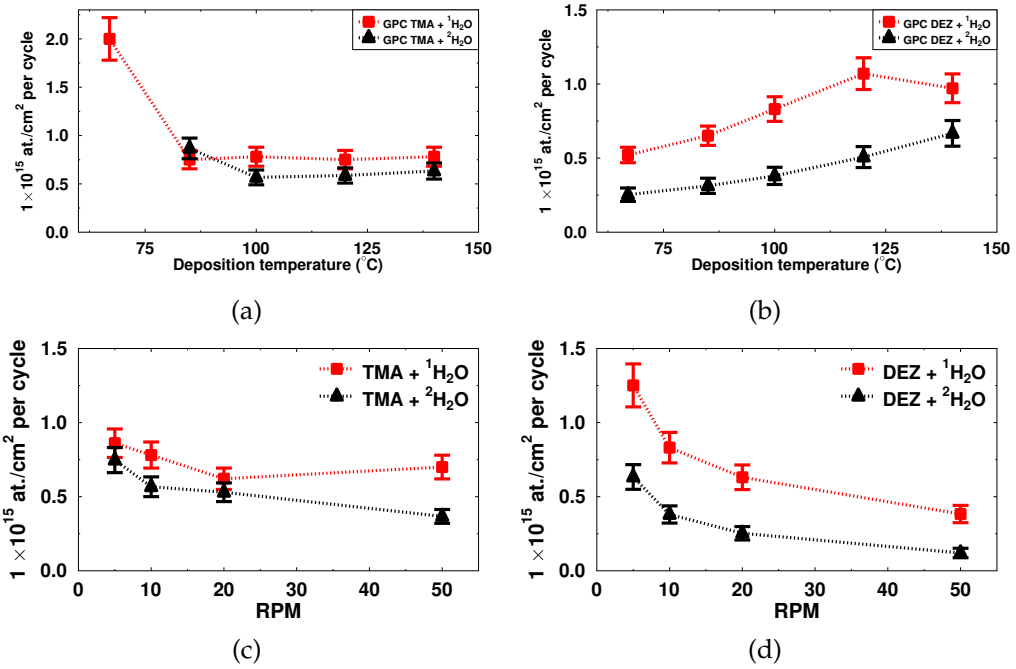

FIGURE 20 Growth per cycle evaluated from the ToF-ERDA depth profiles. GPC of a) Al_2O_3 and b) ZnO as a function of deposition temperature. The sample rotation speed was held at 10 rpm for all the samples. The GPC as a function of the substrate rotation speed at 100 °C for c) Al_2O_3 and d) ZnO. Reprinted with permission from [PIII], Copyright 2022, Elsevier.

ing. Therefore, insufficient precursor exposure can decrease the GPC (Fig. 4a) while too short purging can lead to uncontrolled CVD-like growth (Fig. 4b). In Figs. 20c and 20d the GPCs of Al_2O_3 and ZnO films are shown with different substrate speeds ranging from 5 to 50 rpm at 100 °C. The GPC of Al_2O_3 somewhat decreases with increasing rotation speed e.g. shorter precursor exposure and purging time. In the case of ZnO, slowing down the rotation increases the GPC more significantly. This might be due to the increased exposure time, but as demonstrated with conventional ALD in Fig. 13b, also the purging time plays a role on how much ZnO film is deposited in one cycle.

Even though the GPC decreased with the increasing rotation speed, the throughput, or the growth rate of the Al_2O_3 films deposited with ^1H_2O increase from 0.22 to 1.75×10^{15} at/cm^2 per second when the rotation speed is increased from 5 to 50 rpm. Similarly, ZnO growth rate (with ^1H_2O) increased from 0.31 to 0.92×10^{15} at/cm^2 per second. Because the consumption of precursors is continuous the faster deposition does not only save time but also possibly expensive precursors. Therefore, accessing higher throughput by faster rotation can be tempting for industrial applications but it comes at a cost of higher impurity concentrations as discussed below.

The SALD depositions at low temperature and/or with short purging or fast rotation replicate the results from conventional ALD. The low temperature CVD-like growth of Al_2O_3 is absent with ZnO. This confirms that the onset temperature of CVD-growth is dependent either on the metal precursor or the desorption rate

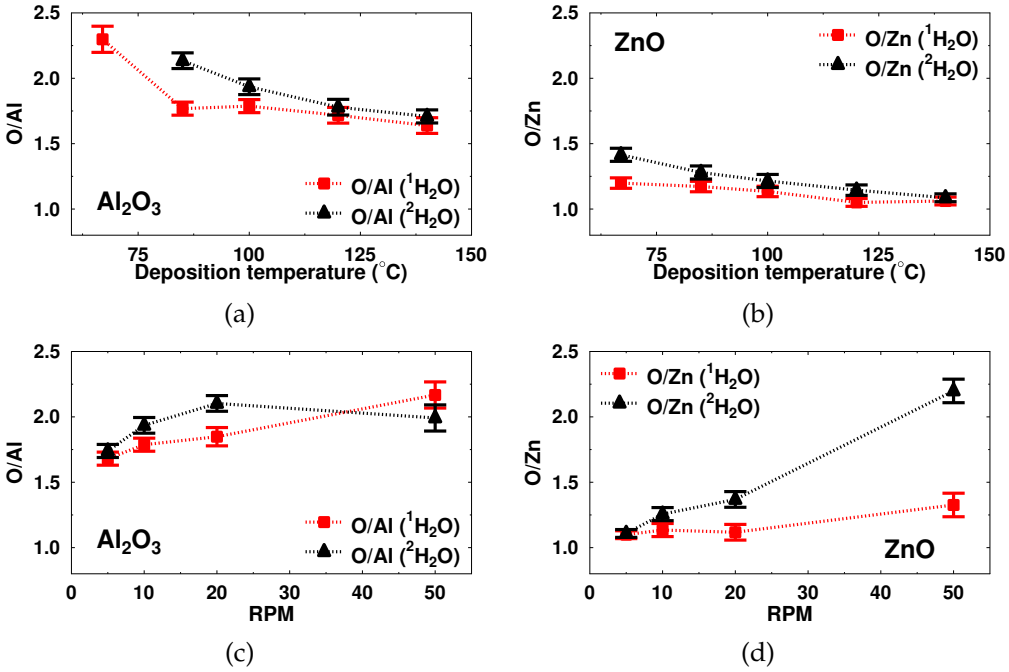

FIGURE 21 Ratio of a) O/Al and b) O/Zn as a function of deposition temperature. The rotation speed was kept at 10 rpm. Ratio of c) O/Al and d) O/Zn as a function of rotation speed. The deposition temperature was kept at 100 °C. Reprinted with permission from [PIII], Copyright 2022, Elsevier.

of water is faster on ZnO than Al_2O_3 surface. The kinetic isotope effect is also visible with SALD and the GPC of heavy water processes for both Al_2O_3 and ZnO is lower than with normal water. Kinetic isotope effect seems to decrease GPC of the ZnO somewhat more than of the Al_2O_3.

The rotation speeds from 5 to 50 rpm corresponds to precursor exposure times of 46 ms at 50 rpm to 458 ms at 5 rpm. While the exposure time is short at 50 rpm, there are reports of much faster depositions. For example, Nandakumar *et al.* demonstrated SALD of ZnO from DEZ and H_2O with exposure time as low as 8 ms [141]. Reflecting on that, even our shortest exposure time of 46 ms should be sufficiently long.

All the samples, both Al_2O_3 and ZnO were oxygen rich as seen in Figs. 21 a–d. Both increasing the deposition temperature and decreasing the rotation speed produce more stoichiometric films. Multiple scattering in ToF-ERDA leads again to a slight underestimation of Zn, which results in higher than actual O/Zn ratio. However, ZnO films deposited at low temperature and with high substrate rotation speed are clearly oxygen rich. The films deposited with heavy water tend to have slightly higher oxygen content than the ones deposited with normal water but only the ZnO films deposited with ^2H_2O at high sample rotation speeds differ significantly from their normal water counterparts. ALD Al_2O_3 films tend to be oxygen rich [82, 98, 99] which is in line with our results. According to our results with temporal ALD the oxygen concentration seems to go up hand in hand with the hydrogen concentration. High oxygen concentration would implicate that a lot of O^2H groups are buried in the film as proposed by Guerra-Nuñes *et al.* [82].

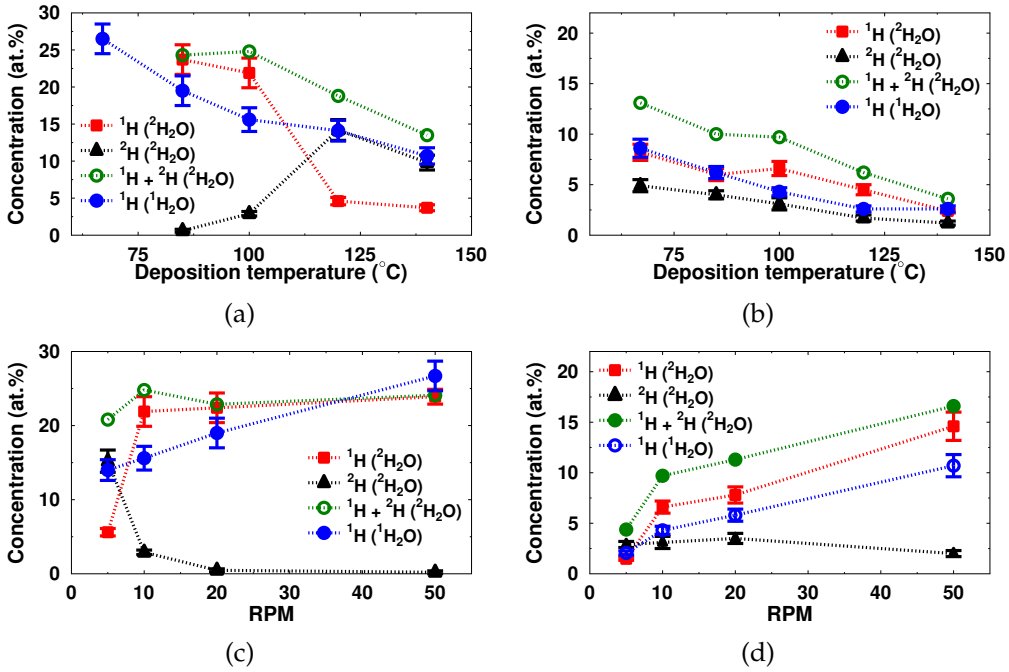

FIGURE 22 ^1H and ^2H concentration of the films as a function of deposition temperature. a) Al_2O_3, b) ZnO. Substrate rotation speed was kept at 10 rpm. ^1H and ^2H concentration of the films as a function of rotation speed deposited at 100 °C. c) Al_2O_3, d) ZnO. Reprinted with permission from [PIII], Copyright 2022, Elsevier.

The hydrogen and deuterium concentrations of SALD Al_2O_3 films deposited with both normal and heavy water are shown in Fig. 22a as a function of the deposition temperature. With both waters, the total hydrogen concentration decreases with increasing deposition temperature. The total hydrogen concentration is somewhat higher with ^2H_2O. Between 100 and 120 °C the major hydrogen isotope in the film changes from ^1H to ^2H. This clearly follows a similar trend to films deposited with conventional ALD. With conventional ALD the change of the major hydrogen isotope occurred between 70 to 80 °C as seen in Fig. 11a. However, as pointed out earlier, the purging time affects the hydrogen isotope incorporation (Fig. 11b) and the purging times are much shorter with spatial ALD compared to conventional ALD. Therefore, the higher temperature where ^1H becomes dominant hydrogen isotope, is not a surprise.

In the case of ZnO in Fig. 22b, ^1H stays the main hydrogen isotope in all studied temperatures. The total hydrogen concentration with both waters decreases with deposition temperature, as expected. It is possible that for ZnO the purging time e.g. the rotation speed of 10 rpm is too high to see the change of the hydrogen isotope. It can be thought that films with higher ^2H than ^1H concentration are grown at more ideal conditions. This is supported by the conventional ALD results where ^1H is the major isotope when the deposition temperature is low or the purging time is short. Films with high ^1H concentration also have low GPC. Reflecting on these conclusions, deposition conditions of SALD ZnO seem to be out of the ideal zone.

The hydrogen incorporation at 100 °C as a function of the sample rotation speed are shown in Figs. 22c and 22d for Al_2O_3 and ZnO, respectively. Again, increasing the rotation speed increases the hydrogen concentration and using heavy water results in higher total hydrogen concentration. For the both film materials ^2H becomes the main hydrogen isotope when the rotation speed is decreased to 5 rpm. For rotation speeds higher than that, films contain more ^1H than ^2H. If the higher ^2H than ^1H concentration is considered as a measurement for ideal ALD reaction as discussed above, rotation speeds higher than 5 rpm at 100 °C are not desired. The effect of the shorter exposure time can not be totally excluded but as shown in Figs. 11b and 18a, sufficient purging time is required to produce films with ^2H being the main isotope.

The high O/Al and O/Zn ratios do not result in as high ^2H concentrations as would be expected if the OH groups would be buried into the film. Similarly to the conventional ALD, also the carbon concentrations of the SALD films do not match with the prediction of buried methyl and ethyl groups when the ^1H concentration is high. The carbon concentration of Al_2O_3 films range from 1.1 to 2.9 at.% and of the ZnO films from 0.7 to 2.8 at.%. For both Al_2O_3 and ZnO the $^1H/C$ ratio is well above the 3 and 2.5, respectively, when deposition temperature is 100 °C or below.

5.4 Kinetic isotope effect on hydrogen concentration

Some ALD studies with heavy water have disregarded the kinetic isotope effect (KIE) which decreases the zero point energy of a bond and therefore decreases the reaction rate as described in Section 2.6. However, our results show that KIE has a significant effect on film composition and GPC. The O/Al and O/Zn ratios of the films, were somewhat oxygen rich with both materials when heavy water was used. Similarly the impurity carbon and total hydrogen concentrations were somewhat higher with heavy water. The most notable difference was in the GPC for both materials as the GPC decreased when heavy water was used. This is emphasized at low deposition temperatures as seen in Figs. 9a and 13a. The gap in GPC between the waters diminishes when there is enough energy for $^1H_2O/^2H_2O$ to overcome the reaction barrier.

In the case of impurity incorporation, the use of heavy water can be regarded as a temperature shift. The effect of using heavy water to total hydrogen concentration is illustrated in Figs. 23a and 23b. The x-values e.g. the temperature of the total ^1H + ^2H concentration of the ^2H_2O process is shifted by 15 °C towards lower temperatures. As a result, the total hydrogen concentration of both water processes matches almost perfectly. This means, that when the results from heavy water processes are compared with the typically used normal water, a temperature shift of roughly 15 °C must be considered for both Al_2O_3 and ZnO. However, it must be noted that some properties, such as crystallinity suffer from the use of heavy water more than by just a simple shift in temperature as showed

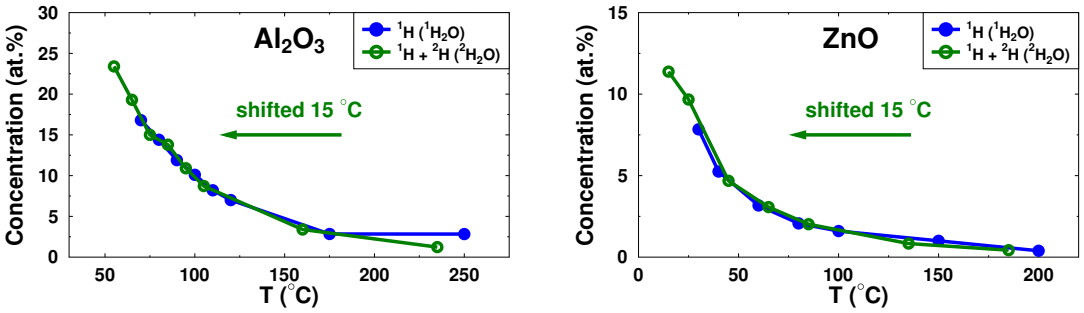

(a) (b)

FIGURE 23 The x-axis of total ^{1}H + ^{2}H concentration of heavy water process (green) is shifted to the lower temperature by 15 °C and it matches with the ^{1}H concentration of the normal water process.

in Fig. 14.

While normal and heavy water have been used as interchangeable precursors in ALD reaction mechanism studies, our results with typical process parameters show that the kinetic isotope effect is something to be considered. On the other hand, when a temperature shift is taken into account, the use of heavy water is well justified in ALD chemistry studies.

5.5 Hydrogen migration

During the studies it was quickly discovered that the deuterium concentration in the films changes if the samples are stored in ambient environment between the deposition and the ToF-ERDA measurements. To avoid this, the as-deposited samples were stored in a vacuum between the deposition and measurements in order to ensure that the composition would not change. We also verified that the vacuum storage did not affect the film composition by measuring samples from the same deposition before and after the vacuum storage.

In order to study this more closely, as-deposited Al_2O_3 films were kept 24 h at 60 °C in 80 % relative humidity (RH). Fig. 24a presents the elemental depth profile of as-deposited Al_2O_3. After the treatment in climate chamber (Fig. 24b) the ^{2}H concentration has decreased dramatically while ^{1}H concentration increased equally. The total amount of hydrogen isotopes presented in green in Figs. 24a and 24b remains almost unchanged even though the concentrations of hydrogen isotopes change significantly.

It is known [44, 106] that ALD Al_2O_3 contain OH groups and as Guerra-Nuñes *et al.* concluded, hydroxyl groups are embedded into the film as impurities. Since deuterium in the films originates from water, it is an easy assumption to make that at least majority of the deuterium is bound to oxygen atoms. In addition, films are oxygen rich as shown in Fig. 10 which suggest that extra oxygen might be in the form of OH groups. In order to study if only the deuterium atoms migrate through the film, or does the whole OH groups move, Al_2O_3 films were

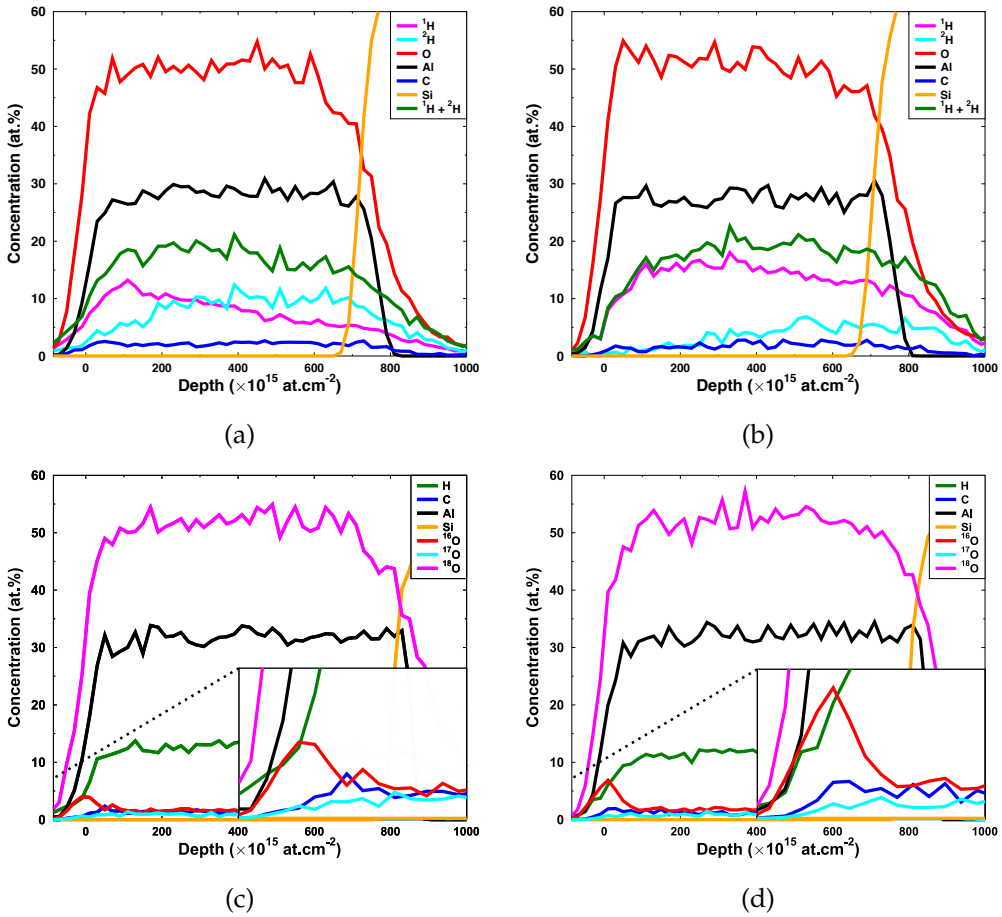

FIGURE 24 Elemental depth profiles of Al_2O_3 films deposited at 100 °C with 150 ms precursor pulses and 3 s purging. a) As-deposited film using TMA and ^2H_2O. The sample was kept at room temperature in air for one day before the characterization. b) The same film as in a) but after 24 h at 60 °C and 80 % RH. c) As-deposited film using TMA and $H_2^{18}O$. The sample was kept for one day at room temperature in air before the characterization. d) The same film as in c) but after 48 h in 60 °C and 80 % RH. Adopted with permission from [PI], Copyright 2021, Elsevier.

deposited using oxygen-18 enriched water, $^1H_2^{18}O$. An elemental depth profile of as-deposited film with $^1H_2^{18}O$ is shown in Fig. 24c. Most of the oxygen in the film is oxygen-18, as expected, and only a few atomic percent of oxygen-16 and oxygen-17 is present. Depth profile of the same film after a 48 h exposure in the climate chamber (60 °C and 80 % RH) in Fig. 24d shows that there is only a small increase in oxygen-16 concentration at the film surface and no other changes. Therefore it is easy to conclude that only $^1H/^2H$ migrates easily in the film.

Al_2O_3 films deposited at 100 °C were also stored in ambient conditions for prolonged period and measured again with ToF-ERDA after the storage. Similar decrease in ^2H and equal increase in ^1H concentration were detected with Al_2O_3 sample that had high initial total hydrogen concentration (Supplementary Fig 27). However, a sample with lower hydrogen concentration, deposited at the same temperature but with longer pulse and purging times, did not show any significant change in hydrogen isotope concentrations even after 5 months of

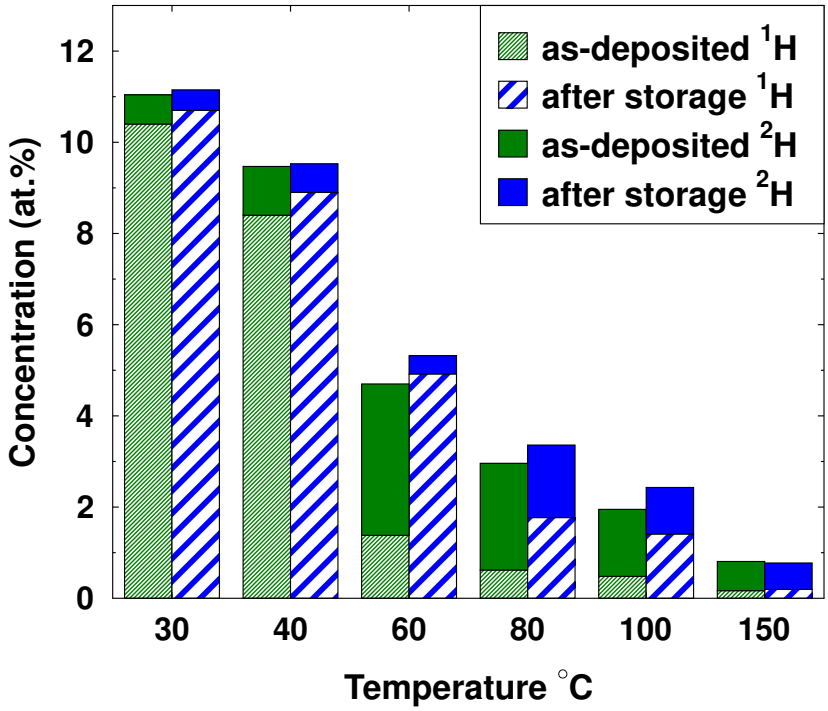

FIGURE 25 Change in the ^{1}H/^{2}H concentration after two months of storage at ambient conditions. For example in the far left bar the film deposited at 30 °C contains 10.4 at.% ^{1}H and 0.64 at.% ^{2}H just after the deposition, and 10.7 at.% ^{1}H and 0.45 at.% ^{2}H after the storage. Reprinted with permission from [PII], Copyright 2021, MDPI.

storage (Supplementary Fig 28). This indicates that there is a threshold hydrogen concentration which is required for the exchange reaction to proceed trough the film. This information can be crucial for applications that suffer from hydrogen induced damage [51–54].

The Al_2O_3 films are thought to be pinhole free after the nucleation step of few tens of cycles [8, 142]. In order to confirm that the migration is not due to porosity of the films, selected samples were investigated with helium ion microscopy. Within the resolution of the images, films appear to be smooth, pinhole free and no signs of cracks were detected as seen in Supplementary Figs. 29a and 29b.

Similar study was done for ZnO films. The films deposited at different temperatures were measured again after 2 months of storage at ambient conditions. Similar to Al_2O_3 films, the deuterium concentration of the samples decreased during the storage as seen in Fig. 25. The total hydrogen concentration had slightly increased between the measurements, but this increase is clear only for samples deposited between 60 and 100 °C. The as-deposited sample grown at 60 °C has the highest initial ^{2}H concentration of all the samples, and the decrease of ^{2}H and the increase of ^{1}H is most pronounced in that sample.

The notable decrease of ^{2}H and only a minor change in total hydrogen con-

centration indicates that hydrogen can exchange with ambient hydrogen (originating from ambient H_2 or H_2O) and therefore also migrate through the film, behaviour similar to Al_2O_3 films. The hydrogen migration seems to be surprisingly similar in both materials even though Al_2O_3 is amorphous and ZnO is polycrystalline.

6 CONCLUSIONS AND OUTLOOK

Hydrogen incorporation in Al_2O_3 and ZnO thin films grown with ALD were investigated using normal water, heavy water and oxygen-18 enriched water. In addition to conventional ALD, a spatial ALD reactor was used. Increase of both the deposition temperature as well as purging times was found to decrease the hydrogen incorporation in the films. Al_2O_3 films deposited at low temperature can contain up to 16.8 at.% and ZnO films 7.8 at.% of hydrogen. By increasing the deposition temperature the hydrogen concentrations decreased to under 2.8 at.% and 0.4 at.% for Al_2O_3 and ZnO, respectively. Lower hydrogen concentrations could also be achieved using longer purging times while keeping the deposition temperature low. Increasing purging times of Al_2O_3 process at 100 °C from 3 to 60 s decreased the hydrogen concentration from 13.0 to 6.0 at.%. In the case of ZnO with heavy water at 60 °C the total hydrogen concentration decreased from 9.5 at.% to 3.7 at.% when total purging time was increased from 3 s after both precursors to 10 s after the DEZ pulse and to 60 s after the heavy water pulse. However, increasing the purging times leads to more than an order of magnitude longer cycle times in both processes.

The main source of impurity hydrogen was found to be dependent on the deposition conditions. Both the deposition temperature, as well as the purging times between the pulses were found to be significant. For both Al_2O_3 and ZnO deposited from TMA and DEZ in combination with water, it seems that in ideal conditions i.e. high enough temperature and/or long purging time, the major hydrogen isotope in the films with heavy water is deuterium. This is in line with the results of Guerra-Nuñes *et al.* who used very long purging times [82]. The suggested mechanism of hydrogen/deuterium incorporation through the rehydroxylation explains the incorporation when purging time is sufficient for the given temperature. However, with less ideal process parameters, the mechanism proposed by Guerra-Nuñes *et al.* does not explain the high ^1H and low ^2H concentration in the films.

The persistent methyl and ethyl groups could well explain the high ^1H concentration found in the films deposited at low temperature or with short purging but for both Al_2O_3 and ZnO the low concentration of carbon in the films con-

tradicts with the explanation. Others have tried to explain the low carbon concentration by the reaction of persistent groups in subsequent cycles [41, 84]. This explanation, however, does not account the very high ^{1}H concentration left in the films. In addition, the high O/(Zn or Al) ratio at low temperatures would predict high ^{2}H concentration, but the results show otherwise. This contradiction remains a puzzle.

Results of the spatial ALD samples show that similar principles govern the impurity incorporation in both ALD methods. Although SALD greatly speeds up the deposition due to the shorter purging times, it also produces films with high impurity concentrations. Therefore, the balance between speed and quality must be considered carefully.

Despite of the similarities of Al_2O_3 and ZnO deposited using TMA and DEZ, respectively, the GPC at low temperature behaves differently. Only TMA + H_2O process suffers on the CVD-like growth. Physisorption and slow desorption of water at low deposition temperature has been argued to be the reason behind high GPC at low temperature. However, the same does not seem to apply to DEZ process.

In addition, deuterium was found to migrate through the film. As the samples were stored in ambient or humid condition, the concentration of deuterium decreased and the concentration of the hydrogen increased equally. The fact that the total amount of hydrogen isotopes in the films did not change significantly during the storage, points to exchange of hydrogen in the film with ambient hydrogen sources, namely H_2O and H_2. In the case of Al_2O_3, ambient conditions resulted in migration of hydrogen only if the initial hydrogen concentration was high enough. This would limit the use of these films as hydrogen barriers. On the other hand, the fact that ALD thin films, especially the low temperature Al_2O_3, contain very high amounts of hydrogen could enable utilizing them in hydrogen storage applications. In addition, the discovered deuterium migration hints that these films could act as proton conductors.

Looking at all the results, it seems evident that the reaction mechanisms and impurity incorporation are more complex than previously thought. This is true especially when short purging times are used. As shown in the thesis, isotopic labelling in combination with ion beam techniques is a powerful tool to study ALD depositions. In this thesis only the water precursor was used for labelling. The use of deuterated metal precursors, like deuterated TMA [41], would give additional information and could be used to validate the method. Furthermore, deuterated ammonia could be used to study nitride depositions.

REFERENCES

[1] J. S. Lim, Y. K. Kim, S. J. Choi, J. H. Lee, Y. S. Kim, B. T. Lee, H. S. Park, Y. W. Park, and S. I. Lee. Novel Al_2O_3 capacitor for high density DRAMs. In *ICVC '99. 6th International Conference on VLSI and CAD (Cat. No.99EX361)*, pages 506–509, 1999.

[2] K. Mistry, C. Allen, C. Auth, B. Beattie, D. Bergstrom, M. Bost, M. Brazier, M. Buehler, A. Cappellani, R. Chau, C.-H. Choi, G. Ding, K. Fischer, T. Ghani, R. Grover, W. Han, D. Hanken, M. Hattendorf, J. He, J. Hicks, R. Huessner, D. Ingerly, P. Jain, R. James, L. Jong, S. Joshi, C. Kenyon, K. Kuhn, K. Lee, H. Liu, J. Maiz, B. McIntyre, P. Moon, J. Neirynck, S. Pae, C. Parker, D. Parsons, C. Prasad, L. Pipes, M. Prince, P. Ranade, T. Reynolds, J. Sandford, L. Shifren, J. Sebastian, J. Seiple, D. Simon, S. Sivakumar, P. Smith, C. Thomas, T. Troeger, P. Vandervoorn, S. Williams, and K. Zawadzki. A 45nm Logic Technology with High-k+Metal Gate Transistors, Strained Silicon, 9 Cu Interconnect Layers, 193nm Dry Patterning, and 100% Pb-free Packaging. In *2007 IEEE International Electron Devices Meeting*, pages 247–250, 2007.

[3] R. W. Johnson, A. Hultqvist, and S. F. Bent. A brief review of atomic layer deposition: from fundamentals to applications. *Materials Today*, 17(5):236–246, 2014.

[4] M. Haruta. When Gold Is Not Noble: Catalysis by Nanoparticles. *The Chemical Record*, 3(2):75–87, 2003.

[5] T. Suntola and J. Antson. Method for producing compound thin films, U.S. Patent 4,058,430, Issued Nov. 25, 1977.

[6] R. L. Puurunen. A Short History of Atomic Layer Deposition: Tuomo Suntola's Atomic Layer Epitaxy. *Chemical Vapor Deposition*, 20(10-11-12):332–344, 2014.

[7] S. M. George. Atomic Layer Deposition: An Overview. *Chemical Reviews*, 110(1):111–131, 2010. PMID: 19947596.

[8] P. F. Carcia, R. S. McLean, M. H. Reilly, M. D. Groner, and S. M. George. Ca test of Al_2O_3 gas diffusion barriers grown by atomic layer deposition on polymers. *Applied Physics Letters*, 89(3):031915, 2006.

[9] T. Hirvikorpi, M. Vähä-Nissi, T. Mustonen, E. Iiskola, and M. Karppinen. Atomic Layer Deposited Aluminum Oxide Barrier Coatings for Packaging Materials. *Thin Solid Films*, 518(10):2654 – 2658, 2010.

[10] T. O. Kääriäinen, P. Maydannik, D. C. Cameron, K. Lahtinen, P. Johansson, and J. Kuusipalo. Atomic layer deposition on polymer based flexible pack-

aging materials: Growth characteristics and diffusion barrier properties. *Thin Solid Films*, 519(10):3146–3154, 2011.

[11] P. S. Maydannik, T. O. Kääriäinen, K. Lahtinen, D. C. Cameron, M. Söderlund, P. Soininen, P. Johansson, J. Kuusipalo, L. Moro, and X. Zeng. Roll-to-roll atomic layer deposition process for flexible electronics encapsulation applications. *Journal of Vacuum Science & Technology A*, 32(5):051603, 2014.

[12] L. Paussa, L. Guzman, E. Marin, N. Isomäki, and L. Fedrizzi. Protection of silver surfaces against tarnishing by means of alumina/titania-nanolayers. *Surface and Coatings Technology*, 206(5):976–980, 2011. Surface Modification of Materials by Ion beams 2009.

[13] J. Huang, X. Yu, P. W. Shum, Z. Zhou, and Y. Ma. Influence of ALD-Al_2O_3 film on anti-scratch and anti-tarnish of silver. *Surface Engineering*, 37(4):490–496, 2021.

[14] X. Xiao, G. Cao, F. Chen, Y. Tang, X. Liu, and W. Xu. Durable superhydrophobic wool fabrics coating with nanoscale Al_2O_3 layer by atomic layer deposition. *Applied Surface Science*, 349:876–879, 2015.

[15] K. Isakov, C. Kauppinen, S. Franssila, and H. Lipsanen. Superhydrophobic Antireflection Coating on Glass Using Grass-like Alumina and Fluoropolymer. *ACS Applied Materials & Interfaces*, 12(44):49957–49962, 2020. PMID: 33084313.

[16] J. Malm, E. Sahramo, M. Karppinen, and R. H. A. Ras. Photo-Controlled Wettability Switching by Conformal Coating of Nanoscale Topographies with Ultrathin Oxide Films. *Chemistry of Materials*, 22(11):3349–3352, 2010.

[17] L.-C. Wang, Y.-Y. Han, K.-C. Yang, M.-J. Chen, H.-C. Lin, C.-K. Lin, and Y.-T. Hsu. Hydrophilic/hydrophobic surface of Al_2O_3 thin films grown by thermal and plasma-enhanced atomic layer deposition on plasticized polyvinyl chloride (PVC). *Surface and Coatings Technology*, 305:158 – 164, 2016.

[18] P. Poodt, V. Tiba, F. Werner, J. Schmidt, A. Vermeer, and F. Roozeboom. Ultrafast atomic layer deposition of alumina layers for solar cell passivation. *Journal of The Electrochemical Society*, 158(9):H937, 2011.

[19] Z. Xing, J. Xiao, T. Hu, X. Meng, D. Li, X. Hu, and Y. Chen. Atomic Layer Deposition of Metal Oxides in Perovskite Solar Cells: Present and Future. *Small Methods*, page 2000588, 2020.

[20] B. Vermang, A. Rothschild, A. Racz, J. John, J. Poortmans, R. Mertens, P. Poodt, V. Tiba, and F. Roozeboom. Spatially separated atomic layer deposition of Al_2O_3, a new option for high-throughput Si solar cell passivation. *Progress in Photovoltaics: Research and Applications*, 19(6):733–739, 2011.

[21] C.-H. Chao, C.-T. Hsieh, W.-J. Ke, L.-W. Lee, Y.-F. Lin, H.-W. Liu, S. Gu, C.-C. Fu, R.-S. Juang, B. C. Mallick, Y. A. Gandomi, and C.-Y. Su. Roll-to-roll atomic layer deposition of titania coating on polymeric separators for lithium ion batteries. *Journal of Power Sources*, 482:228896, 2021.

[22] K. Sharma, D. Routkevitch, N. Varaksa, and S. M. George. Spatial atomic layer deposition on flexible porous substrates: ZnO on anodic aluminum oxide films and Al_2O_3 on Li ion battery electrodes. *Journal of Vacuum Science & Technology A*, 34(1):01A146, 2016.

[23] B. J. O'Neill, D. H. K. Jackson, J. Lee, C. Canlas, P. C. Stair, C. L. Marshall, J. W. Elam, T. F. Kuech, J. A. Dumesic, and G. W. Huber. Catalyst Design with Atomic Layer Deposition. *ACS Catalysis*, 5(3):1804–1825, 2015.

[24] D. La Zara, F. Sun, F. Zhang, F. Franek, K. Balogh Sivars, J. Horndahl, S. Bates, M. Brännström, P. Ewing, M. J. Quayle, G. Petersson, S. Folestad, and J. R. van Ommen. Controlled Pulmonary Delivery of Carrier-Free Budesonide Dry Powder by Atomic Layer Deposition. *ACS Nano*, 15(4):6684–6698, 2021. PMID: 33769805.

[25] R. L. Garcea, N. M. Meinerz, M. Dong, H. Funke, S. Ghazvini, and T. W. Randolph. Single-administration, thermostable human papillomavirus vaccines prepared with atomic layer deposition technology. *NPJ Vaccines*, 5:45, 2020.

[26] V. Miikkulainen, M. Leskelä, M. Ritala, and R. Puurunen. Crystallinity of inorganic films grown by atomic layer deposition: Overview and general trends. *Journal of Applied Physics*, 113(2):021301, 2013.

[27] A.J. M. Mackus, J. R. Schneider, C. MacIsaac, J. G. Baker, and S. F. Bent. Synthesis of Doped, Ternary, and Quaternary Materials by Atomic Layer Deposition: A Review. *Chemistry of Materials*, 31(4):1142–1183, 2019.

[28] H. C. M. Knoops, T. Faraz, K. Arts, and W. M. M. Kessels. Status and prospects of plasma-assisted atomic layer deposition. *Journal of Vacuum Science & Technology A*, 37(3):030902, 2019.

[29] A. Rahtu, T. Alaranta, and M. Ritala. In situ quartz crystal microbalance and quadrupole mass spectrometry studies of atomic layer deposition of aluminum oxide from trimethylaluminum and water. *Langmuir*, 17(21):6506–6509, 2001.

[30] A. Rahtu and M. Ritala. Reaction mechanism studies on titanium isopropoxide-water atomic layer deposition process. *Chemical Vapor Deposition*, 8(1):21–28, 2002.

[31] M. Juppo, A. Rahtu, M. Ritala, and M. Leskelä. In Situ Mass Spectrometry Study on Surface Reactions in Atomic Layer Deposition of Al_2O_3 Thin

Films from Trimethylaluminum and Water. *Langmuir*, 16(8):4034–4039, 2000.

[32] R. Matero, A. Rahtu, and M. Ritala. In Situ Reaction Mechanism Studies on the Atomic Layer Deposition of Al_2O_3 from $(CH_3)_2AlCl$ and Water. *Langmuir*, 21(8):3498–3502, 2005. PMID: 15807594.

[33] H. Azizpour, M. Talebi, F.D. Tichelaar, R. Sotudeh-Gharebagh, J. Guo, J.R. van Ommen, and N. Mostoufi. Effective coating of titania nanoparticles with alumina via atomic layer deposition. *Applied Surface Science*, 426:480–496, 2017.

[34] K. S. An, W. T. Cho, K. W. Sung, S. S. Lee, and Y. S. Kim. Preparation of Al_2O_3 Thin Films by Atomic Layer Deposition Using Dimethylaluminum Isopropoxide and Water and Their Reaction Mechanisms. *Bulletin of the Korean Chemical Society*, 46(26):1659–1663, 2003.

[35] T. S. Yang, W. Cho, M. Kim, K.-S. An, T.-M. Chung, C. G. Kim, and Y. Kim. Atomic layer deposition of nickel oxide films using $Ni(dmamp)_2$ and water. *Journal of Vacuum Science & Technology A*, 23(4):1238–1243, 2005.

[36] J. Niinistö, A. Rahtu, M. Putkonen, M. Ritala, M. Leskelä, and L. Niinistö. In Situ Quadrupole Mass Spectrometry Study of Atomic-Layer Deposition of ZrO_2 Using $Cp_2Zr(CH_3)_2$ and Water. *Langmuir*, 21(16):7321–7325, 2005. PMID: 16042461.

[37] K. Knapas, A. Rahtu, and M. Ritala. Reaction Mechanism Studies on Atomic Layer Deposition of Nb_2O_5 from $Nb(OEt)_5$ and Water. *Langmuir*, 26(2):848–853, 2010. PMID: 19795848.

[38] Y. Tomczak, K. Knapas, M. Sundberg, M. Leskelä, and M. Ritala. In Situ Reaction Mechanism Studies on the New ^{t}BuN=M$(NEt_2)_3$ -Water and ^{t}BuN=M$(NEt_2)_3$ - Ozone (M = Nb,Ta) Atomic Layer Deposition Processes. *Chemistry of Materials*, 24(9):1555–1561, 2012.

[39] Y. Tomczak, K. Knapas, S. Haukka, M. Kemell, M. Heikkilä, M. Ceccato, M. Leskelä, and M. Ritala. In Situ Reaction Mechanism Studies on Atomic Layer Deposition of $Al_xSi_yO_z$ from Trimethylaluminium, Hexakis(ethylamino)disilane, and Water. *Chemistry of Materials*, 24(20):3859–3867, 2012.

[40] Y. Tomczak, K. Knapas, M. Leskelä, and M. Ritala. In situ reaction mechanism studies on the $Ti(NMe_2)_2(O^iPr)_2$-D_2O and $Ti(O^iPr)_3[MeC(N^iPr)_2]$-$D_2O$ atomic layer deposition processes. *Journal of Vacuum Science & Technology A*, 32(1):01A121, 2014.

[41] V. Vandalon and W. M. M. Kessels. Revisiting the Growth Mechanism of Atomic Layer Deposition of Al_2O_3: A Vibrational Sum-frequency Generation Study. *Journal of Vacuum Science & Technology A*, 35(5):05C313, 2017.

[42] V. Vandalon and W. M. M. Kessels. What is limiting low-temperature atomic layer deposition of Al_2O_3? A vibrational sum-frequency generation study. *Applied Physics Letters*, 108(1):011607, 2016.

[43] L. Ye, J. A. Kropp, and T. Gougousi. In situ infrared spectroscopy study of the surface reactions during the atomic layer deposition of TiO_2 on GaAs (100) surfaces. *Applied Surface Science*, 422:666–674, 2017.

[44] A.C. Dillon, A.W. Ott, J.D. Way, and S.M. George. Surface chemistry of Al_2O_3 deposition using $Al(CH_3)_3$ and H_2O in a binary reaction sequence. *Surface Science*, 322(1):230–242, 1995.

[45] E. Kokkonen, M. Kaipio, H.-E. Nieminen, F. Rehman, V. Miikkulainen, M. Putkonen, M. Ritala, S. Huotari, J. Schnadt, and S. Urpelainen. Ambient pressure X-ray photoelectron spectroscopy setup for synchrotron-based in situ and operando atomic layer deposition research. *Review of Scientific Instruments*, 93(1):013905, 2022.

[46] M. Shirazi and S. D. Elliott. Cooperation between adsorbates accounts for the activation of atomic layer deposition reactions. *Nanoscale*, 7:6311–6318, 2015.

[47] T. Weckman and Laasonen K. First principles study of the atomic layer deposition of alumina by TMA-H_2O-process. *Physical Chemistry Chemical Physics*, 17:17322–17334, 2015.

[48] T. Weckman and K. Laasonen. Atomic Layer Deposition of Zinc Oxide: Diethyl Zinc Reactions and Surface Saturation from First-Principles. *The Journal of Physical Chemistry C*, 120(38):21460–21471, 2016.

[49] T. Weckman and K. Laasonen. Atomic Layer Deposition of Zinc Oxide: Study on the Water Pulse Reactions from First-Principles. *The Journal of Physical Chemistry C*, 122(14):7685–7694, 2018.

[50] G. P. Gakis, H. Vergnes, E. Scheid, C. Vahlas, A. G. Boudouvis, and B. Caussat. Detailed investigation of the surface mechanisms and their interplay with transport phenomena in alumina atomic layer deposition from TMA and water. *Chemical Engineering Science*, 195:399–412, 2019.

[51] D. Sohrabi Baba Heidary, W. Qu, and C. A. Randall. Evaluating the Merit of ALD Coating as a Barrier Against Hydrogen Degradation in Capacitor Components. *RSC Adv.*, 5:50869–50877, 2015.

[52] Y. Lee, T. Nam, S. Seo, H. Yoon, I.-K. Oh, C. H. Lee, H. Yoo, H. J. Kim, W. Choi, S. Im, J. Y. Yang, D. W. Choi, C. Yoo, H.-J. Kim, and H. Kim. Hydrogen Barriers Based on Chemical Trapping Using Chemically Modulated Al_2O_3 Grown by Atomic Layer Deposition for InGaZnO Thin-Film Transistors. *ACS Applied Materials & Interfaces*, 13(17):20349–20360, 2021. PMID: 33818057.

[53] V. Kolkovsky. Hydrogen-Related Defects in Insulators. *Physica Status Solidi (A)*, 218:2100213, 2021.

[54] A. Schmid, C. Fischer, D. Skorka, A. Herguth, C. Winter, A. Zuschlag, and G. Hahn. On the Role of AlO_x Thickness in AlO_x/SiN_y: H Layer Stacks Regarding Light- and Elevated Temperature-Induced Degradation and Hydrogen Diffusion in c-Si. *IEEE Journal of Photovoltaics*, 11(4):967–973, 2021.

[55] P. F. Carcia, R. S. McLean, and M. H. Reilly. Permeation measurements and modeling of highly defective Al_2O_3 thin films grown by atomic layer deposition on polymers. *Applied Physics Letters*, 97(22):221901, 2010.

[56] T. Suntola. Atomic layer epitaxy. *Materials Science Reports*, 4(5):261–312, 1989.

[57] R. Puurunen. Surface chemistry of atomic layer deposition: A case study for the trimethylaluminum/water process. *Journal of Applied Physics*, 97(12):121301, 2005.

[58] N. E. Richey, C. de Paula, and S. F. Bent. Understanding chemical and physical mechanisms in atomic layer deposition. *The Journal of Chemical Physics*, 152(4):040902, 2020.

[59] R. L. Puurunen. Correlation between the growth-per-cycle and the surface hydroxyl group concentration in the atomic layer deposition of aluminum oxide from trimethylaluminum and water. *Applied Surface Science*, 245(1):6–10, 2005.

[60] J. M. Lownsbury, J. A. Gladden, C. T. Campbell, I. S. Kim, and A. B. F. Martinson. Direct Measurements of Half-Cycle Reaction Heats during Atomic Layer Deposition by Calorimetry. *Chemistry of Materials*, 29(20):8566–8577, 2017.

[61] E. B. Yousfi, J. Fouache, and D. Lincot. Study of atomic layer epitaxy of zinc oxide by in-situ quartz crystal microgravimetry. *Applied Surface Science*, 153(4):223 – 234, 2000.

[62] V. H. Nguyen, A. Sekkat, C. Jiménez, D. Muñoz, D. Bellet, and D. Muñoz-Rojas. Impact of precursor exposure on process efficiency and film properties in spatial atomic layer deposition. *Chemical Engineering Journal*, 403:126234, 2021.

[63] D. Muñoz-Rojas, V. H. Nguyen, C. Masse de la Huerta, S. Aghazadehchors, C. Jiménez, and D. Bellet. Spatial Atomic Layer Deposition (SALD), an emerging tool for energy materials. Application to new-generation photovoltaic devices and transparent conductive materials. *Comptes Rendus Physique*, 18(7):391 – 400, 2017.

[64] D. Muñoz-Rojas, T. Maindron, A. Esteve, F. Piallat, J.C.S. Kools, and J.-M. Decams. Speeding up the unique assets of atomic layer deposition. *Materials Today Chemistry*, 12:96–120, 2019.

[65] A. S. Asundi, J. A. Raiford, and S. F. Bent. Opportunities for Atomic Layer Deposition in Emerging Energy Technologies. *ACS Energy Letters*, 4(4):908–925, 2019.

[66] C.H. Frijters, P. Poodt, and A. Illiberi. Atmospheric spatial atomic layer deposition of Zn(O,S) buffer layer for Cu(In,Ga)Se_2 solar cells. *Solar Energy Materials and Solar Cells*, 155:356–361, 2016.

[67] D. H. Levy, D. Freeman, S. F. Nelson, P. J. Cowdery-Corvan, and L. M. Irving. Stable ZnO thin film transistors by fast open air atomic layer deposition. *Applied Physics Letters*, 92(19):192101, 2008.

[68] S. Moitzheim, J. E. Balder, P. Poodt, S. Unnikrishnan, S. De Gendt, and P. M. Vereecken. Chlorine Doping of Amorphous TiO_2 for Increased Capacity and Faster Li^+-Ion Storage. *Chemistry of Materials*, 29(23):10007–10018, 2017.

[69] A. Illiberi, R. Scherpenborg, Y. Wu, F. Roozeboom, and P. Poodt. Spatial Atmospheric Atomic Layer Deposition of $Al_xZn_{1-x}O$. *ACS Applied Materials & Interfaces*, 5(24):13124–13128, 2013. PMID: 24295211.

[70] H. Choi, S. Shin, Y. Choi, Y. Choi, J. Kim, S. Kim, H. Kim, J. Park, S. C. Chung, H. Jeon, and K. Oh. High Throughput and Scalable Spatial Atomic Layer Deposition of Al_2O_3 as a Moisture Barrier for Flexible OLED Display. *SID Symposium Digest of Technical Papers*, 46(1):1043–1046, 2015.

[71] K. L. Jarvis and P. J. Evans. Growth of thin barrier films on flexible polymer substrates by atomic layer deposition. *Thin Solid Films*, 624:111–135, 2017.

[72] M. Aghaee, P. S. Maydannik, P. Johansson, J. Kuusipalo, M. Creatore, T. Homola, and D. C. Cameron. Low temperature temporal and spatial atomic layer deposition of TiO_2 films. *Journal of Vacuum Science & Technology A*, 33(4):041512, 2015.

[73] K. Lahtinen, T. Kääriäinen, P. Johansson, S. Kotkamo, P. Maydannik, T. Seppänen, J. Kuusipalo, and D. C. Cameron. UV protective zinc oxide coating for biaxially oriented polypropylene packaging film by atomic layer deposition. *Thin Solid Films*, 570:33–37, 2014.

[74] M. B. M. Mousa, J. S. Ovental, A. H. Brozena, C. J. Oldham, and G. N. Parsons. Modeling and experimental demonstration of high-throughput flow-through spatial atomic layer deposition of Al_2O_3 coatings on textiles at atmospheric pressure. *Journal of Vacuum Science & Technology A*, 36(3):031517, 2018.

[75] M.D. Groner, J.W. Elam, F.H. Fabreguette, and S.M. George. Electrical Characterization of Thin Al_2O_3 Films Grown by Atomic Layer Deposition on Silicon and Various Metal Substrates. *Thin Solid Films*, 413(1):186 – 197, 2002.

[76] R. Y. Khosa, E. B. Thorsteinsson, M. Winters, N. Rorsman, R. Karhu, J. Hassan, and E. Ö. Sveinbjörnsson. Electrical Characterization of Amorphous Al_2O_3 Dielectric Films on n-type 4H-SiC. *AIP Advances*, 8(2):025304, 2018.

[77] J. Acharya, J. Wilt, B. Liu, and J. Wu. Probing the Dielectric Properties of Ultrathin $Al/Al_2O_3/Al$ Trilayers Fabricated Using in Situ Sputtering and Atomic Layer Deposition. *ACS Applied Materials & Interfaces*, 10(3):3112–3120, 2018.

[78] S.-H. Ko Park, J. Oh, C.-S. Hwang, J.-I. Lee, Y. S. Yang, H. Y. Chu, and K.-Y. Kang. Ultra Thin Film Encapsulation of Organic Light Emitting Diode on a Plastic Substrate. *ETRI Journal*, 27(5):545–550, 2005.

[79] A. P. Ghosh, L. J. Gerenser, C. M. Jarman, and J. E. Fornalik. Thin-film Encapsulation of Organic Light-emitting Devices. *Applied Physics Letters*, 86(22):223503, 2005.

[80] L. Aarik, H. Mändar, P. Ritslaid, A. Tarre, J. Kozlova, and J. Aarik. Low-Temperature Atomic Layer Deposition of α-Al_2O_3 Thin Films. *Crystal Growth & Design*, 21(7):4220–4229, 2021.

[81] G. S. Higashi and C. G. Fleming. Sequential surface chemical reaction limited growth of high quality Al_2O_3 dielectrics. *Applied Physics Letters*, 55(19):1963–1965, 1989.

[82] C. Guerra-Nunẽz, M. Döbeli, J. Michler, and I. Utke. Reaction and growth mechanisms in Al_2O_3 deposited via atomic layer deposition: Elucidating the hydrogen source. *Chemistry of Materials*, 29(20):8690–8703, 2017.

[83] C. Soto and W. T. Tysoe. The reaction pathway for the growth of alumina on high surface area alumina and in ultrahigh vacuum by a reaction between trimethyl aluminum and water. *Journal of Vacuum Science & Technology A*, 9(5):2686–2695, 1991.

[84] B. A. Sperling, B. Kalanyan, and J. E. Maslar. Atomic Layer Deposition of Al_2O_3 Using Trimethylaluminum and H_2O: The Kinetics of the H_2O Half-Cycle. *The Journal of Physical Chemistry C*, 124(5):3410–3420, 2020.

[85] A. Werbrouck, M. Shirazi, F. Mattelaer, S. D. Elliott, J. Dendooven, and C. Detavernier. A secondary reaction pathway for the alumina atomic layer deposition process with trimethylaluminum and water, revealed by full-range, time-resolved in situ mass spectrometry. *The Journal of Physical Chemistry C*, 124(48):26443–26454, 2020.

[86] J. Malm, E. Sahramo, J. Perälä, Sajavaara T., and Karppinen M. Low-temperature atomic layer deposition of ZnO thin films: Control of crystallinity and orientation. *Thin Solid Films*, 519(16):5319 – 5322, 2011.

[87] J. Cai, Z. Ma, U. Wejinya, M. Zou, Y. Liu, H. Zhou, and X. Meng. A revisit to atomic layer deposition of zinc oxide using diethylzinc and water as precursors. *Journal of Materials Science*, 54(7):5236–5248, 2019.

[88] E. Guziewicz, I. A. Kowalik, M. Godlewski, K. Kopalko, V. Osinniy, A. Wójcik, S. Yatsunenko, E. Łusakowska, W. Paszkowicz, and M. Guziewicz. Extremely low temperature growth of ZnO by atomic layer deposition. *Journal of Applied Physics*, 103(3):033515, 2008.

[89] M.-J. Zhao, Z.-T. Sun, C.-H. Hsu, P.-H. Huang, X.-Y. Zhang, W.-Y. Wu, P. Gao, Y. Qiu, S.-Y. Lien, and W.-Z. Zhu. Zinc oxide films with high transparency and crystallinity prepared by a low temperature spatial atomic layer deposition process. *Nanomaterials (Basel, Switzerland)*, 10(3):459, 03 2020.

[90] Z. Gao and P. Banerjee. Review Article: Atomic layer deposition of doped ZnO films. *Journal of Vacuum Science & Technology A*, 37(5):050802, 2019.

[91] Z. Kan, Z. Wang, Y. Firdaus, M. Babics, H. N. Alshareef, and P. M. Beaujuge. Atomic-layer-deposited AZO outperforms ITO in high-efficiency polymer solar cells. *J. Mater. Chem. A*, 6:10176–10183, 2018.

[92] D.-J. Lee, H.-M. Kim, J.-Y. Kwon, H. Choi, S.-H. Kim, and K.-B. Kim. Structural and Electrical Properties of Atomic Layer Deposited Al-Doped ZnO Films. *Advanced Functional Materials*, 21(3):448–455, 2011.

[93] M.-L. Kääriäinen, C.K. Weiss, S. Ritz, S. Pütz, D.C. Cameron, V. Mailänder, and K. Landfester. Zinc release from atomic layer deposited zinc oxide thin films and its antibacterial effect on *Escherichia coli*. *Applied Surface Science*, 287:375 – 380, 2013.

[94] J. W. Elam and S. M. George. Growth of ZnO/Al_2O_3 Alloy Films Using Atomic Layer Deposition Techniques. *Chemistry of Materials*, 15(4):1020–1028, 2003.

[95] A. J. M. Mackus, C. MacIsaac, W.-H. Kim, and S. F. Bent. Incomplete elimination of precursor ligands during atomic layer deposition of zinc-oxide, tin-oxide, and zinc-tin-oxide. *The Journal of Chemical Physics*, 146(5):052802, 2017.

[96] K. Morishige, S. Kittaka, T. Moriyasu, and T. Morimoto. Thermal desorption study of surface hydroxyls on ZnO. *J. Chem. Soc., Faraday Trans. 1*, 76:738–745, 1980.

[97] S. Kim, S. Lee, S.-Y. Ham, D.-H. Ko, S. Shin, Z. Jin, and Y.-S. Min. A kinetic study of ZnO atomic layer deposition: Effects of surface hydroxyl concentration and steric hindrance. *Applied Surface Science*, 469:804–810, 2019.

[98] M. D. Groner, F. H. Fabreguette, J. W. Elam, and S. M. George. Low-Temperature Al_2O_3 Atomic Layer Deposition. *Chemistry of Materials*, 16(4):639–645, 2004.

[99] S. E. Potts, G. Dingemans, C. Lachaud, and W. M. M. Kessels. Plasma-enhanced and thermal atomic layer deposition of Al_2O_3 using dimethylaluminum isopropoxide, $[Al(CH_3)_2(\mu\text{-}O^iPr)]_2$, as an alternative aluminum precursor. *Journal of Vacuum Science & Technology A*, 30(2):021505, 2012.

[100] A. Hiraiwa, T. Saito, D. Matsumura, and H. Kawarada. Isotope analysis of diamond-surface passivation effect of high-temperature H_2O-grown atomic layer deposition-Al_2O_3 films. *Journal of Applied Physics*, 117(21):215304, 2015.

[101] J. Panigrahi, P.K. Singh, G. Gupta, and Vandana. Growth and luminescence characteristics of zinc oxide thin films deposited by ALD technique. *Journal of Luminescence*, 233:117797, 2021.

[102] G. Dingemans, M. C. M. van de Sanden, and W. M. M. Kessels. Influence of the Deposition Temperature on the c-Si Surface Passivation by Al_2O_3 Films Synthesized by ALD and PECVD. *Electrochemical and Solid-State Letters*, 13(3):H76, 2010.

[103] L.E. Black, B.W.H. van de Loo, B. Macco, J. Melskens, W.J.H. Berghuis, and W.M.M. Kessels. Explorative studies of novel silicon surface passivation materials: Considerations and lessons learned. *Solar Energy Materials and Solar Cells*, 188:182–189, 2018.

[104] B. Macco, H.C.M. Knoops, M. A. Verheijen, W. Beyer, M. Creatore, and W. M.M. Kessels. Atomic layer deposition of high-mobility hydrogen-doped zinc oxide. *Solar Energy Materials and Solar Cells*, 173:111–119, 2017. Proceedings of the 7th international conference on Crystalline Silicon Photovoltaics.

[105] J. L. van Hemmen, S. B. S. Heil, J. H. Klootwijk, F. Roozeboom, C. J. Hodson, M. C. M. van de Sanden, and W. M. M. Kessels. Plasma and Thermal ALD of Al_2O_3 in a Commercial 200 mm ALD Reactor. *Journal of The Electrochemical Society*, 154(7):G165, 2007.

[106] V Verlaan, L. R. J. G. van den Elzen, G. Dingemans, M. C. M. van de Sanden, and W. M. M. Kessels. Composition and bonding structure of plasma-assisted ALD Al_2O_3 films. *physica status c*, 7(3-4):976–979, 2010.

[107] E. Guziewicz, W. Wozniak, S. Mishra, R. Jakiela, M. Guziewicz, V. Y. Ivanov, E. Lusakowska, and R. Schifano. Hydrogen in As-Grown and Annealed

ZnO Films Grown by Atomic Layer Deposition. *physica status solidi a*, 218(1):2000318, 2021.

[108] M. Napari, J. Malm, R. Lehto, J. Julin, K. Arstila, T. Sajavaara, and M. Lahtinen. Nucleation and growth of ZnO on PMMA by low-temperature atomic layer deposition. *Journal of Vacuum Science & Technology A*, 33(1):01A128, 2015.

[109] B. Xia, J.J. Ganem, E. Briand, S. Steydli, H. Tancrez, and I. Vickridge. The carbon and hydrogen contents in ALD-grown ZnO films define a narrow ALD temperature window. *Vacuum*, 190:110289, 2021.

[110] O. M.E. Ylivaara, X. Liu, L. Kilpi, J. Lyytinen, D. Schneider, M. Laitinen, J. Julin, S. Ali, S. Sintonen, M. Berdova, E. Haimi, T. Sajavaara, H. Ronkainen, H. Lipsanen, J. Koskinen, S-P. Hannula, and R. L. Puurunen. Aluminum oxide from trimethylaluminum and water by atomic layer deposition: The temperature dependence of residual stress, elastic modulus, hardness and adhesion. *Thin Solid Films*, 552:124–135, 2014.

[111] CIAAW, Isotopic compositions of the elements 2019. Available online at www.ciaaw.org, 2021.

[112] K. Bae, K. S. Son, J. W. Kim, S. W. Park, J. An, F. B. Prinz, and J. H. Shim. Proton incorporation in yttria-stabilized zirconia during atomic layer deposition. *International Journal of Hydrogen Energy*, 39(6):2621–2627, 2014.

[113] Y. Wu, B. Macco, D. Vanhemel, S. Kölling, M.A. Verheijen, P. M. Koenraad, W. M. M. Kessels, and F. Roozeboom. Atomic Layer Deposition of In_2O_3:H from InCp and H_2O/O_2: Microstructure and Isotope Labeling Studies. *ACS Applied Materials & Interfaces*, 9(1):592–601, 2017. PMID: 27977925.

[114] A. C. Kozen, M. A. Schroeder, K. D. Osborn, C. J. Lobb, and G. W. Rubloff. Examining the role of hydrogen in the electrical performance of in situ fabricated metal-insulator-metal trilayers using an atomic layer deposited Al_2O_3 dielectric. *Applied Physics Letters*, 102(17):173501, 2013.

[115] T. Nguyen, N. Valle, J. Guillot, J. Bour, N. Adjeroud, Y. Fleming, M. Guennou, J.-N. Audinot, B. El Adib, R. Joly, D. Arl, G. Frache, and J. Polesel-Maris. Elucidating the growth mechanism of ZnO films by atomic layer deposition with oxygen gas via isotopic tracking. *J. Mater. Chem. C*, 9:4307–4315, 2021.

[116] N. Leick, S. Agarwal, A. J. M. Mackus, S. E. Potts, and W. M. M. Kessels. Catalytic Combustion Reactions During Atomic Layer Deposition of Ru Studied Using $^{18}O_2$ Isotope Labeling. *The Journal of Physical Chemistry C*, 117(41):21320–21330, 2013.

[117] B. Xia, J.J. Ganem, S. Steydli, H. Tancrez, and I. Vickridge. RBS and NRA analysis for films with high growth rate prepared by atomic layer deposition. *Nuclear Instruments and Methods in Physics Research Section B: Beam Interactions with Materials and Atoms*, 489:20–25, 2021.

[118] B.-W. Shih, W.-P. Hsieh, J.-J. Shyue, and F.-Y. Tsai. Enhanced thermoelectric properties of atomic-layer-deposited Hf:Zn^{16}O/^{18}O superlattice films by interface-engineering. *Ceramics International*, 46(6):7122–7130, 2020.

[119] M. Juppo, A. Rahtu, and M. Ritala. In Situ Mass Spectrometry Study on Surface Reactions in Atomic Layer Deposition of TiN and Ti(Al)N Thin Films. *Chemistry of Materials*, 14(1):281–287, 2002.

[120] K. Torii, T. Kawahara, and K. Shiraishi. Improvement of interfacial layer reliability by incorporation of deuterium into $HfAlO_x$ formed by D_2/O-ALD. *IEEE Electron Device Letters*, 26(10):722–724, 2005.

[121] T. Lee, H.-K. Ko, J. Ahn, I.-S. Park, H. Sim, H. Park, and H. Hwang. Electrical Properties of Atomic Layer Deposited HfO_2 Gate Dielectric Film Using D_2O as Oxidant for Improved Reliability. *Japanese Journal of Applied Physics*, 45(9A):6993–6995, 2006.

[122] J. Bigeleisen and M. Goeppert Mayer. Calculation of equilibrium constants for isotopic exchange reactions. *The Journal of Chemical Physics*, 15(5):261–267, 1947.

[123] M. Gómez-Gallego and M. Sierra. Kinetic Isotope Effects in the Study of Organometallic Reaction Mechanisms. *Chemical Reviews*, 111(8):4857–4963, 2011. PMID: 21545118.

[124] M. Putkonen, T. Sajavaara, L. Niinistö, and J. Keinonen. Analysis of ALD-processed thin films by ion-beam techniques. *Analytical and Bioanalytical Chemistry*, 382(8):1791–1799, 2005.

[125] M. Laitinen, M. Rossi, J. Julin, and T. Sajavaara. Time-of-flight – Energy spectrometer for elemental depth profiling – Jyväskylä design. *Nuclear Instruments and Methods in Physics Research Section B: Beam Interactions with Materials and Atoms*, 337:55 – 61, 2014.

[126] K. Arstila, J. Julin, M.I. Laitinen, J. Aalto, T. Konu, S. Kärkkäinen, S. Rahkonen, M. Raunio, J. Itkonen, J.-P. Santanen, T. Tuovinen, and T. Sajavaara. Potku – New analysis software for heavy ion elastic recoil detection analysis. *Nuclear Instruments and Methods in Physics Research Section B: Beam Interactions with Materials and Atoms*, 331:34 – 41, 2014. 11th European Conference on Accelerators in Applied Research and Technology.

[127] K. Arstila, T. Sajavaara, and J. Keinonen. Monte Carlo simulation of multiple and plural scattering in elastic recoil detection. *Nuclear Instruments and*

Methods in Physics Research Section B: Beam Interactions with Materials and Atoms, 174(1):163–172, 2001.

[128] T. Degen, M. Sadki, E. Bron, U. König, and G Nénert. The HighScore suite (v. 4.9). *Powder Diffraction* **29 S2**, 2014, S13-S18.

[129] International Centre for Diffraction Data, ICDD-PDF4+, Release 2020, 12 Campus Boulevard, Newton Square, Pennsylvania USA, 2020.

[130] J. Notte, B. Ward, N. Economou, R. Hill, R. Percival, L. Farkas, and S. McVey. An Introduction to the Helium Ion Microscope. *AIP Conference Proceedings*, 931(1):489–496, 2007.

[131] M. Schmidt, J. M. Byrne, and I. J. Maasilta. Bio-imaging with the helium-ion microscope: A review. *Beilstein Journal of Nanotechnology*, 12:1–23, 2021.

[132] E. Guziewicz, T. A. Krajewski, E. Przezdziecka, K. P. Korona, N. Czechowski, L. Klopotowski, and P. Terziyska. Zinc Oxide Grown by Atomic Layer Deposition: From Heavily n-Type to p-Type Material. *physica status solidi (b)*, 257(2):1900472, 2020.

[133] M. Napari, M. Lahtinen, A. Veselov, J. Julin, E. Østreng, and T. Sajavaara. Room-temperature plasma-enhanced atomic layer deposition of ZnO: Film growth dependence on the PEALD reactor configuration. *Surface and Coatings Technology*, 326:281–290, 2017.

[134] R. Peter, K. Salamon, A. Omerzu, J. Grenzer, I. J. Badovinac, I. Saric, and M. Petravic. Role of Hydrogen-Related Defects in Photocatalytic Activity of ZnO Films Grown by Atomic Layer Deposition. *The Journal of Physical Chemistry C*, 124(16):8861–8868, 2020.

[135] E. Przezdziecka, E. Guziewicz, D. Jarosz, D. Snigurenko, A. Sulich, P. Sybilski, R. Jakiela, and W. Paszkowicz. Influence of oxygen-rich and zinc-rich conditions on donor and acceptor states and conductivity mechanism of ZnO films grown by ALD-Experimental studies. *Journal of Applied Physics*, 127(7):075104, 2020.

[136] H. K. Park, B. S. Yang, S. Park, M. S. Kim, J. C. Shin, and J. Heo. Purge-time-dependent growth of ZnO thin films by atomic layer deposition. *Journal of Alloys and Compounds*, 605:124–130, 2014.

[137] H. Wang, Z. Wang, X. Xu, Y. Liu, C. Chen, P. Chen, W. Hu, and Y. Duan. Multiple short pulse process for low-temperature atomic layer deposition and its transient steric hindrance. *Applied Physics Letters*, 114(20):201902, 2019.

[138] T. Muneshwar and K. Cadien. AxBAxB... pulsed atomic layer deposition: Numerical growth model and experiments. *Journal of Applied Physics*, 119(8):085306, 2016.

[139] H. Salami, A. Poissant, and R. A. Adomaitis. Anomalously high alumina atomic layer deposition growth per cycle during trimethylaluminum under-dosing conditions. *Journal of Vacuum Science & Technology A*, 35(1):01B101, 2017.

[140] S. F. Nelson, D. H. Levy, L. W. Tutt, and M. Burberry. Cycle time effects on growth and transistor characteristics of spatial atomic layer deposition of zinc oxide. *Journal of Vacuum Science & Technology A*, 30(1):01A154, 2012.

[141] N. Nandakumar, B. Dielissen, D. Garcia-Alonso, Z. Liu, R. Görtzen, W. M. M. Kessels, A. G. Aberle, and B. Hoex. Resistive Intrinsic ZnO Films Deposited by Ultrafast Spatial ALD for PV Applications. *IEEE Journal of Photovoltaics*, 5(5):1462–1469, 2015.

[142] G. P. Gakis, C. Vahlas, H. Vergnes, S. Dourdain, Y. Tison, H. Martinez, J. Bour, D. Ruch, A. G. Boudouvis, B. Caussat, and E. Scheid. Investigation of the initial deposition steps and the interfacial layer of Atomic Layer Deposited (ALD) Al_2O_3 on Si. *Applied Surface Science*, 492:245–254, 2019.

APPENDIX 1 SUPPLEMENTARY FIGURES

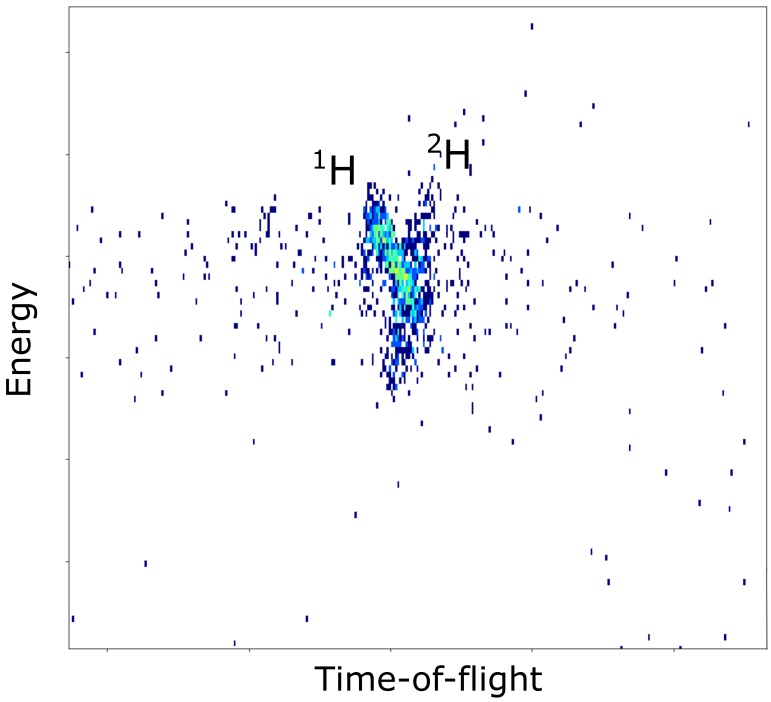

FIGURE 26 Overlapping ToF-E data of ^{1}H and ^{2}H with 10.215 MeV ^{35}Cl beam.

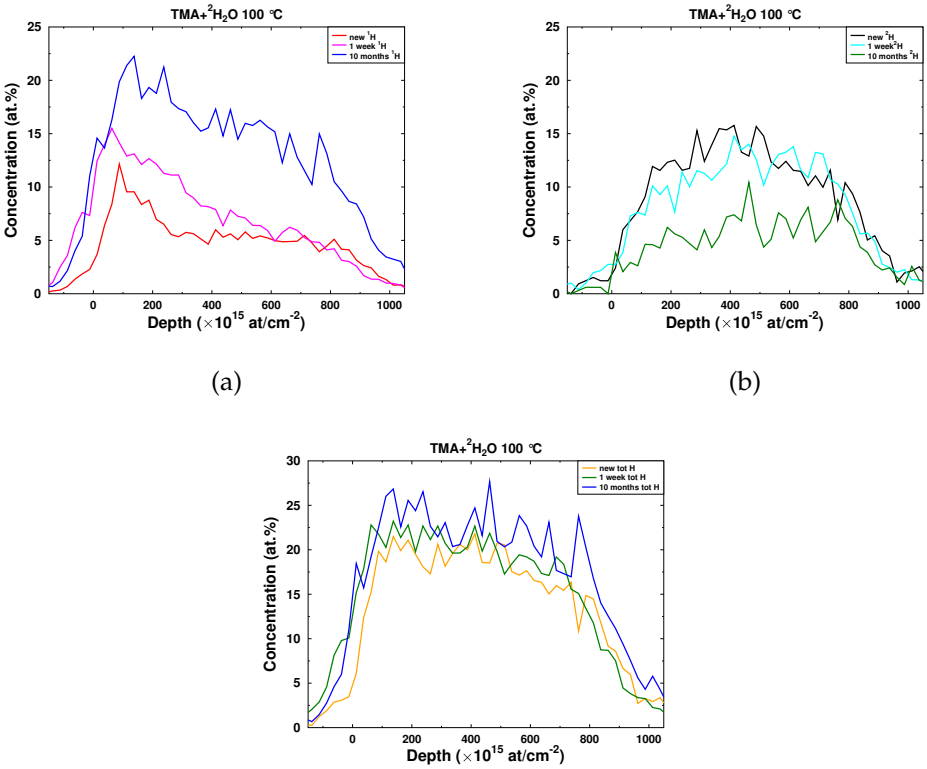

FIGURE 27 Al_2O_3 sample was deposited from TMA and ^2H_2O at 100 °C using 150 ms pulses and 3 s purging making the hydrogen concentration high. The sample was stored in ambient condition and measured again later. The ^1H concentration increased as the ^2H concentration decreased equally. a) Elemental depth profile of ^1H, b) ^2H and c) the sum of ^1H and ^2H presented in a) and b). Reprinted with permission from [PI], Copyright 2021, Elsevier.

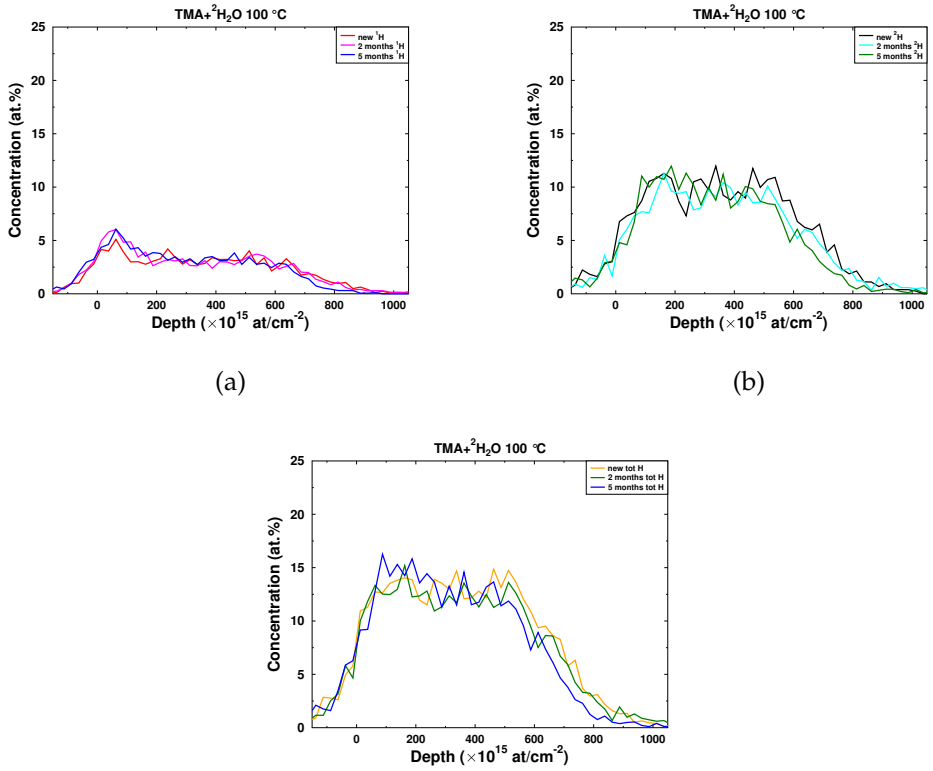

FIGURE 28 Al_2O_3 sample was deposited from TMA and ^2H_2O at 100 °C using 300 ms pulses and 10 s purging and was stored in ambient conditions and measured again later. a) Elemental depth profile of ^1H, b) ^2H and c) the sum of ^1H and ^2H presented in a) and b). Reprinted with permission from [PI], Copyright 2021, Elsevier.

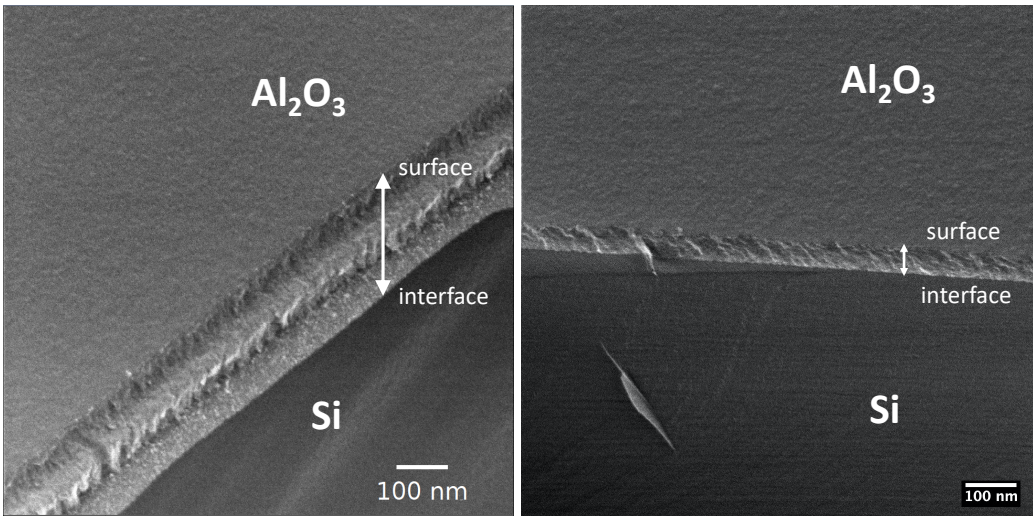

(a) (b)

FIGURE 29 Cleaved 100 nm thick Al_2O_3 film at 30° angle imaged with HIM. a) The film was deposited with TMA and ^2H_2O at 100 °C using 150 ms precursor pulses and 3 s purging. b) The film was deposited with same recipe as in a) but using TMA + $^1H_2^{18}O$. Reprinted with permission from [PI], Copyright 2021, Elsevier.

ORIGINAL PAPERS

PI

Al_2O_3 ALD FILMS GROWN USING TMA + RARE ISOTOPE $^2H_2^{16}O$ AND $^1H_2^{18}O$ PRECURSORS

by

S. Kinnunen, K. Arstila and T. Sajavaara

Applied Surface Science, 546 (2021), 148909

Applied Surface Science 546 2021) 148909

Contents lists available at ScienceDirect

Applied Surface Science

journal homepage: www.elsevier.com/locate/apsusc

Full Length cle

l 2O3 ALD films grown using TMA + rare sotope $^{2}H_{2}^{16}O$ and $^{1}H_{2}^{18}O$ precursors

S. Kinnunen *, K. rstila, T. Sajavaara

Department Physics, University Jyvaskyla, P. O. Box 35, FI-40014 University Jyvaskyla, Finland

A R T I C L E I N F O

Keywords:
LD
l 2O3
Low emperature
Heavy water
Hydrogen migration
TMA

B S T R A C T

In his work hydrogen and oxygen migration and exchange reactions n the atomic layer deposited (ALD) Al_2O_3 thin films were studied together with ydrogen incorporation by varying deposition parameters. l 2O3 films deposited at low temperatures can contain more than 20 at.% of ydrogen. Both higher temperature and longer purge length decrease the hydrogen and carbon concentrations significantly. In order to ack the hydrogen and oxygen movement n he films, heavy water ($^{2}H_{2}^{16}O$) and oxygen-18 enriched water ($^{1}H_{2}^{18}O$) were used as precursors in combination with trimethylaluminium (TMA). Different sotopes of he same element were quantified by means of time-of-flight elastic recoil detection analysis (ToF-ERDA). It was found out at $^{1}H/^{2}H$ exchange eactions take place even at room emperature f e hydrogen concentration s high enough. On he other and, oxygen atoms n the films do not migrate notably.

1. Introduction

Atomic layer deposited (ALD) amorphous aluminium oxide (Al_2O_3) is both extensively used and much s udied hin film material. Alumina films have been studied, for example, as a high-k material for semiconductor ndustry [1–3] as well for gas permeation barriers [4–6]. There are numerous ALD processes for Al_2O_3 but especially e process with trimethylaluminium (TMA) and water as precursors s widely studied (www.atomiclimits.com ALD database mentions almost 300 articles as to date [7]) and e reaction mechanism is also believed to be quite well understood [8,9].

One early identified application for amorphous ALD-oxide films has been o use it for moisture and gas permeation barriers [10]. Thin moisture barriers are needed n packaging materials where flexibility of the barrier s of mportance. Another example is organic light emitting diodes (OLED) which equire ransparent moisture barrier. OLEDs a e known to be sensitive to water vapour and oxygen, and in o der to n-crease heir lifespan diffusion of hese gases must be prevented [11]. When considering gas and moisture barriers, atomic layer deposi on is an deal deposition method. Due o the self erminating reactions of LD, conformal and pinhole-free films can be grown even on complex and porous substrates [12,13]. It s also possible to deposit e ALD-films at low temperatures equired by he organic substrates. Therefore coating polymers with e ALD is an attractive option.

LD thin films often contain significant amounts of ydrogen, especially when grown at low deposition temperatures. In addition o water vapour [4] and oxygen [6], also ydrogen can cause degradation for example in capacitors components [14]. l 2O3 thin films along with other LD-oxides have been studied as H_2 barriers for this purpose and has been s own at the diffusion of ydrogen to a capacitor dielectric material decreases s gnificantly if a protective ALD film s appl ed [15]. However, in some applications ydrogen is a desirable element n e film. Hydrogen from e ALD capping film can, for example, passivate the Si-interface n solar-cells by binding to dangling bonds which are responsible for the charge carrier ecombination esulting in suboptimal energy conversion efficiency [16].

Metal–organic ALD precursors are frequently used and the organic ligands very often contain ydrogen. In addition, ydrogen containing coreactants such as $^{1}H_2O$ and NH_3 are extensively used for depositing oxides and n des, espectively. Therefore ydrogen is a common m-purity in all thin films but it s quite often disregarded because only a few measuring techniques, such as elastic recoil detection analysis (ERDA) and secondary ion mass spectrometry (SIMS), can directly detect hydrogen atoms n he films. The advantage of ERDA and especially time-of-flight ERDA (ToF-ERDA) over SIMS s he possibility of quantative elemental depth profiling [17].

For example n he case of TMA and $^{1}H_2O$ process both precursors contain ydrogen that can be ncorporated n he film. l 2O3 can be deposited from he TMA and water at as low as 33 °C but e mpurity contents a e en very gh [18]. In o der to decrease e esidual

* Corresponding author.

ps://doi.org/10.1016/j.apsusc.2020.148909
Received 17 August 2020; Received n revised form 17 December 2020; Accepted 30 December 2020
Available online 21 January 2021

ydrogen concentration n Al_2O_3 films, one can ncrease the deposition emperature [19]. Alternatively, post deposition annealing can also be used o decrease e hydrogen content [20]. On he other and, many of the applications equiring gas barriers involve polymers or other o ganic substrates and elevated temperatures can not be used during or after e deposition.

The use of precursors containing rare s able sotopes can g ve nformation not only on reaction mechanism but also on sources of impurities n the films. For example, ydrogen as two stable sotopes, ^1H (99.985%) and ^2H (0.015%) [21] and n he following ext ydrogen efers o ^1H and deuterium o ^2H. Similarly, water efers o ^1H_2O and heavy water to ^2H_2O.

Deuterated precursors ave been used n various s udies [9,19,22,23]. By using heavy water instead of water in TMA + ^1H_2O process the source of ydrogen impurity can be detected. I is often presumed that as he elements do not c ange, heavy water can be treated as equivalent to normal water [9,24,25].

These isotope studies ave given detailed information on eacti on mechanism and TMA + H_2O process [9,19,25] is probably the most widely studied ALD process. That said, even e reason of he most important aspect of ALD – the self terminating reaction – in the case of this process is still under debate. Saturation of e eaction is often contributed o he steric hindrance of the ligands which popula e e surface so at e reactive sites are blocked [9,26]. On he other and, Vandalon et al. propose at the steric hindrance can not be e sole cause of erminating reaction. Their claim s that non-reactive methyl groups cause eactions to stop at least n he lower emperatures [25]. However, there are open questions such as why he persistent -CH_3 groups are not ncorporated n he film as a carbon impurity since e deposited films contain only a small concentration of carbon even at low deposition emperatures [25,27].

In his work we studied ow ydrogen is ncorporated n he films. In addition, he migration of ydrogen (and oxygen) n he films is s udied. In o der o do so, both heavy water (^2H_2O) and oxygen-18 (natural abundance 0.2% [21]) enriched water ($H_2^{18}O$) were used as oxygen sources. The effect of d fferent ALD conditions, such as the deposition temperature and purge lengths, were also studied. It was found at e impurities decrease with increasing deposition temperature. In addition, the migration of ydrogen was only detected f hydrogen concent ation n he film was gh.

. Experimental details

l $_2O_3$ films were deposited using Beneq TFS 200 side flow eactor. Nitrogen from Inmatec PN 1150 nitrogen generator (99.999%) was used as a carrier gas as well as for purging between he precursor pulses. Pressure during the deposition n e reaction chamber was 1–2 mbar. TMA (Strem >98%) was used as an aluminium source for he process. Three types of water were used as an oxygen source: normal wate $^1H_2^{16}O$, heavy water $^2H_2^{16}O$ (Medical Isotopes Inc. 99.99%) and oxygen-18 enriched water $^1H_2^{18}O$ (Medical Isotopes Inc. 97%). Deposition emperature was varied between 70 °C and 250 °C. Pulse lengths for both precursors were kept constant at 300 ms which is double e time for our ypical l_2O_3 processes. The longer pulse length was used o ensure a complete saturation of he substrate surfaces. Purging time was n most depositions 10 s after both precursor pulses but the effect of the purging time was also investigated and en t was varied between 3 and 60 s. ll films were deposited on n-type (100) silicon chips cut from a b gger wafer with native S O_x layer. Sample pieces were distributed in f ont, back and sides of e eactor in order o ensure film conformality all over e reactor. To minimise H-contamination prior he TMA + ^2H_2O deposition, e eactor was treated with 50 ^2H_2O pulses (150 ms).

As-deposited samples were also exposed o elevated temperature and humid conditions by storing em n a climate chamber (Weiss WK3-180/40) for 24 or 48 h at 60 °C and n 80% elative umidity (RH) at atmospheric pressure.

The elemental composition and depth profiles of he films were measured with a time-of-flight elastic recoil detection analysis (ToF-ERDA) using 11.915 MeV $^{63}Cu^{6+}$ ons [28]. Recoiled species were detected at 41° angle using mirror measuring geometry. Analysis and elemental depth profiles were made with Potku analysis software [29]. Surface and nterface egions of the films were excluded f om e elemental analysis and compositions were calculated from he bulk of the film.

l $_2O_3$ films were investigated with elium ion microscopy (HIM) (Zeiss Orion Nanofab) n order o study the porosity of he films.

Thicknesses of he films were measured with Rudolph AUTO EL III ellipsometer with 632.8 nm laser.

3. Results and discussion

The deposition rate decreases about one hird when normal water is changed o ^2H_2O as seen n e Fig. 1a when every other parameter s kept constant. Similar decrease in growth-per-cycle (GPC) is eported by Hiraiwa et al. [24]. This s most probably due to the kinetic sotope effect, which is utilised for example in c emical eaction mechan sm studies [30]. This effect aises he activation energy of e reaction and erefore educes e eaction rate which could explain e results. s mentioned n he Introduction, e interchangeability of ^1H_2O and ^2H_2O is often assumed. On the other and, one can not ule out at e changes in activation energies can also change he probabilities of different reaction paths making some paths more favourable han o ers compared to situation with normal water. For example reaction w e TMA and oxygen bridge site (.e. l–O– l) [31] does not nvolve deuterium which may favour his eaction oute f e eaction rate with O^{2}H-groups s decreased.

The GPC of he TMA + ^1H_2O process has been eported to ncrease as a function of he deposition emperature aving e highest GPC a 200–300 °C depending on the source [22,24,32,33]. Our results are compareable and he growth ate s arts to decrease between 200 and 250 °C (Fig. 1a). This as been attributed o he decrease of reactive OH-sites due to dehydration [25,33]. On he other and, deposition with ^2H_2O changes the situation so at the growth ate continues o increase even at 250 °C and approaches en he GPC of e ^1H_2O process. I seems at the extra energy f om e higher emperature drives e eaction more han what the dehydration slows it. When considering purging times (Fig. 1b), it seems at he purging length does not play a significant role n ^1H_2O process at 100 °C, but longer purging increases the GPC slightly n ^2H_2O process. This s another ndication of slower eaction ates due o the isotope effect.

Composition and elemental depth profiles of he samples were produced from coincidence me-of-flight and energy data (Fig. 2). Elemental composition of all the samples can be found n Supplementary (Table .1 and .2) .

l $_2O_3$ films grown at low emperatures end o have oxygen ch composition and the O/Al atio closes o the stoichiometric value of 1.5 only at 200 °C and above [9,18,34]. Our similar results are shown n Fig. 3a. Also purging time c anges the O/Al atio of films deposited a 100 °C (Fig. 3b) although even he 60 s long purging time produces O-rich film. Even ough the GPC decreases when he oxygen source s changed from ^1H_2O o ^2H_2O (Fig. 1a), it does not affect e ratio between the main components of he film. In s egard, using ^2H_2O instead of ^1H_2O is well justified.

While O/Al atio is ndependent of he oxygen precursor, ere is a difference n the amount of ydrogen ncorporated n he films (Fig. 4a). Films deposited with heavy water end o have slightly gher otal amount of ^1H and ^2H compared o hydrogen content n he films deposited with normal water. In earlier s udies he equivalence between the use of ^1H_2O or ^2H_2O have been justified by s milar otal ydrogen concentrations [9,19]. Somewhat similar esults to ours, with gher otal ydrogen when ^1H_2O was replaced with ^2H_2O, were obtained by

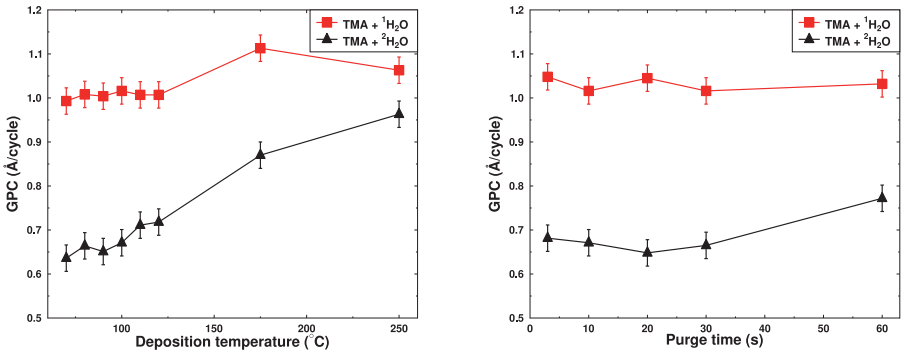

(a) (b)

Fig. 1. a) Growth-per-cycle as a function of he deposition temperature. Films were deposited using 300 ms precursor pulses and 10 s N_2 purges between he pulses. b) Growth-per-cycle of he films deposited at 100 °C. Nitrogen purge was varied between 3 and 60 s.

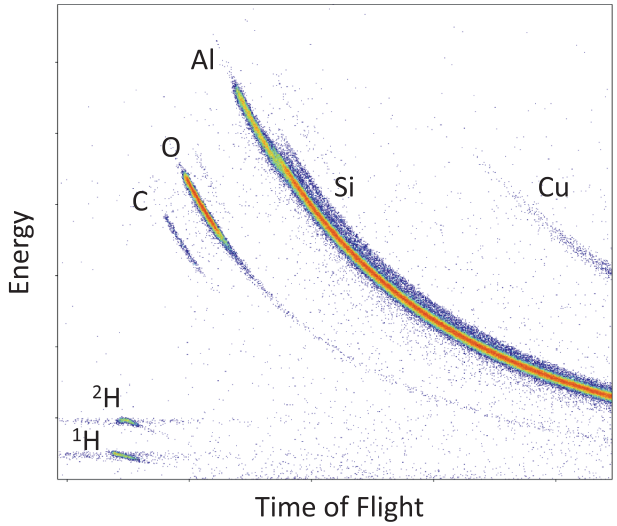

Fig. . Coincidence time-of-flight and energy histogram of a ToF-ERDA measurement. Elements and sotopes differentiate according o ei r masses. Film was deposited using 1000 cycles of TMA and ^2H_2O at 100 °C. Scattered ^{63}Cu beam used for he measurement is also visible.

Hiraiwa et al. [24]. However, their conclusion was at the difference s not significant and can be neglected. Nevertheless, e otal ydrogen concentration follows a similar trend with both oxygen precursors even ough he use of ^2H_2O esults in somewhat gher otal ydrogen concentration an ^1H_2O.

The deposition temperature plays a major ole n ydrogen incorporation n LD-Al $_2O_3$ films. gh emperatures e hydrogen concentration decreases as s own n Fig. 4a and goes below 5 at.% only above 175 °C. The main ydrogen source s from water s nce ere s more deuterium an ydrogen n he film when he deposition temperature s gher han 70 °C. I is notable at in our s udy the majority ydrogen isotope changes from ydrogen to deuterium between 70 and 80 °C. Films deposited at 70 °C, based on visual nspection as well as with thickness profiles given by he ellipsometer, appeared completely fine; films were uniform n hickness all around e reactor and visually looked s milar to ones deposited at gher emperatures. When e deposition temperature was decreased o 60 °C clear signs of CVD-growth were observed (See Supplementary .7) for the TMA + ^2H_2O process. Films deposited with ^1H_2O were uniform. The drastic change n ^1H and ^2H composition at 70 °C would herefore be an ndication of CVD component n e reaction. I is known [18] that water molecules physisorpt o "cold" surfaces and require long pumping (i.e. purging) time. If the purging time is not sufficient, physisorption leads to higher than monolayer surface concentration of ^1H_2O or OH which is s ll present when TMA s pulsed o e reactor. However, as seen n Fig. 4a, the deuterium concentration drops significantly at 70 °C, ndicating at deuterium from water s not ncorporated n he film n large quantities.

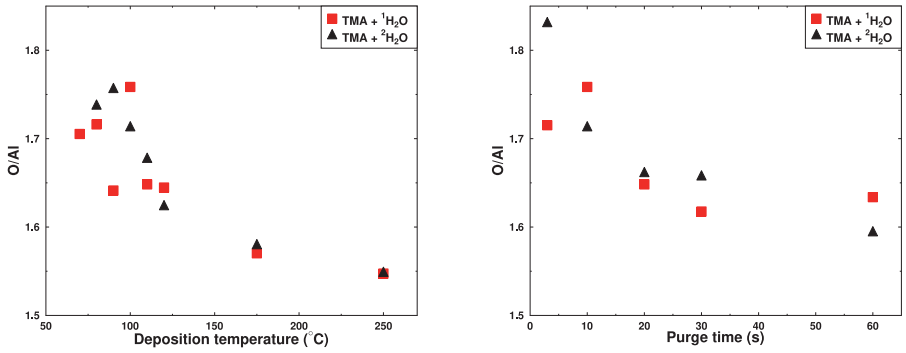

(a) (b)

Fig. 3. a) O/Al ratio as a function of he deposition temperature. Samples were deposited using 300 ms precursor pulses and 10 s purging. b) O/Al atio as a function of he purging time. Samples were deposited at 100 °C.

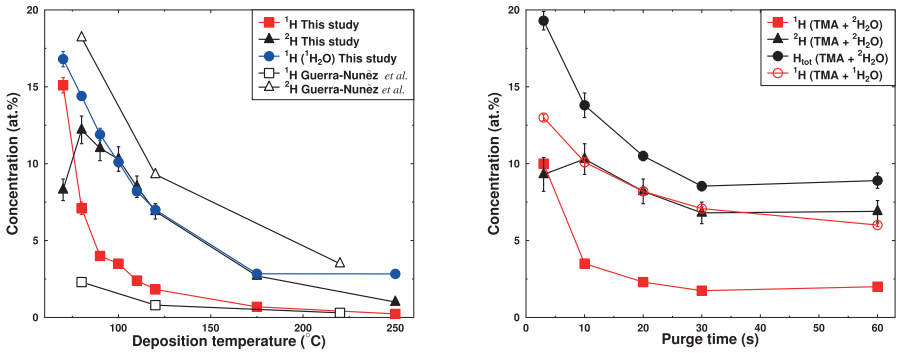

(a) (b)

Fig. 4. a) ^{1}H and ^{2}H impurity concentrations at different deposition temperatures. Films were deposited using 300 ms precursor pulses and 10 s pu ging mes. Comparison to Guerra-Nunẽz et al. [9] is also shown. b) ^{1}H and ^{2}H concentrations as a function of purge ime. Deposited at 100 °C using 300 ms precursor pulses.

In addition, CVD-growth would ncrease he GPC which was not observed at 70 °C (Fig. 1a). This can be explained by he studies of Vandalon et al. [22,25] where they s owed at ere is a certain emperature limit where water is not eactive enough owards the CH_3-groups at the substrate surface which leaves excessive amount of persistent CH_3-groups n he film. As Vandalon et al. pointed out, also simulations suggest at e isolated CH_3-groups ave gher eaction barrier compared o he multiple methyl g oups in close proximi y o each o er [35]. These isolated unreactive methyl groups could be e source of e gh hydrogen concentration n he film deposited at 70 °C.

As seen n Fig. 5a and b, he carbon concentration follows very similar end o e hydrogen concentration and decreases with e increasing deposition temperature and purge length. Carbon concenation is not high even at low emperatures and he use of ^2H_2O nstead of ^1H_2O does not ave a significant effect on carbon concentration. However, emains as an open question what appens o the carbon since even at 70 °C the amount of carbon n he films is only 2.3±0.2 at. % (Fig. 5a). If ydrogen would be n he film n the form of methyl groups we should expect carbon concentration to be closer to 5 at.%. Same observation was done by Vandalon et al. and hey proposed at these methyl groups can eact with water in subsequent cycles.

Comparison of ^{1}H and ^{2}H impurities with previous work by Guerra-Nunẽz et al. s made also n Fig. 4a. General trends are similar although our esults show slightly higher deuterium content but somewhat lower ydrogen ncorporation. ll our samples n Fig. 4a are deposited with 300 ms precursor pulses and 10 s N_2 purges while Guerra-Nunẽz et al. used 1 s pulses, 2 s exposure time and 60 s purging. While this long LD cycle can mprove he film quality, it also makes he deposition very long and maybe impractical for industrial purposes.

The length of he purge has a significant effect on e hydrogen ncorporation n he film as seen n Fig. 4b. Both e hydrogen and deuterium concentration decrease as the purging mes increases. Although deposited films are conformal n hickness (less than 2% variation over he area of e reactor) even with the shorter purging times, and herefore seem o represent pure and self-limiting LD-growth, the films are far from dentical. Reactions are observed o go o completion at quite slow ate at low emperatures, equiring 30 s purging even as high as at 100 °C before e hydrogen concentration saturates. S milar rend s observed for ^1H_2O process which is somewhat surprising since the GPC does not change with increasing purging mes (Fig. 1b).

The mass gain per cycle is a more direct indication of slow reaction rate and desorption of eaction species at low emperatures compared o measuring only GPC, as films with similar thickness can ave different mass density. It s shown on quartz crystal microbalance (QCM) studies at the mass gain per cycle decreases as he purging times are inc eased at low emperatures [18,36]. In addition, he mass loss after he precursor pulse can continue for ens of seconds ndicating at e eactions a e slow and e desorption of eaction products and physisorbed surface species equire long purging times at low emperatures. This supports our finding that long purging times decrease hydrogen, carbon and excess oxygen content n e film.

This purging time ssue is one example of a sources of nconsis ency n LD research pointed out by Sønsteby et al. n e recent paper [37]. They address the problems on LD reproducibility and relate, fo example, gher han expected GPC to short purging times possibly

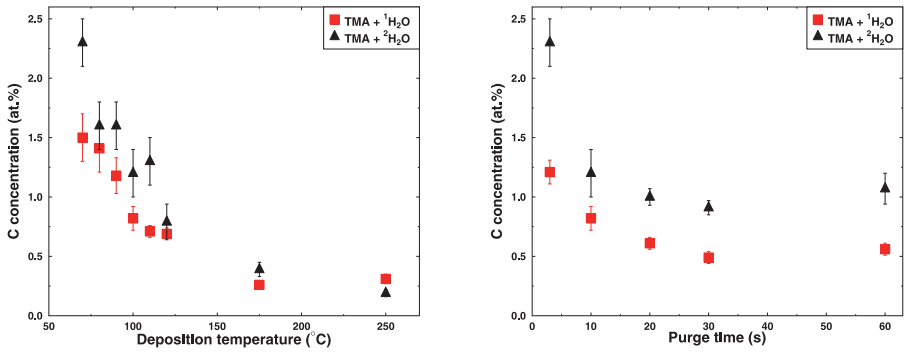

(a) (b)

Fig. 5. a) Carbon concentration of films deposited at different temperatures using 300 ms pulses and 10 s purging times. b) Carbon concentration as a function of purging times, films were deposited at 100 °C using 300 ms pulses.

leading to CVD like growth. This s all true, but looking only at the GPC does not guarantee at e results are comparable as we have s own above. Even if purging times are adequate o produce conformal films, purging can be short enough o also c ange he composition of he film as seen n Fig. 4b even f the GPC does not change (See Fig. 1b). In addition, e reactor used will nfluence e required purging (and pulsing) imes. Details, such as vacuum level, reactor geometry and gas flows will have an effect on deposition and film growth. I is mportant o note s ssue when comparing e results obtained by he different groups. This ssue is most pronounced at low emperatures. As seen n Fig. 4a, our esults are somewhat different compared o hose measured by Guerra-Nuñez et al. The difference between our and heir esults is of order of a few at.% which is larger an he margin of error. T erefore the discrepancy must come from he different pulsing and purging mes, reactor geometry and deposition pressure, and it s important o report all the deposition parameters n order o compare e results reliably.

We also studied the hydrogen migration in the Al_2O_3 films. A depth profile of an as-deposited TMA + ^2H_2O film s presented n Fig. 6a). The films were deposited using 150 ms precursor pulses and 3 s purging at 100 °C which makes em ydrogen rich. In Fig. 6b) he same film s shown after 24 h exposure n a climate chamber. The conditions n e chamber were kept constant at 60 °C and at 80% elative umidity. fter e eatment the deuterium concentration was dramatically decreased and at the same me the concentration of ^1H ad increased equally keeping e total amount of elemental ydrogen constant. This can be explained by e hydrogen exchange eactions. Hydrogen in water vapour and gaseous H_2 can exchange ydrogen atoms with e mpurity ydrogen/deuterium n the film. Since the natural abundance of deuterium (0.02%) is much lower an e atio n hese films, e percentage of e ^2H drops due o these exchanges. Interestingly, e exchange does not appen only at the surface but also all the way ough e 80 nm hick films. T s equires migration of ydrogen for rather long distances even n these low emperature annealing conditions. Other possibility s at the film s porous and gases penetrate e film easily.

However, ere is a hreshold for ydrogen concentration at s needed for he exchange eaction to proceed ough he whole film. Sample deposited at 100 °C with 300 ms pulses and 10 s purging mes contain ~15 at.% of otal ydrogen (^1H + ^2H). When his sample s exposed to climate chamber conditions, there are no major changes n either hydrogen or deuterium concentrations (See Supplementary .9).

We can observe n Fig. 6a that both ^1H and ^2H are unevenly distributed n he film. There is more ^1H at he surface and more ^2H at e interface. This s an example of a similar exchange eaction at happens also at oom emperature n air given enough ime (1 day) between e deposition and characterization (see Supplementary Fig. .8). Therefore data shown n Figs. 1, 3, 4 and 5 were measured from he samples hat were kept in a load-lock under a vacuum condition (<1 mbar) until exposed o a very briefly just before e characterization.

It s known based on IR-studies at e ydrogen impurities n LD- l $_2O_3$ films are found at least in the form of OH-groups [38,39]. Signal from OH stretching has been shown o increase as e hydrogen content of he film ncreases, supporting the claim at ydrogen is found n e films in form of OH-groups [38]. Films deposited at low emperature a e also oxygen ch nting at there are undercoordinated oxygen atoms.

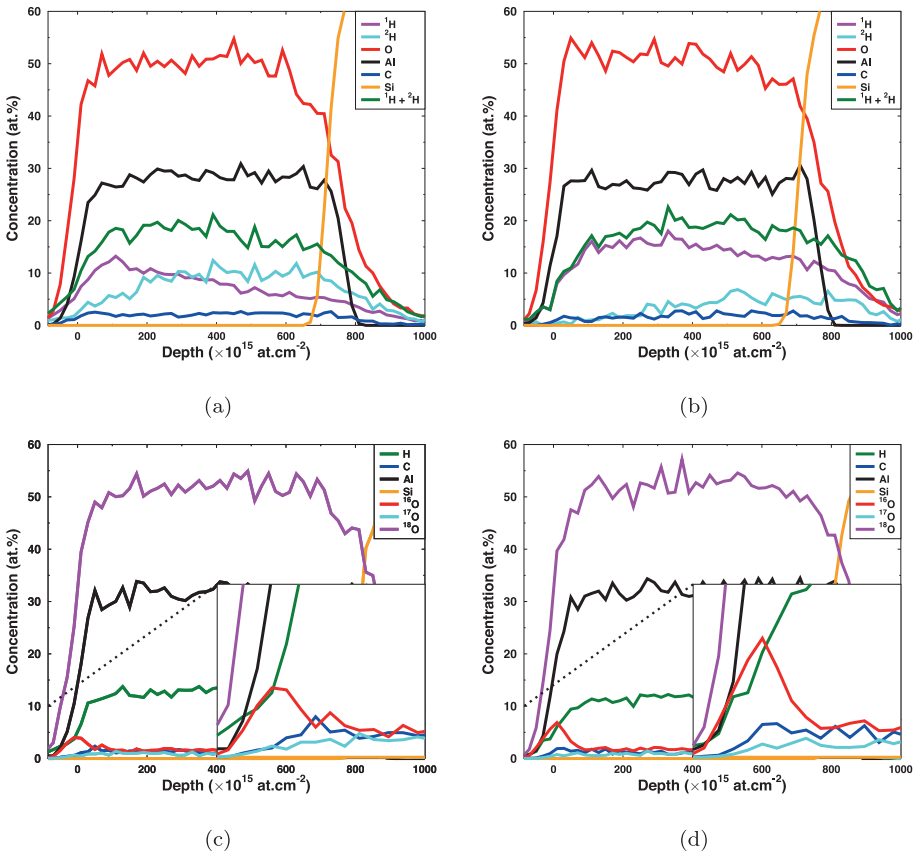

Fig. 6. Elemental depth profiles of l_2O_3 films deposited at 100 °C with 150 ms precursor pulses and 3 s purging. a) As-deposited film using TMA and ^2H_2O. T e sample was kept at room emperature in air for one day before he characterization. b) The same film as in a) but after 24 h at 60 °C and 80% RH. c) As-deposited film using TMA and $H_2^{18}O$. The sample was kept for one day at room temperature n air before the characterization. d) The same film as in c) but after 48 n 60 °C and 80% RH.

Relatively low carbon concentration rules out the speculation at e majority of e ydrogen would be n e form of CH_3-groups. Furthermore, in the films grown with TMA + ^2H_2O, ^2H atoms are most likely bound o oxygen as they originate f om e water.

In order o see f e hydrogen migration is elated o he movement of he whole OH-group or f ere is any oxygen diffusion from e ambient present, films using TMA and $H_2^{18}O$ as precursors were deposited. The depth profile of an as-deposited film grown at 100 °C is presented n Fig. 6c). We see that oxygen-18 enriched water produces films that contain less ydrogen an he films deposited with ^2H_2O. However, hydrogen concentration n Fig. 6c is comparable o he samples deposited with ^1H_2O. This s expected since small change n oxygen mass does not ave a great effect on the activation energy and herefore kinetic isotope effect is not noticeable. fter 48 n he climate chamber at 60 °C and at 80% RH the films show only very minor difference at the surface as seen n Fig. 6d). Inside the film he amount of oxygen-18 does not c ange, ndicating that oxygen even in OH-groups can not efficiently exchange with oxygen from O_2 or H_2O at similar rate compared o hydrogen. This ndicates that only ydrogen is m grating n he film, not whole OH-groups. F om e esults it s also clear at the oxygen at s bonded o aluminium does not exchange with oxygen atoms from O_2 or ^1H_2O molecules.

Dingemann et al. s owed at hydrogen effuses from e l $_2O_3$ films n he form of both H_2 and ^1H_2O when annealed at 200 to 1000 °C n high vacuum (10^{-7} mbar) conditions [20]. That process, owever, must be different compared to process reported n this paper. The gh emperature annealing removes and so decreases he amount of hydrogen n the films. Here we observe only an (isotope) exchange eaction and e total amount of ydrogen n he film does not change. Considering at e $^1H/^2H$-exchange eaction is chemically similar o the H/H-exchange, it s clear at e hydrogen moves ough the films easily f the film as been deposited at low emperature and as gh hydrogen content. Hydrogen diffusion studies done by Cameron et al. with adioact ve ydrogen sotope tritium (^3H) s ow at hydrogen can d ffuse ough also n atomic form [40], which is n agreement with our findings.

Porosity of he film could ncrease both he efficiency of e hydrogen exchange and ydrogen permeation n he film enabling gases to penetrate and nteract also deeper n the film. Many amorphous LD films are known to be pinhole f ee [4,41] and this was confirmed also here with elium ion microscopy (HIM) (See Supplementary A.10a and .10b). With the nominal HIM esolution of 0.5 nm no detectable porosity could be observed.

4. Conclusions

lthough ALD alumina films have been suggested and used as possible gas barriers, is clear hat at least ydrogen is able o ansport ough the film rather easily in a warm and humid environment if the nitial hydrogen concentration of he film s high. Our esults ndicate at e ydrogen transport proceeds via hydrogen exchange eac ons. Therefore is possible to decrease e ydrogen transport by controlling e amount of hydrogen left in the film during the deposition. T s can be achieved by careful selection of precursors o ncreasing e deposition temperature and using very long purging times. Optionally also post-deposition annealing can be applied. However, the coated material in barrier applications s commonly a polymer, which many imes ules out high deposition temperatures. Longer purges n urn increase e deposition times, possibly by an order of magnitude, which reduces e throughput significantly making e LD-Al $_2O_3$ films as ydrogen permeation barriers not so attractive method.

As demonstrated here, a significant amount of ydrogen is stored in the films and hydrogen can also move ough he film f the concen- ation s high. Oddly enough, this could open opportunities us ng LD- l $_2O_3$ films as proton conductors [42]. ALD also offers various ways o control e hydrogen content and d ffusion.

In o der o study e ydrogen ncorporation n he films, we eplaced ^1H_2O with ^2H_2O. Change of sotope in a molecule should not change he chemistry since the element is not changed. However, n e case of ydrogen, eplacing hydrogen with deuterium doubles the mass of he atom and it affects he film growth. Growth per cycle is decreased and impurity carbon and otal ydrogen ncorporated n he film s ncreased when ^2H_2O is used. On e other and, he ratio between the main components, oxygen and aluminium, s independent of oxygen precursor. While there are differences n he films depending on e oxygen precursor, he general trends are similar and erefore e comparison is justified when done carefully.

It s also noteworthy to keep n mind at in addition to pulsing mes and deposition temperature, purging times affect greatly he film quality and this should be taken nto account especially when comparing esults from different studies. Our work clearly demonstrates hat even ough a quick glance at the samples does not show any difference, e re can be a significant difference n the compositions. If his s the case even with the close o " deal" ALD process of TMA and water, even more care should be taken when nterpreting results obtained with limited c ar- acterization techniques from more demanding processes.

CRediT a thorship contribution statement

S. K nnunen: Investigation, Visualization, Writing - original d aft. **K. Arstila:** Investigation, Writing - eview & editing. **T. Sajavaara:** Supervision, Writing - eview & editing.

Declaration of Competing Interest

The authors declare at ey ave no known competing financial interests or personal elationships that could ave appeared o nfluence the work eported in this paper.

Appendix A. Supplementary material

Supplementary data associated with this article can be found, n e online version, at ps://doi.org/10.1016/j.apsusc.2020.148909 .

References

[1] M. Groner, J. Elam, F. Fabreguette, S. George, Electrical characterization of n l $_2O_3$ films grown by atomic layer deposition on silicon and various me al substrates, Thin Solid Films 413 (2002) 186–197.
[2] R.Y. Khosa, E.B. Thorsteinsson, M. Winters, N. Rorsman, R. Karhu, J. Hassan, E. Sveinbjörnsson, Electrical characterization of amorphous l $_2O_3$ dielectric films on n-type 4H-SiC, IP dv. 8 (2018) 025304.
[3] J. Acharya, J. Wilt, B. Liu, J. Wu, Probing the dielectric properties of ultrathin Al/ l $_2O_3$/Al trilayers fabricated using in situ sputtering and atomic layer deposition, CS Appl. Mater. Interf. 10 (2018) 3112–3120. PMID: 29293311.
[4] P.F. Carcia, R.S. McLean, M.H. Reilly, M.D. Groner, S.M. George, Ca est of l_2O_3 gas diffusion barriers grown by atomic layer deposition on polymers, Appl. Phys. Lett. 89 (2006) 031915.
[5] S.-H.K. Park, J. Oh, C.-S. Hwang, J.-I. Lee, Y.S. Yang, H.Y. Chu, K.-Y. Kang, Ultra thin film encapsulation of organic light emitting diode on a plastic substrate, ETRI Journal 27 (2005) 545–550.
[6] T. Hirvikorpi, M. Vähä-Nissi, T. Mustonen, E. Iiskola, M. Karppinen, tomic layer deposited aluminum oxide barrier coatings for packaging materials, Thin Solid Films 518 (2010) 2654–2658.
[7] omicLimits, ALD database, doi:10.6100/alddatabase, 2020. ps://www.atomi climits.com/alddatabase/.
[8] V. Miikkulainen, M. Leskelä, M. Ritala, R. Puurunen, Crystallinity of norganic films grown by atomic layer deposition: Overview and general trends, J. ppl. Phys. 113 (2013) 021301.
[9] C. Guerra-Nunëz, M. Döbeli, J. Michler, I. Utke, Reaction and growth mechanisms n l_2O_3 deposited via atomic layer deposition: Elucidating e hydrogen source, Chem. Mater. 29 (2017) 8690–8703.
[10] A.P. Ghosh, L.J. Gerenser, C.M. Jarman, J.E. Fornalik, Thin-film encapsulation of organic light-emitting devices, ppl. Phys. Lett. 86 (2005) 223503.
[11] M. Schaer, F. Nüesch, D. Berner, W. Leo, L. Zuppiroli, Water vapor and oxygen degradation mechanisms n organic light emitting diodes, Adv. Funct. Mater. 11 (2001) 116–121.
[12] M. Ritala, M. Leskelä, J.-P. Dekker, C. Mutsaers, P.J. Soininen, J. Skarp, Perfectly Conformal TiN and l $_2O_3$ films deposited by atomic layer deposition, Chem. Vap. Deposition 5 (1999) 7–9.

[13] I. Iatsunskyi, M. Kempíski, M. Jancelewicz, K. Załeski, S. Jurga, V. Smyntyna, Structural and XPS characterization of LD l $_2O_3$ coated porous silicon, Vacuum 113 (2015) 52–58.
[14] D. Sohrabi Baba Heidary, C.A. Randall, nalysis of he degradation of $BaTiO_3$ resistivity due o ydrogen on incorporation: mpedance spectroscopy and diffusion analysis, Acta Mater. 96 (2015) 344–351.
[15] D. Sohrabi Baba Heidary, W. Qu, C.A. Randall, Evaluating the merit of ALD coating as a barrier against ydrogen degradation in capacitor components, RSC Adv. 5 (2015) 50869–50877.
[16] L. Black, B. van de Loo, B. Macco, J. Melskens, W. Berghuis, W. Kessels, Explorative studies of novel silicon surface passivation materials: considerations and lessons learned, Sol. Energy Mater. Sol. Cells 188 (2018) 182–189.
[17] S. Giangrandi, T. Sajavaara, B. Brijs, K. stila, A. Vantomme, W. Vandervorst, Low-energy heavy-ion TOF-ERDA setup for quantitative depth profiling of n films, Nucl. Instrum. Methods Phys. Res., Sect. B 266 (2008) 5144–5150.
[18] M.D. Groner, F.H. Fabreguette, J.W. Elam, S.M. George, Low-temperature l $_2O_3$ atomic layer deposition, Chem. Mater. 16 (2004) 639–645.
[19] M. Juppo, A. Rahtu, M. Ritala, M. Leskelä, In situ mass spectrometry study on surface eactions n atomic layer deposition of l_2O_3 thin films from trimethylaluminum and water, Langmuir 16 (2000) 4034–4039.
[20] G. Dingemans, F. Einsele, W. Beyer, M.C.M. van de Sanden, W.M.M. Kessels, Influence of annealing and l $_2O_3$ properties on e hydrogen-induced passivation of he Si/SiO_2 interface, J. ppl. Phys. 111 (2012) 093713.
[21] CIAAW, Isotopic compositions of the elements 2019. Available online at www.ciaaw.org, 2020. URL p://www.ciaaw.org .
[22] V. Vandalon, W.M.M. Kessels, What is limiting low-temperature atomic layer deposition of l_2O_3: a vibrational sum-frequency generation study, Appl. Phys. Lett. 108 (2016) 011607.
[23] G. Dingemans, W. Beyer, M.C.M. van de Sanden, W.M.M. Kessels, Hydrogen induced passivation of S interfaces by l_2O_3 films and SiO_2/Al_2O_3 stacks, ppl. Phys. Lett. 97 (2010) 152106.
[24] A. Hiraiwa, T. Saito, D. Matsumura, H. Kawarada, Isotope analysis of diamond-surface passivation effect of high-temperature H_2O-grown atomic layer deposition-l $_2O_3$ films, J. Appl. Phys. 117 (2015) 215304.
[25] V. Vandalon, W.M.M. Kessels, Revisiting the growth mechanism of atomic layer deposition of Al_2O_3: a vibrational sum-frequency generation study, J. Vacuum Sci. Technol. 35 (2017) 05C313.
[26] R.L. Puurunen, Surface chemistry of atomic layer deposition: a case study for e trimethylaluminum/water process, J. Appl. Phys. 97 (2005) 121301.
[27] O.M. Ylivaara, X. Liu, L. Kilpi, J. Lyytinen, D. Schneider, M. Laitinen, J. Julin, S. li, S. Sintonen, M. Berdova, E. Haimi, T. Sajavaara, H. Ronkainen, H. L psanen, J. Koskinen, S.-P. Hannula, R.L. Puurunen, Aluminum oxide f om trimethylaluminum and water by atomic layer deposition: e temperature dependence of residual stress, Elastic Modulus Hardness Adhesion Thin Solid Films 552 (2014) 124–135.
[28] M. Laitinen, M. Rossi, J. Julin, T. Sajavaara, Time-of-flight – Energy spectrometer for elemental depth profiling – Jyväskylä design, Nucl. Instrum. Methods Phys. Res., Sect. B 337 (2014) 55–61.
[29] K. rstila, J. Julin, M. Laitinen, J. Aalto, T. Konu, S. Kärkkäinen, S. Rahkonen, M. Raunio, J. Itkonen, J.-P. Santanen, T. Tuovinen, T. Sajavaara, Potku – New analysis software for eavy ion elastic recoil detection analysis, Nucl. Instrum. Methods Phys. Res. Section B: Beam Interact. Mater. Atoms 331 (2014) 34–41. 11th European Conference on Accelerators n Applied Research and Tec nology.
[30] M. Gómez-Gallego, M. Sierra, Kinetic sotope effects n he study of organometallic reaction mechanisms, Chem. Rev. 111 (2011) 4857–4963. PMID: 21545118.
[31] R. Puurunen, M. L ndblad, A. Rootc, A. Krausea, Successive eac tions of gaseous trimethylaluminium and ammonia on porous alumina, PCCP 3 (2001) 1093–1102. Cited By 76.
[32] R. Matero, A. Rahtu, M. Ritala, M. Leskelä, T. Sajavaara, Effect of water dose on e atomic layer deposition rate of oxide thin films, Thin Solid Films 368 (2000) 1–7.
[33] G.P. Gakis, H. Vergnes, E. Scheid, C. Vahlas, A.G. Boudouvis, B. Caussat, Detailed investigation of he surface mechanisms and their nterplay wit ansport phenomena in alumina atomic layer deposition from TMA and water, Chem. Eng. Sci. 195 (2019) 399–412.
[34] S.E. Potts, G. Dingemans, C. Lachaud, W.M.M. Kessels, Plasma-enhanced and thermal atomic layer deposition of l_2O_3 using dimethylaluminum sopropoxide, $[Al(CH_3)_2(\mu\text{-O Pr})]_2$, as an alternative aluminum precursor, J. Vacuum Sci. Technol. 30 (2012) 021505.
[35] M. Shirazi, S.D. Elliott, Cooperation between adsorbates accounts for he activation of atomic layer deposition reactions, Nanoscale 7 (2015) 6311–6318.
[36] R.A. Wind, S.M. George, Quartz crystal microbalance studies of l $_2O_3$ atomic layer deposition using trimethylaluminum and water at 125 °C, J. Phys. Chem. A 114 (2010) 1281–1289. PMID: 19757806.
[37] H.H. Sønsteby, A. Yanguas-Gil, J.W. Elam, Consistency and eproducibil y n atomic layer deposition, J. Vacuum Sci. Technol. 38 (2020) 020804.
[38] V. Verlaan, L.R.J.G. van den Elzen, G. Dingemans, M.C.M. van de Sanden, W.M. M. Kessels, Composition and bonding structure of plasma-assisted LD l $_2O_3$ films, Phys. Status Solidi C 7 (2010) 976–979.
[39] A. Dillon, A. Ott, J. Way, S. George, Surface chemistry of l_2O_3 deposition using l $(CH_3)_3$ and H_2O in a binary reaction sequence, Surf. Sci. 322 (1995) 230–242.
[40] A.A. Dameron, S.D. Davidson, B.B. Burton, P.F. Carcia, R.S. McLean, S.M. George, Gas diffusion barriers on polymers using multilayers fabricated by l $_2O_3$ and apid SiO_2 atomic layer deposition, J. Phys. Chem. C 112 (2008) 4573–4580.
[41] .I. Abdulagatov, Y. Yan, J.R. Cooper, Y. Zhang, Z.M. Gibbs, A.S. Cavanagh, R. G. Yang, Y.C. Lee, S.M. George, Al_2O_3 and TiO_2 atomic layer deposition on copper for water corrosion esistance, CS Appl. Mater. Interf. 3 (2011) 4593–4601. PMID: 22032254.
[42] H. Zhang, L. Guo, Q. Wan, Nanogranular l_2O_3 proton conducting films for low-voltage oxide-based omojunction n-film ransistors, J. Mater. Chem. C 1 (2013) 2781–2786.

PII

HYDROGEN AND DEUTERIUM INCORPORATION IN ZnO FILMS GROWN BY ATOMIC LAYER DEPOSITION

by

S. Kinnunen, M. Lahtinen, K. Arstila and T. Sajavaara

Coatings 11, (2021), 542

coatings

MDPI

Article

Hydrogen and Deuterium Incorporation in ZnO Films Grown by Atomic Layer Deposition

Sami Kinnunen[1,2,*], Manu Lahtinen [3], Kai Arstila [1,2] and Timo Sajavaara [1,2]

[1] Department of Physics, University of Jyvaskyla, P.O. Box 35, FI-40014 Jyväskylä, Finland; kai.arstila@jyu.fi (K.A.); timo.sajavaara@jyu.fi (T.S.)
[2] Nanoscience Center, University of Jyvaskyla, P.O. Box 35, FI-40014 Jyväskylä, Finland
[3] Department of Chemistry, University of Jyvaskyla, P.O. Box 35, FI-40014 Jyväskylä, Finland; manu.k.lahtinen@jyu.fi
* Correspondence: samantki@jyu.fi

Abstract: Zinc oxide (ZnO) thin films were grown by atomic layer deposition using diethylzinc (DEZ) and water. In addition to depositions with normal water, heavy water (^2H_2O) was used in order to study the reaction mechanisms and the hydrogen incorporation at different deposition temperatures from 30 to 200 °C. The total hydrogen concentration in the films was found to increase as the deposition temperature decreased. When the deposition temperature decreased close to room temperature, the main source of impurity in hydrogen changed from ^1H to ^2H. A sufficiently long purging time changed the main hydrogen isotope incorporated in the film back to ^1H. A multiple short pulse scheme was used to study the transient steric hindrance. In addition, the effect of the storage of the samples in ambient conditions was studied. During the storage, the deuterium concentration decreased while the hydrogen concentration increased an equal amount, indicating that there was an isotope exchange reaction with ambient H_2 and/or H_2O.

Keywords: ZnO; ALD; heavy water; diethylzinc; ToF-ERDA

Citation: Kinnunen, S.; Lahtinen, M.; Arstila, K.; Sajavaara, T. Hydrogen and Deuterium Incorporation in ZnO Films Grown by Atomic Layer Deposition. *Coatings* **2021**, *11*, 542. https://doi.org/10.3390/coatings11050542

Academic Editor:Alessio Lamperti

Received: 28 March 2021
Accepted: 29 April 2021
Published: 3 May 2021

1. Introduction

Atomic layer deposition (ALD) is a thin film deposition technique that is widely adopted in integrated circuits [1] and other modern devices such as in organic light emitting diodes (OLEDs) [2] and perovskite solar cells [3]. Unique to ALD is its ability to control the film thickness with subnanometer precision and to produce a conformal film on top of complex three-dimensional objects as well as on porous substrates [4,5].

Zinc oxide, ZnO, is an optically transparent wide band gap semiconductor ($E_g \sim 3.3$ eV) [6]. The electrical properties of ZnO can be tailored with doping, which makes it a versatile material for numerous applications [7]. The unique assets of ALD have attracted the attention of ALD-grown ZnO films for various applications. For example, the excellent conformality enables the deposition of ZnO on high surface area powders used in catalysis [8]. Doped ZnO can be used as transparent conductive oxide (TCO) for optoelectronics [9] and ZnO can be deposited at near room temperature [6,10–13], making ALD a suitable deposition method for temperature-sensitive substrates such as polymers. Recently, spatial atomic layer deposition (SALD) has been harnessed for high throughput and large area depositions, making ALD more interesting for industrial use [6]. In addition, ALD ZnO has been studied for its reversible wettability [14,15], and it has been found to have antibacterial properties [16].

The atomic layer deposition of ZnO using diethylzinc (DEZ) and water as precursors has been widely studied. ZnO films deposited with DEZ and water are polycrystalline with a hexagonal wurtzite crystal structure [10,17]. While the crystal structure itself does not change, the preferred orientation of the crystals can change with the deposition temperature [10,13,18]. In addition, the substrate [17] and the process parameters such as pulse and purging times [19] have been found to affect the crystal orientation.

The ideal reaction mechanism for DEZ and H_2O is as follows [20]:

$$||-OH + Zn(CH_2CH_3)_2\,(g) \longrightarrow ||-O-Zn(CH_2CH_3) + CH_3CH_3\,(g) \quad (1)$$

$$||-OH-Zn(CH_2CH_3) + H_2O\,(g) \longrightarrow ||-O-Zn-OH + CH_3CH_3\,(g). \quad (2)$$

In the first half reaction (1), DEZ reacts with the surface OH-group, releasing ethane. The half reaction stops when all the OH-groups have reacted and the whole surface is saturated with monoethylzinc. In the second half reaction (2), water is pulsed and removes ethyl groups from zinc atoms and renews the surface with OH-groups. In the ideal case, the saturation of the surface is reached when all of the hydroxyl or ethyl groups are removed from the surface.

However, in reality, the reaction is more complex, and less than a monolayer of material is deposited in each cycle. This phenomenon is often related to the steric hindrance caused by the ligand molecules. Bulky ligands, such as ethyl groups, can cover reactive sites, and the saturation of growth is reached before every reactive site is occupied [21]. At high temperatures, the desorption of molecules providing reactive sites can also decrease the growth-per-cycle (GPC), and the self-limiting reaction is terminated due to the lack of reactive sites rather than steric hindrance [21].

Furthermore, at low temperatures, the saturation of the surface can be due to the low reactivity of the ligands. The termination of the half cycle for the low-temperature deposition of Al_2O_3 from trimethylaluminium (TMA) and H_2O was experimentally studied by Vandalon and Kessels [22]. They showed that after the H_2O pulse, there were persistent CH_3-groups at the surface. Their conclusion was that, at low temperatures, water is not reactive enough towards the methyl surface species, resulting in saturation. Similar results were obtained by Mackus et al. for DEZ and H_2O [23]. There is also strong theoretical evidence of persistent surface groups. Both the DEZ and H_2O half cycles were studied computationally by Weckman and Laasonen [24,25]. They found out that DEZ is reactive towards water even at room temperature, but water is not able to remove all the ethyl groups and the water pulse would therefore be the growth-limiting step in the reaction.

Some sensitive substrates, such as organic materials and plastics, may require a low deposition temperature. Reaction rates at these temperatures are not only slower but also the mechanism of saturation of the half cycle might be different than at higher temperatures. As a result, significant amounts of precursor-derived impurities, such as carbon and hydrogen, are incorporated in the film due to incomplete reactions. While hydrogen incorporation is sometimes even desired [26], more often, high-purity films are required, and hydrogen impurities can have a negative effect on the film properties [27]. The hydrogen concentration of ALD ZnO films has also been found to be related to the conductivity of the films [28,29].

In this study, we used heavy water, ^2H_2O, as an oxygen source in order to probe the impurities and to study the reaction mechanisms of ZnO films deposited at low temperatures using DEZ. Hydrogen originating from the precursors is a common impurity in ALD films, and with ^2H_2O, it is possible to distinguish whether the hydrogen in the film originates from DEZ or water. In addition, this can reveal valuable information regarding the reaction mechanisms. Heavy water is, in principle, chemically identical to normal water as none of the elements change. However, the heavier hydrogen isotope has some effect on the reactions, as discussed in the text below.

Earlier reaction mechanism studies have been performed with precursors containing rare stable isotopes, such as heavy water [30–36]. There are a few techniques that can be utilized to differentiate isotopes from each other. Quadrupole mass spectrometry (QMS) can be used to detect reaction side-products in the gas phase [31–33]. Ion beam techniques, such as time-of-flight elastic recoil detection analysis (ToF-ERDA) [30,37] and secondary ion beam mass spectrometry (SIMS) [35], can detect different isotopes within the film. In addition, IR spectroscopy can be used to resolve different isotopes [34]. In our study,

we utilized ToF-ERDA, which can directly and quantitatively measure hydrogen and its isotopes as well as the elemental composition of the films.

2. Materials and Methods

Thin films were deposited using a Beneq TFS 200 ALD-reactor. Nitrogen from an Inmatec PN 1150 nitrogen generator (99.999% purity) was used as a purging gas. Diethylzinc (Strem Chemicals, min. 95%) was used as a zinc precursor. Both normal deionized water $^{1}H_2O$ and heavy water $^{2}H_2O$ (Medical Isotopes Inc., Pelham, NH, USA. 99.9%) were used as oxygen sources. Depositions were performed at 1–2 mbar of base pressure with a constant (300 sccm) N_2 flow. The effect of the temperature on ZnO films was studied using 150 ms and 500 ms pulses for DEZ and $^{1}H_2O/^{2}H_2O$, respectively. The purging time after the DEZ pulse was 10 s, and 20 s after $^{1}H_2O/^{2}H_2O$. In addition, ZnO samples were deposited using variety of purging times at 60 °C and with a multiple short pulsing (MSP) scheme at 40 °C.

Atomic force microscopy (AFM), helium ion microscopy (HIM) and powder X-ray diffraction (XRD) were used to study the crystallinity of the deposited films. AFM imaging was done using Bruker Dimension Icon in the peak force tapping mode. XRD measurements were carried out using a Malvern Pananalytical X'Pert PRO diffractometer with Cu K_α radiation (λ = 1.54187 Å via Ni β-filter; 45 kV, 40 mA). Data processing and search-match phase analyses were carried out using the program X'pert HighScore Plus v. 4.9 and ICDD-PDF4+ database (version 2020) [38,39]. Cross sections of cleaved ZnO samples were imaged with a Carl Zeiss Orion NanoFab helium ion microscope using a 30 keV helium beam at a 45° angle.

Thin film elemental depth profiles were measured with ToF-ERDA using a 13.615 MeV $^{127}I^{7+}$ ion beam [40]. Analysis was done using Potku-software [41].

Film thicknesses were measured with a Rudolph AUTO EL III ellipsometer using a 632.8 nm wavelength.

3. Results and Discussion

All the deposited ZnO films were found to be slightly oxygen rich according to the ToF-ERDA measurements. The measured O/Zn ratio varied between 1.33 and 1.09, and the O/Zn ratio decreased with increasing deposition temperature. Due to the scattering effects, the amount of Zn in the film was slightly underestimated [42]. However, oxygen rich ZnO films deposited with ALD, especially at low deposition temperatures, have been reported previously [10,27,43–45]. The high oxygen concentration in the ZnO films was attributed to the zinc vacancies [44] in the crystal as well as to the oxygen interstitials [43]. In addition, hydrogen impurities were proposed to occupy the Zn-sites in the crystal [27].

The growth-per-cycle increased with increasing deposition temperature, reaching 1.7 Å/cycle at 150 °C when $^{1}H_2O$ was used (Figure 1a and Table 1). When the deposition temperature was further increased to 200 °C, the GPC decreased. This expected and well-documented decrease in GPC has been attributed to both the loss of OH-groups at elevated temperatures and the desorption of precursors before reacting on the surface [11,20,25]. The loss of OH-groups decreases the number of reactive sites for DEZ and results in a lower GPC. The GPC results in this study are somewhat lower than previously reported in the literature [10,11,20] but still comparable. The observed differences could have originated from multiple sources such as reactor design, reactor pressure and purging times [46]. When heavy water was used instead of normal water (Figure 1a), the GPC was significantly lower, especially at low temperatures. This can be attributed to the kinetic isotope effect. The use of a heavier hydrogen isotope increased the activation energy of the reaction, which slowed down the reaction rate. Therefore, the kinetic isotope effect can be thought of as equivalent to the decrease in the temperature. The effect became less significant as the temperature increased and there was enough energy for the reaction to reach completion. The kinetic isotope effect is utilized, for example, in chemical reaction

mechanism studies [47], where an isotopic substitution changes the reaction rate if a bond at or near the substitute plays a role in the reaction.

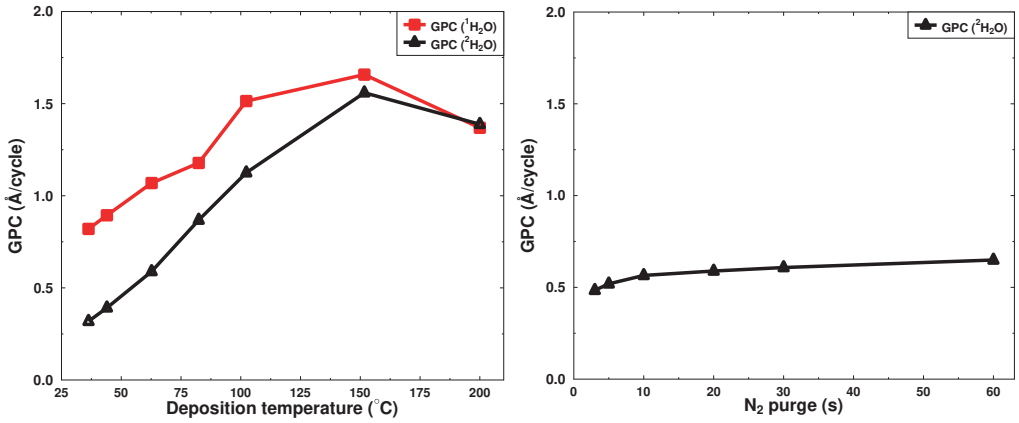

(**a**) (**b**)

Figure 1. (**a**) Growth-per-cycle as a function of the deposition temperature. One ALD cycle consisted of a 150 ms DEZ pulse, 10 s purge, 500 ms $^1H_2O/^2H_2O$ pulse and 20 s purge. (**b**) Growth-per-cycle as a function of the purging time using DEZ and ^2H_2O as precursors at 60 °C. The purging times after both precursors were kept the same when the purging time was 3, 5 or 10 s. For the longer purging times, only the purge after ^2H_2O was increased, and the purge after DEZ was kept at 10 s.

Table 1. The main results of ZnO samples deposited with both ^1H_2O and ^2H_2O at different deposition temperatures. Each cycle consisted of a 150 ms DEZ pulse, 10 s purge, 500 ms $^1H_2O/^2H_2O$ pulse and 20 s purge.

Sample	T (°C)	^{1}H (at.%)	^{2}H (at.%)	C (at.%)	Thickness (nm)	RMS Roughness (nm)	GPC (Å/cycle)
DEZ+^2H_2O							
D30	30	10.7	0.7	1.3	45	3.6	0.32
D40	40	8.7	1.0	0.8	47	3.5	0.39
D60	60	1.4	3.3	0.3	59	3.4	0.59
D80	80	0.7	2.4	0.2	87	5.7	0.87
D100	100	0.5	1.6	0.2	113	7.5	1.13
D150	150	0.1	0.7	0.2	156	6.2	1.56
D200	200	>0.1	0.4	>0.1	139	-	1.39
DEZ+^1H_2O							
H30	30	7.8	-	0.5	82	4.5	0.82
H40	40	5.3	-	0.3	89	4.3	0.89
H60	60	3.2	-	0.1	107	4.6	1.07
H80	80	2.1	-	0.2	118	6.8	1.18
H100	100	1.6	-	0.2	155	9.2	1.55
H150	150	1.0	-	0.2	133	3.1	1.66
H200	200	0.4	-	0.1	137	-	1.37

The increase of the purging time slightly increased the growth per cycle (Figure 1b and Table 2), but the effect was only minor at 60 °C when DEZ and ^2H_2O were used. Park et al. reported that long purging times have a considerable impact on the film properties [48]. In their study, they observed that at 170 °C, the GPC decreased from 2.2 Å/cycle to 1.6 Å/cycle when the purging time after the ^1H_2O pulse was increased from 20 s to 120 s, thus leading them to conclude that the decrease in the GPC was due to the loss of OH-groups via dehydration, which led to a decreased concentration of the reaction sites for DEZ molecules in the next precursor pulse. A comparison with our results indicates that the effect of purging on GPC is dependent on the deposition temperature. The GPC at 60 °C is not

limited due to the loss of OH-groups during the purge step but rather due to the slow reactivity of the precursors. Longer purging times at low temperatures are often favored in order to avoid uncontrolled CVD-like growth resulting in a high GPC. However, no indication of CVD growth was detected, even at very short purging times, as seen in Figure 1b. The increase of the GPC with increasing purging time at 60 °C could have been due to slow reactions and the desorption of by-products. If the by-products were not desorbed from the surface when the next precursor arrived, they could block reactive sites which in turn would reduce the GPC. This transient steric hindrance is discussed later in the text. At higher deposition temperatures, the reactions and desorption of by-products would likely be fast enough so that other factors, such as the concentration of the reactive sites, would become the limiting factors to the GPC.

Table 2. The main results of the ZnO samples deposited at 60 °C with varying purging times. The precursor pulse times were kept at 150 ms and 500 ms for DEZ and ^2H_2O, respectively.

Sample	N_2 Purge (s)	^1H (at.%)	^2H (at.%)	C (at.%)	Thickness (nm)	RMS Roughness (nm)	GPC (Å/cycle)
N3	3	8.5	1.0	0.7	48	3.3	0.48
N5	5	3.4	4.2	0.7	52	2.7	0.52
N10	10	1.9	3.4	0.3	57	3.3	0.57
N20	20	1.4	3.3	0.3	59	3.4	0.59
N30	30	1.3	3.1	0.3	61	3.1	0.61
N60	60	1.0	2.7	0.2	65	3.4	0.65

The effect of using ^2H_2O instead of ^1H_2O on film crystallinity and surface morphology was studied with XRD, AFM and HIM. The diffraction peaks characteristic to the wurtzite structure in Figure 2 (JCPDS 01-084-6784 [49]) show a transformation of preferred orientation from (002) to (100), as reported by Malm et al. [10] and also by Cai et al. [11] and Guziewicz et al. [12]. At low temperatures (40 °C and 60 °C), the preferred orientation of the crystals was (002), and this transformed to (100) at higher temperatures (100 °C). However, the crystallinity in the films was quite low, as indicated by the broad peak profiles and low intensities of the characteristic peaks. The films deposited with ^1H_2O were more crystalline than the films deposited with ^2H_2O. Some of this difference can be attributed to thinner films due to the lower GPC, as seen in Table 1. The film deposited at 40 °C with ^2H_2O was 47 nm thick, while the film deposited with ^1H_2O was 89 nm thick. At 100 °C, the thicknesses were 113 and 155 nm, respectively. However, the trend of change in the orientation was similar for both ^1H_2O and ^2H_2O.

The mtomic force microscope micrographs in Figure 3 confirm the transformation of the preferred crystal orientation from (002) to (100). The change in crystal orientation is visible in AFM micrographs at lower temperatures than in XRD patterns. The same transformation is also evident from the HIM images in Figure 4a,b. Cross-sectional HIM images also reveal that neither the crystallinity nor the orientation changed considerably within the film. HIM images of ZnO films deposited at 40, 60, 100 and 150 °C with both normal and heavy water are presented in Supplementary Figures S1 and S2. The root-mean-square (RMS) roughness (calculated from the AFM micrographs) of the films with a preferred (002) orientation varied from 3.4 to 4.5 nm, as seen in Table 1. The roughness increased at higher temperatures when the (100) orientation became visible, with its highest value of 9.2 nm in the case of the sample deposited with ^1H_2O at 100 °C. When ^1H_2O was used as an oxygen source, crystals with (100) orientation were visible already at the deposition temperature of 60 °C. In the case of heavy water, the (100) oriented crystals became visible only at 80 °C and above as seen in Figure 3. This also supports the earlier claim that the use of ^2H_2O has a similar effect on the deposition process as the decrease in the deposition temperature.

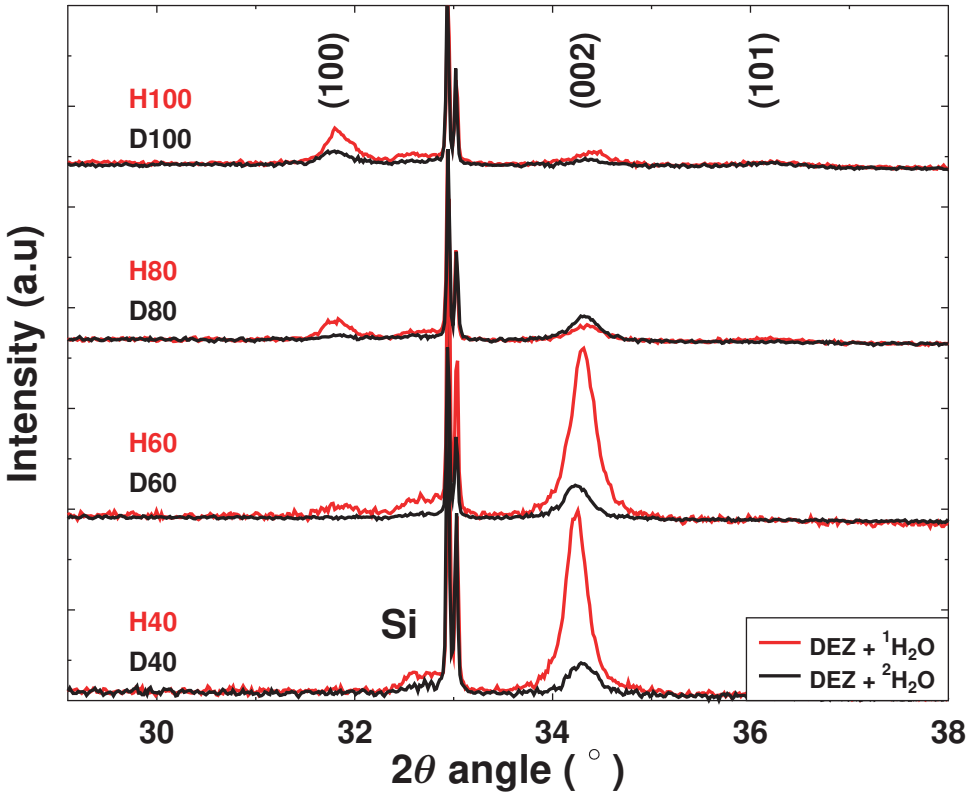

Figure 2. XRD patterns of selected ZnO films deposited at different temperatures with both ^1H_2O (red) and ^2H_2O (black). Films deposited with ^2H_2O are thinner than the films deposited with ^1H_2O, which affects the peak intensity. The double peak at 33° originates from the silicon substrate.

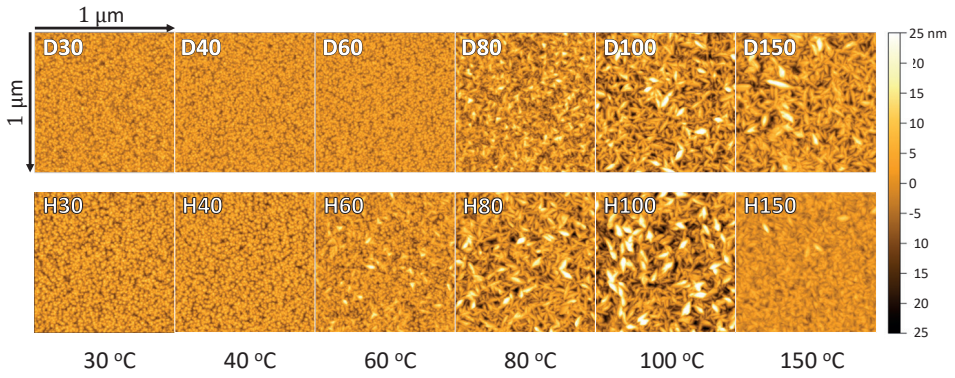

Figure 3. AFM micrographs of ZnO films deposited with DEZ and either ^1H_2O or ^2H_2O at different temperatures. The preferred crystal orientation changes as the temperature is raised. The lengths of the sides in each image are 1 µm.

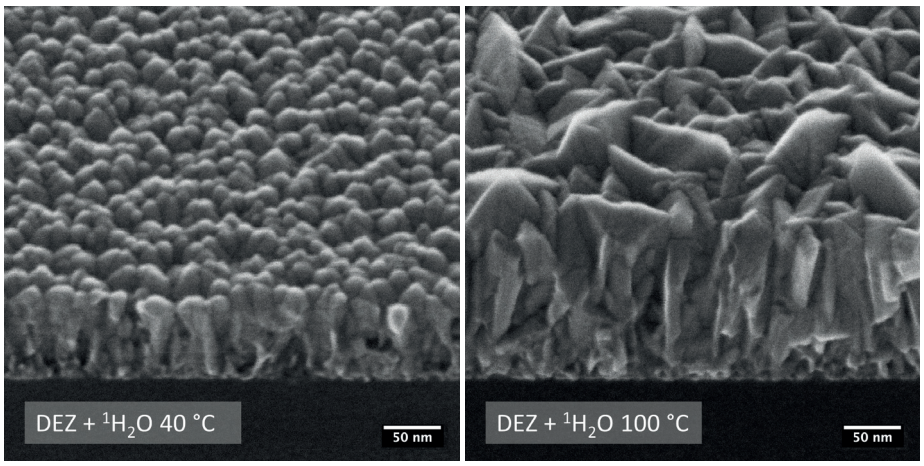

(**a**) (**b**)

Figure 4. Cross-sectional HIM images of ZnO films deposited with normal water at (**a**) 40 °C and (**b**) 100 °C. The cleaved samples are imaged at a 45° angle relative to the beam.

Figure 5a presents the hydrogen isotope concentrations in the ZnO films as a function of the deposition temperature (also in Table 1). As expected, the total hydrogen concentration decreased with the increasing deposition temperature. The use of heavy water yielded a higher total hydrogen concentration than when using normal water, but the general trend is very similar. The higher total hydrogen concentration of the ^2H_2O process can be attributed to the kinetic isotope effect and similarly to the GPC and change in preferred crystal orientation; the use of ^2H_2O induced a temperature shift to the concentration values. A heavier hydrogen isotope raises the activation energy of the reaction, and this effect is visible especially in the lower deposition temperatures as shown in Figure 5.

In a recent work, Guziewicz et al. [36] deposited ZnO with DEZ and ^2H_2O. Using SIMS, they found that both deuterium and hydrogen concentrations decrease as the deposition temperature is increased from 100 to 200 °C, which is in agreement with our findings. Their ^1H and ^2H concentrations are slightly lower than in our measurements. The difference is evident especially in ZnO films deposited with heavy water at 100 °C. According to our study, these films contain 1.6 at.% deuterium, while Guziewicz et al. report a value around 0.5 at.%. A possible explanation for this discrepancy could be the different pulsing and purging times used in our studies. For example, the purging time can affect the impurity composition significantly, as discussed later.

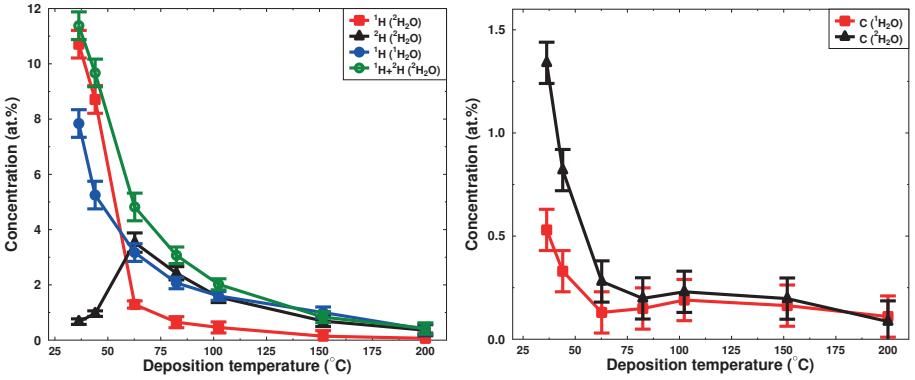

(**a**) (**b**)

Figure 5. (**a**) Hydrogen isotope and (**b**) carbon concentration of the films deposited at different temperatures using 150 ms DEZ and 500 ms ^1H_2O or ^2H_2O pulses. Purging times after the precursor pulses were 10 and 20 s, respectively.

Guziewicz et al. [36] studied the $^{1}H/^{2}H$ incorporation above 100 °C. Interestingly, the major hydrogen isotope changed from deuterium to hydrogen when the deposition temperature was decreased below 50 °C, as seen in Figure 5a. A similar phenomenon was observed in our previous study when Al_2O_3 films were deposited from trimethyl aluminum (TMA) and heavy water [37]. Both TMA and DEZ are organometallic alkyls whose chemical characteristics could be expected to be similar. However, the TMA + H_2O process produces amorphous films even at 600 °C [17], whereas ZnO films deposited using DEZ+H_2O are crystalline even near the room temperature, as seen in Figures 2 and 3 and shown by Malm et al. earlier [10]. Therefore, the crystallinity of the film does not seem to be a contributing factor for impurity incorporation.

The high ^{1}H concentration at low temperature can be attributed to persistent ethyl groups [23,25] which behave similarly to persistent methyl groups in the case of the TMA+H_2O process [22,34]. In these earlier studies, it was shown both computationally and experimentally that at low temperatures water is not reactive enough to remove all the methyl/ethyl groups from the surface. The persistent alkyl-groups remain at the surface even after multiple water exposures. There is also some evidence for co-operative mechanisms of surface groups, as it has been shown that multiple methyl/ethyl groups react with a lower reaction barrier compared to isolated groups [24,50]. These isolated alkyl groups are then buried into the film during the next ALD cycles.

The carbon concentration of the ZnO films follows a similar increasing trend with the hydrogen concentration as the deposition temperature is decreased, as seen in the Figure 5b, and the carbon concentration starts to increase rapidly as the deposition temperature goes below 50 °C. However, it must be noted that the films contain much more ^{1}H or much less carbon than what would be expected if these impurities only originated from persistent ethyl groups. If hydrogen originated mainly from the unreacted ethyl groups, the majority of the carbon in the film would need to escape via some yet unknown mechanism. One possible mechanism studied by Weckman and Laasonen was the β-elimination of two Zn-CH_2CH_3 surface groups following a release of gaseous C_2H_4 and C_2H_6. However, according to their calculations, the activation energy (2.52 eV) for β-elimination is too high to play any significant role on skewing the $C/^{1}H$ ratio [25].

At low temperatures, the reduced desorption rate of molecular water from the surface is thought to be a problem for ideal ALD-growth. The growth would therefore not be self-limited, as more than a monolayer of water stays on the surface even after long purging times. However, as mentioned above, a decrease in the deposition temperature (Figure 5a) or in the purging time (Figure 6b) decreases the amount of deuterium dramatically as the concentration of hydrogen increases. It would be an easy assumption to make that the physisorbed heavy water would lead to a higher deuterium concentration and/or to uncontrolled chemical vapor deposition-like (CVD) growth. However, no evidence of uncontrolled CVD growth with very high GPC was found, as can be seen in Figure 1a,b. More interestingly, in our previous study, the TMA +$^{2}H_2O$ process showed CVD-like growth already at 60 °C [37]. In addition, the Al_2O_3 films investigated in that study contained roughly two times more hydrogen than ZnO films deposited at the same temperature. It could be assumed that if the uncontrolled growth were mainly due to the adsorption of multiple layers of water, the CVD-growth should be clearly visible for both DEZ and TMA at equivalent temperature. Thus, our observations indicate that there exists either some DEZ/TMA related CVD-growth or the water sticks on the Al_2O_3 surface more tightly than on the ZnO surface.

The effect of the purging time on the impurity composition of the ZnO films was studied by pulsing DEZ and $^{2}H_2O$ at 60 °C with different purging schemes. Both hydrogen and deuterium concentrations and corresponding carbon concentrations are tabulated in Table 2 and plotted in Figure 6a,b, respectively. The effect of the purging shows a very similar trend as that obtained by changing the deposition temperature. Longer purging times resulted in lower ^{2}H and ^{1}H concentrations, while very short purging times resulted in a dramatic drop in ^{2}H and an increase in ^{1}H concentrations.The higher ^{1}H concentration was also correlated with the higher carbon concentration. These results indicate that the

change of the primary hydrogen isotope at low temperatures is also related to the purge time, as a shortening of the purge time has a similar effect to decreasing the deposition temperature. The effect of the purging on the roughness and crystallinity of the films was also studied with AFM (Table 2), but no noticeable difference on surface morphology was observed between the samples with different purging times.

For short purging times, the cause of the low deuterium and high hydrogen concentrations is more difficult to explain. Cai et al. used a quartz crystal microbalance (QCM) to measure the mass change during the DEZ and H_2O pulses [11]. In principle, the mass change during the water pulse should be negative, since the heavier ethyl-group is replaced by a lighter OH-group. However, Cai et al. observed that the mass change during the water pulse was slightly positive. Similar results have previously been reported also by Yousfi et al. [20] and Elam and George [51]. Elam and George concluded that the DEZ molecule reacts with more than one OH-group, leaving the bare zinc atoms on the surface. Water can then react with these undercoordinated Zn atoms, balancing the mass loss from ethyl–water exchange reactions. According to Cai et al., approximately 1.5 OH-groups react with each DEZ molecule when the deposition temperature is between 80 and 250 °C, but at 30 °C, DEZ reacts with two OH-groups. This could well explain our observation of the smaller amount of deuterium at low temperatures. On the other hand, DEZ reacting with the OH-groups should also lead to low ^{1}H and C concentrations, which contradicts our results. In addition, Weckman and Laasonen calculated that the second ligand exchange leading to bare zinc atoms has a high reaction barrier, making the second ligand exchange feasible only at higher temperatures [24].

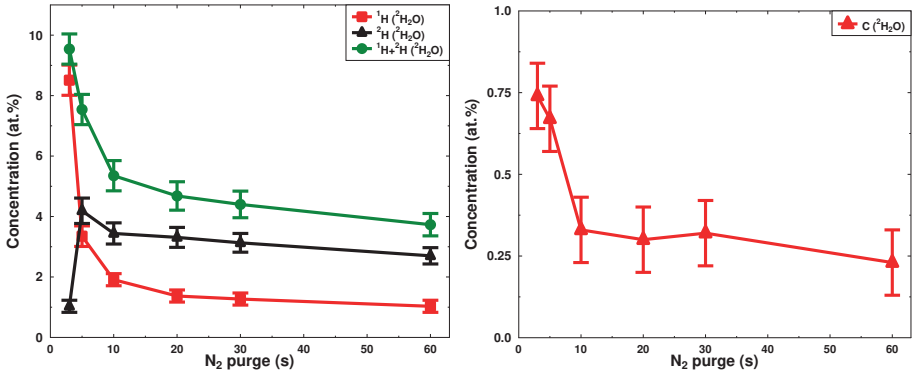

(**a**) (**b**)

Figure 6. (**a**) Hydrogen and (**b**) carbon concentration as a function of the N_2 purge time. All the samples were deposited at 60 °C using 150 ms DEZ pulses and 500 ms ^2H_2O pulses. The purging time between the pulses was varied. The purging times after both precursors were kept the same when the purging time was 3, 5 or 10 s. For longer purging times, only the purge after ^2H_2O was increased, and the purge after DEZ was kept at 10 s.

A question arises regarding whether the purging of DEZ and ^2H_2O is more important than the deposition temperature for the incorporation of the impurities and $^1H/^2H$ concentrations. Therefore, more detailed purging experiments were performed at 60 °C with purging schemes of 3/3 s, 3/10 s, 10/3 s and 10/10 s after DEZ and ^2H_2O pulses, respectively. Results shown in Figure 7a indicate that there was a small preference for a lower total hydrogen concentration when purging after a longer DEZ pulse. However, there was no significant difference in ^{1}H or ^{2}H concentrations if the purging was changed from 3/10 s to 10/3 s. It seems that the total purging time of the ALD cycle is a more important factor in the hydrogen and deuterium incorporation. A longer purge also led to a somewhat higher GPC, as shown in Figure 7b. It is also possible that the ligands from the previous pulse, which had not yet reacted, or by-products which had not yet desorbed from the surface, could block reactive sites when the next precursor pulse arrived.

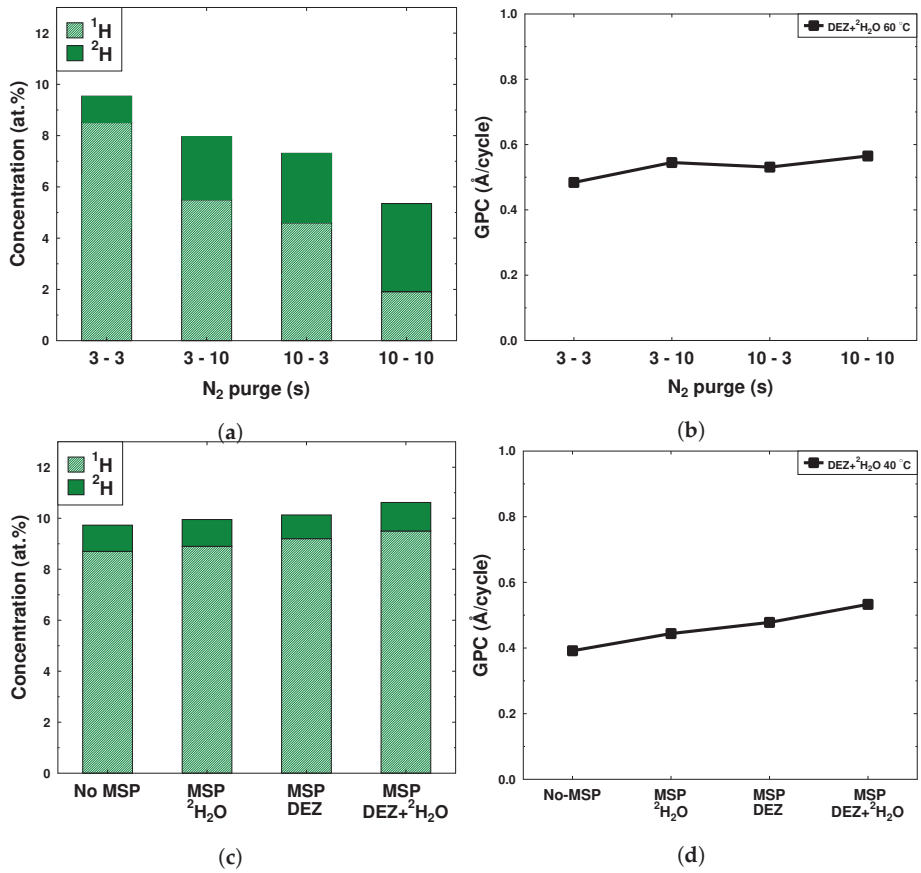

Figure 7. (**a**) Hydrogen and deuterium concentration with different N_2 purge schemes deposited at 60 °C. (**b**) Growth per cycle with different N_2 purging schemes deposited at 60 °C. (**c**) Hydrogen and deuterium concentration when multiple short pulses (see text) were used at 40 °C. (**d**) Growth per cycle using multiple short pulsing at 40 °C.

We also studied whether the transient steric hindrance proposed by Wang et al. [52] could explain our data. Wang et al. deposited ZnO films from DEZ and ^1H_2O using multiple short pulses (MSP), and they divided one pulse into shorter separated pulses while keeping the total pulse time (i.e., precursor exposure) the same. Using the MSP increased the growth per cycle, and their conclusion was that the slow desorption of byproducts and unreacted precursor molecules blocked some of the reactive sites when a single pulse was used. Multiple short pulses gives more time for desorption, allowing more precursors to adsorb, leading to a higher overall intake of material per cycle. It is known from the QCM studies that the decrease of the surface species (i.e., weight) can take seconds even at 177 °C [51].

In order to study this hypothesis, ZnO films were deposited at 40 °C using a recipe in which the pulses were divided into three shorter pulses so that the total precursor dose remained unchanged. This was done using 3 × 50 ms pulses for DEZ and 3 × 167 ms for heavy water. The purge time between the short pulses was set to 1 s. In order to keep the total cycle time the same as in the previous depositions, purging times of 8 s and 18 s were used instead of 10 s and 20 s after DEZ and heavy water, respectively. Three different samples were deposited: MSP for both DEZ and water, MSP only with ^2H_2O and MSP only with DEZ.

Hydrogen and deuterium concentrations of the films deposited with the MSP process along with conventional single pulse deposition are shown in Figure 7c. Multiple short pulses did not significantly change the ^2H concentration but slightly increased the ^1H concentration in each case. The highest total hydrogen concentration was measured when MSP was used for both DEZ and ^2H_2O, and at the same time, the GPC increased more

than 25% from 0.40 to 0.53 Å/cycle. These two results are somewhat contradictory, as an increase in the GPC would be an indication of the transient steric hindrance proposed by Wang et al. [52]. On the other hand, this should lead to a film with fewer impurities, but our results indicated the opposite. The reason behind the contradiction remains unknown and requires further studies. It seems that the total purging time is the most significant factor affecting the film composition, as shown in Figure 7a. Nevertheless, the MSP seems to increase the GPC significantly without increasing the cycle time, and the faster low-temperature deposition is beneficial for industrial applications.

In order to study the hydrogen (deuterium) migration and exchange reactions in the film, samples deposited with ^2H_2O were measured again after two months of storage in ambient conditions. The results (Figure 8) show that the sum of the hydrogen and deuterium in the film increased slightly during the storage. Simultaneously, the ^2H concentration in the film decreased considerably while the ^1H concentration increased. Especially in the sample deposited at 60 °C, which had the highest deuterium concentration to begin with, almost all the deuterium was replaced with hydrogen.

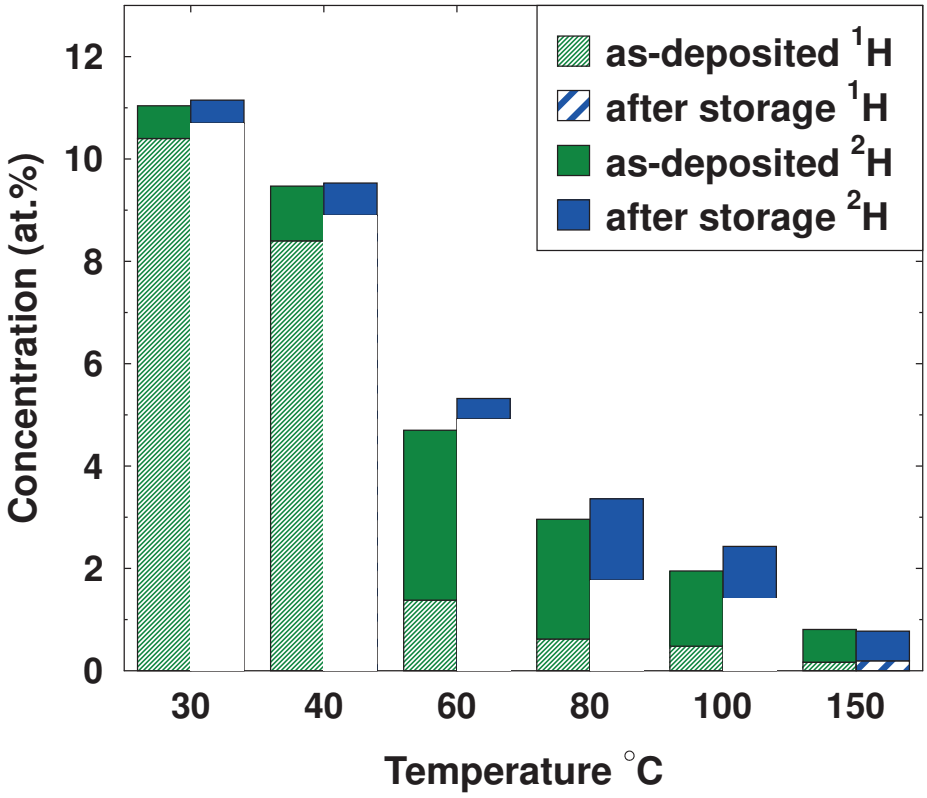

Figure 8. Change in the $^1H/^2H$ concentration after two months of storage at ambient conditions. For example, in the far left bar, the film deposited at 30 °C contains 10.4 at.% ^1H and 0.64 at.% ^2H immediately after the deposition and 10.7 at.% ^1H and 0.45 at.% ^2H after the storage.

This decrease in the deuterium concentration was most likely caused by an exchange reaction between the deuterium atoms in the film surface and hydrogen atoms from either molecular hydrogen H_2 or from water vapor, which are found in air. Since these gases contain only a very minor amount of deuterium, the deuterium concentration in the film would decrease. This exchange does not only take place in the film surface, but the deuterium concentration also decreases through the cross-section of the film, even if it is 100 nm thick. Analogous results were obtained in our previous study with Al_2O_3 [37]. However, the ALD ZnO films are crystalline whereas Al_2O_3 films are amorphous.

4. Conclusions

The atomic layer deposition of ZnO at low temperatures is a complex process. Our study shows that there are probably multiple processes that occur at the same time, including the fast primary reactions of the ALD growth and the slower secondary reactions that can take place even below the outermost layer of atoms. This is demonstrated by varying the purging time, which has a significant effect on the impurity levels of the films. All the films deposited in this study had a uniform thickness throughout the reactor and did not show any hint of CVD-growth even though the elemental compositions of the films were significantly different. This can influence the film properties. Therefore, it is important to describe the deposition conditions in great detail. This also means that great care must be taken when the results from multiple studies are compared, especially at low deposition temperatures.

The use of stable isotopes gives valuable information regarding the reactions, especially when the deposition conditions are not ideal; i.e., at low temperatures where the reaction rate can be slow and adequate purging times impractically long. The high ^{1}H and low ^{2}H concentrations in ZnO films at low temperatures and with short purging times indicate the existence of some unidentified mechanism that may govern the growth in these non-ideal conditions. The second ligand exchange reaction suggested by Cai et al. [11] was found to be an unlikely candidate at low temperatures, since ^{1}H and C concentrations increased rapidly at low temperature.

The high ^{1}H and low ^{2}H concentration at low deposition temperatures could be an indication of persistent non-reactive ligands, as suggested by Weckman et al. [25] and Mackus et al. [23]. More reactive DEZ would remove practically all the possible OH-groups, leading to decreased ^{2}H and increased ^{1}H concentrations. However, there are two observations contradicting this explanation: firstly, there was a lower concentration of carbon in the film than what would be expected based on the ^{1}H concentration or vice versa; secondly, shortening the purging time led to a similar effect as decreasing the deposition temperature, which also implies the existence of some slower yet unknown reaction mechanism, as discussed above.

There is also a transient steric hindrance component which decreases the GPC at low temperature. Multiple short pulses can be used to tackle this problem, as a higher GPC can be achieved without increasing the ALD cycle time, making the low-temperature process faster. Changing from a single pulse to the MSP does not, however, change the impurity concentrations of the films. This can be achieved only through longer purging, as shown above. The longer purging times also lead to a somewhat higher GPC. Therefore, there might be a transient steric hindrance component related also to this slower process of removing the persistent methyl groups from the film. These species can also block the reactive sites which become available to the precursor only after the long purging.

The kinetic isotope effect due to heavier deuterium induces an effect similar to decreasing the deposition temperature, which must be taken into account when comparing our results with results from different studies. However, replacing normal water with heavy water seems to reproduce similar trends in terms of the GPC, impurity concentration and crystallinity, validating the use of heavy water when studying the DEZ + H_2O ALD-process.

Supplementary Materials: The following are available online at https://www.mdpi.com/2079-6412/11/5/542/s1, Figure S1: HIM-$^{1}H_2O$, Figure S2: HIM-$^{2}H_2O$.

Author Contributions: Investigation, S.K., M.L. and K.A.; Writing—original draft, S.K.; Writing—review and editing M.L., K.A. and T.S. All authors have read and agreed to the published version of the manuscript.

Funding: This research received no external funding.

Institutional Review Board Statement: Not applicable.

Informed Consent Statement: Not applicable.

Data Availability Statement: Not applicable.

Conflicts of Interest: The authors declare no conflict of interest.

Abbreviations

The following abbreviations are used in this manuscript:

AFM	Atomic force microscopy
ALD	Atomic layer deposition
CVD	Chemical vapor deposition
DEZ	Diethylzinc
GPC	Growth per cycle
HIM	Helium ion microscopy
IR	Infrared
MSP	Multiple short pulses
OLED	Organic light emitting diode
QCM	Quartz crystal microbalance
QMS	Quadrupole mass spectrometry
RMS	Root-mean-square
SIMS	Secondary ion mass spectrometry
TMA	Trimethylaluminium
ToF-ERDA	Time-of-flight elastic recoil detection analysis
XRD	X-ray diffraction

References

1. Choi, J.; Mao, Y.; Chang, J. Development of hafnium based high-k materials—A review. *Mater. Sci. Eng. R Rep.* **2011**, *72*, 97–136. [CrossRef]
2. Li, Y.; Xiong, Y.; Yang, H.; Cao, K.; Chen, R. Thin film encapsulation for the organic light-emitting diodes display via atomic layer deposition. *J. Mater. Res.* **2020**, *35*, 681–700. [CrossRef]
3. Xing, Z.; Xiao, J.; Hu, T.; Meng, X.; Li, D.; Hu, X.; Chen, Y. Atomic Layer Deposition of Metal Oxides in Perovskite Solar Cells: Present and Future. *Small Methods* **2020**, *4*, 2000588. [CrossRef]
4. Ritala, M.; Leskelä, M.; Dekker, J.P.; Mutsaers, C.; Soininen, P.J.; Skarp, J. Perfectly Conformal TiN and Al_2O_3 Films Deposited by Atomic Layer Deposition. *Chem. Vap. Depos.* **1999**, *5*, 7–9. [CrossRef]
5. Iatsunskyi, I.; Kempiński, M.; Jancelewicz, M.; Załęski, K.; Jurga, S.; Smyntyna, V. Structural and XPS Characterization of ALD Al_2O_3 Coated Porous Silicon. *Vacuum* **2015**, *113*, 52–58. [CrossRef]
6. Zhao, M.J.; Sun, Z.T.; Hsu, C.H.; Huang, P.H.; Zhang, X.Y.; Wu, W.Y.; Gao, P.; Qiu, Y.; Lien, S.Y.; Zhu, W.Z. Zinc Oxide Films with High Transparency and Crystallinity Prepared by a Low Temperature Spatial Atomic Layer Deposition Process. *Nanomaterials* **2020**, *3*, 459. [CrossRef]
7. Gao, Z.; Banerjee, P. Review Article: Atomic layer deposition of doped ZnO films. *J. Vac. Sci. Technol. A* **2019**, *37*, 050802. [CrossRef]
8. Ingale, P.; Knemeyer, K.; Piernavieja Hermida, M.; Naumann d'Alnoncourt, R.; Thomas, A.; Rosowski, F. Atomic Layer Deposition of ZnO on Mesoporous Silica: Insights into Growth Behavior of ZnO via In-Situ Thermogravimetric Analysis. *Nanomaterials* **2020**, *10*, 981. [CrossRef]
9. Choi, Y.J.; Gong, S.C.; Park, C.S.; Lee, H.S.; Jang, J.G.; Chang, H.J.; Yeom, G.Y.; Park, H.H. Improved Performance of Organic Light-Emitting Diodes Fabricated on Al-Doped ZnO Anodes Incorporating a Homogeneous Al-Doped ZnO Buffer Layer Grown by Atomic Layer Deposition. *ACS Appl. Mater. Interfaces* **2013**, *5*, 3650–3655.
10. Malm, J.; Sahramo, E.; Perälä, J.; Sajavaara, T.; Karppinen, M. Low-temperature atomic layer deposition of ZnO thin films: Control of crystallinity and orientation. *Thin Solid Film.* **2011**, *519*, 5319–5322. [CrossRef]
11. Cai, J.; Ma, Z.; Wejinya, U.; Zou, M.; Liu, Y.; Zhou, H.; Meng, X. A revisit to atomic layer deposition of zinc oxide using diethylzinc and water as precursors. *J. Mater. Sci.* **2019**, *54*, 5236–5248. [CrossRef]
12. Guziewicz, E.; Godlewski, M.; Krajewski, T.; Wachnicki, Ł.; Szczepanik, A.; Kopalko, K.; Wójcik-Głodowska, A.; Przeździecka, E.; Paszkowicz, W.; Łusakowska, E.; et al. ZnO grown by atomic layer deposition: A material for transparent electronics and organic heterojunctions. *J. Appl. Phys.* **2009**, *105*, 122413. [CrossRef]
13. Di Mauro, A.; Cantarella, M.; Nicotra, G.; Privitera, V.; Impellizzeri, G. Low temperature atomic layer deposition of ZnO: Applications in photocatalysis. *Appl. Catal. B Environ.* **2016**, *196*, 68–76. [CrossRef]
14. Wang, L.C.; Han, Y.Y.; Yang, K.C.; Chen, M.J.; Lin, H.C.; Lin, C.K.; Hsu, Y.T. Hydrophilic/hydrophobic surface of Al_2O_3 thin films grown by thermal and plasma-enhanced atomic layer deposition on plasticized polyvinyl chloride (PVC). *Surf. Coatings Technol.* **2016**, *305*, 158–164. [CrossRef]

15. Kekkonen, V.; Hakola, A.; Kajava, T.; Sahramo, E.; Malm, J.; Karppinen, M.; Ras, R.H.A. Self-erasing and rewritable wettability patterns on ZnO thin films. *Appl. Phys. Lett.* **2010**, *97*, 044102. [CrossRef]
16. Kääriäinen, M.L.; Weiss, C.; Ritz, S.; Pütz, S.; Cameron, D.; Mailänder, V.; Landfester, K. Zinc release from atomic layer deposited zinc oxide thin films and its antibacterial effect on *Escherichia coli*. *Appl. Surf. Sci.* **2013**, *287*, 375–380. [CrossRef]
17. Miikkulainen, V.; Leskelä, M.; Ritala, M.; Puurunen, R. Crystallinity of inorganic films grown by atomic layer deposition: Overview and general trends. *J. Appl. Phys.* **2013**, *113*, 021301. [CrossRef]
18. Fang, M.; Qi, L.; Zhang, Z.; Chen, Q. Effects of thickness and deposition temperature of ALD ZnO on the performance of inverted polymer solar cells. *J. Mater. Sci. Mater. Electron.* **2016**, *27*, 10252–10258. [CrossRef]
19. Guziewicz, E.; Kowalik, I.A.; Godlewski, M.; Kopalko, K.; Osinniy, V.; Wójcik, A.; Yatsunenko, S.; Łusakowska, E.; Paszkowicz, W.; Guziewicz, M. Extremely low temperature growth of ZnO by atomic layer deposition. *J. Appl. Phys.* **2008**, *103*, 033515. [CrossRef]
20. Yousfi, E.B.; Fouache, J.; Lincot, D. Study of atomic layer epitaxy of zinc oxide by in-situ quartz crystal microgravimetry. *Appl. Surf. Sci.* **2000**, *153*, 223–234. [CrossRef]
21. Puurunen, R.L. Surface chemistry of atomic layer deposition: A case study for the trimethylaluminum/water process. *J. Appl. Phys.* **2005**, *97*, 121301. [CrossRef]
22. Vandalon, V.; Kessels, W.M.M. What is limiting low-temperature atomic layer deposition of Al_2O_3: A vibrational sum-frequency generation study. *Appl. Phys. Lett.* **2016**, *108*, 011607. [CrossRef]
23. Mackus, A.J.M.; MacIsaac, C.; Kim, W.H.; Bent, S.F. Incomplete elimination of precursor ligands during atomic layer deposition of zinc-oxide, tin-oxide, and zinc-tin-oxide. *J. Chem. Phys.* **2017**, *146*, 052802. [CrossRef]
24. Weckman, T.; Laasonen, K. Atomic Layer Deposition of Zinc Oxide: Diethyl Zinc Reactions and Surface Saturation from First-Principles. *J. Phys. Chem. C* **2016**, *120*, 21460–21471. [CrossRef]
25. Weckman, T.; Laasonen, K. Atomic Layer Deposition of Zinc Oxide: Study on the Water Pulse Reactions from First-Principles. *J. Phys. Chem. C* **2018**, *122*, 7685–7694. [CrossRef]
26. Macco, B.; Knoops, H.C.; Verheijen, M.A.; Beyer, W.; Creatore, M.; Kessels, W.M. Atomic layer deposition of high-mobility hydrogen-doped zinc oxide. *Sol. Energy Mater. Sol. Cells* **2017**, *173*, 111–119.
27. Peter, R.; Salamon, K.; Omerzu, A.; Grenzer, J.; Badovinac, I.J.; Saric, I.; Petravic, M. Role of Hydrogen-Related Defects in Photocatalytic Activity of ZnO Films Grown by Atomic Layer Deposition. *J. Phys. Chem. C* **2020**, *124*, 8861–8868. [CrossRef]
28. Przezdziecka, E.; Guziewicz, E.; Jarosz, D.; Snigurenko, D.; Sulich, A.; Sybilski, P.; Jakiela, R.; Paszkowicz, W. Influence of oxygen-rich and zinc-rich conditions on donor and acceptor states and conductivity mechanism of ZnO films grown by ALD—Experimental studies. *J. Appl. Phys.* **2020**, *127*, 075104. [CrossRef]
29. Beh, H.; Hiller, D.; Bruns, M.; Welle, A.; Becker, H.W.; Berghoff, B.; Sürgers, C.; Merz, R.; Zacharias, M. Quasi-metallic behavior of ZnO grown by atomic layer deposition: The role of hydrogen. *J. Appl. Phys.* **2017**, *122*, 025306. [CrossRef]
30. Guerra-Nunẽz, C.; Döbeli, M.; Michler, J.; Utke, I. Reaction and Growth Mechanisms in Al_2O_3 deposited via Atomic Layer Deposition: Elucidating the Hydrogen Source. *Chem. Mater.* **2017**, *29*, 8690–8703. [CrossRef]
31. Rahtu, A.; Ritala, M. Reaction Mechanism Studies on Titanium Isopropoxide-Water Atomic Layer Deposition Process. *Chem. Vap. Depos.* **2002**, *8*, 21–28. [CrossRef]
32. Juppo, M.; Rahtu, A.; Ritala, M.; Leskelä, M. In Situ Mass Spectrometry Study on Surface Reactions in Atomic Layer Deposition of Al_2O_3 Thin Films from Trimethylaluminum and Water. *Langmuir* **2000**, *16*, 4034–4039. [CrossRef]
33. Juppo, M.; Rahtu, A.; Ritala, M. In Situ Mass Spectrometry Study on Surface Reactions in Atomic Layer Deposition of TiN and Ti(Al)N Thin Films. *Chem. Mater.* **2002**, *14*, 281–287. [CrossRef]
34. Vandalon, V.; Kessels, W.M.M. Revisiting the Growth Mechanism of Atomic Layer Deposition of Al_2O_3: A Vibrational Sum-frequency Generation Study. *J. Vac. Sci. Technol. A* **2017**, *35*, 05C313. [CrossRef]
35. Hiraiwa, A.; Saito, T.; Matsumura, D.; Kawarada, H. Isotope Analysis of Diamond-surface Passivation Effect of High-temperature H_2O-grown Atomic Layer Deposition-Al_2O_3 Films. *J. Appl. Phys.* **2015**, *117*, 215304, [CrossRef]
36. Guziewicz, E.; Wozniak, W.; Mishra, S.; Jakiela, R.; Guziewicz, M.; Ivanov, V.Y.; Lusakowska, E.; Schifano, R. Hydrogen in As-Grown and Annealed ZnO Films Grown by Atomic Layer Deposition. *Phys. Status Solidi (a)* **2021**, *218*, 2000318. [CrossRef]
37. Kinnunen, S.; Arstila, K.; Sajavaara, T. Al_2O_3 ALD films grown using TMA + rare isotope $^2H_2^{16}O$ and $^1H_2^{18}O$ precursors. *Appl. Surf. Sci.* **2021**, 148909. [CrossRef]
38. Degen, T.; Sadki, M.; Bron, E.; König, U.; Nénert, G. The HighScore suite (v. 4.9). *Powder Diffr.* **2014**, *29*, S13–S18. [CrossRef]
39. International Centre for Diffraction Data, ICDD-PDF4+ Database. Avaliable online: https://www.icdd.com/ (accessed on 3 May 2021)
40. Laitinen, M.; Rossi, M.; Julin, J.; Sajavaara, T. Time-of-flight—Energy spectrometer for elemental depth profiling—Jyväskylä design. *Nucl. Instruments Methods Phys. Res. Sect. B Beam Interact. Mater. Atoms* **2014**, *337*, 55–61. [CrossRef]
41. Arstila, K.; Julin, J.; Laitinen, M.; Aalto, J.; Konu, T.; Kärkkäinen, S.; Rahkonen, S.; Raunio, M.; Itkonen, J.; Santanen, J.P.; Tuovinen, T.; Sajavaara, T. Potku—New analysis software for heavy ion elastic recoil detection analysis. *Nucl. Instruments Methods Phys. Res. Sect. B Beam Interact. Mater. Atoms* **2014**, *331*, 34–41.
42. Arstila, K.; Sajavaara, T.; Keinonen, J. Monte Carlo simulation of multiple and plural scattering in elastic recoil detection. *Nucl. Instruments Methods Phys. Res. Sect. B Beam Interact. Mater. Atoms* **2001**, *174*, 163–172. [CrossRef]

43. Guziewicz, E.; Krajewski, T.A.; Przezdziecka, E.; Korona, K.P.; Czechowski, N.; Klopotowski, L.; Terziyska, P. Zinc Oxide Grown by Atomic Layer Deposition: From Heavily n-Type to p-Type Material. *Phys. Status Solidi (b)* **2020**, *257*, 1900472. [CrossRef]
44. Panigrahi, J.; Singh, P.; Gupta, G.; Vandana. Growth and luminescence characteristics of zinc oxide thin films deposited by ALD technique. *J. Lumin.* **2021**, *233*, 117797. [CrossRef]
45. Napari, M.; Lahtinen, M.; Veselov, A.; Julin, J.; Østreng, E.; Sajavaara, T. Room-temperature plasma-enhanced atomic layer deposition of ZnO: Film growth dependence on the PEALD reactor configuration. *Surf. Coatings Technol.* **2017**, *326*, 281–290. [CrossRef]
46. Sønsteby, H.H.; Yanguas-Gil, A.; Elam, J.W. Consistency and Reproducibility in Atomic Layer Deposition. *J. Vac. Sci. Technol. A* **2020**, *38*, 020804. [CrossRef]
47. Gómez-Gallego, M.; Sierra, M. Kinetic Isotope Effects in the Study of Organometallic Reaction Mechanisms. *Chem. Rev.* **2011**, *111*, 4857–4963.
48. Park, H.K.; Yang, B.S.; Park, S.; Kim, M.S.; Shin, J.C.; Heo, J. Purge-time-dependent growth of ZnO thin films by atomic layer deposition. *J. Alloys Compd.* **2014**, *605*, 124–130. [CrossRef]
49. Dos Reis, P.M.; de Oliveira, A.S.; Pecoraro, E.; Ribeiro, S.J.; Góes, M.S.; Nascimento, C.S.; Gonçalves, R.R.; dos Santos, D.P.; Schiavon, M.A.; Ferrari, J.L. Photoluminescent and structural properties of ZnO containing Eu^{3+} using PEG as precursor. *J. Lumin.* **2015**, *167*, 197–203. [CrossRef]
50. Shirazi, M.; Elliott, S.D. Cooperation between adsorbates accounts for the activation of atomic layer deposition reactions. *Nanoscale* **2015**, *7*, 6311–6318. [CrossRef]
51. Elam, J.W.; George, S.M. Growth of ZnO/Al_2O_3 Alloy Films Using Atomic Layer Deposition Techniques. *Chem. Mater.* **2003**, *15*, 1020–1028. [CrossRef]
52. Wang, H.; Wang, Z.; Xu, X.; Liu, Y.; Chen, C.; Chen, P.; Hu, W.; Duan, Y. Multiple short pulse process for low-temperature atomic layer deposition and its transient steric hindrance. *Appl. Phys. Lett.* **2019**, *114*, 201902. [CrossRef]

PIII

SPATIAL ALD OF Al_2O_3 AND ZnO USING HEAVY WATER

by

S. Kinnunen and T. Sajavaara

Surface & Coatings Technology 441, (2022), 128456

Surface Coatings Technology 441 2022) 128456

Contents lists available at ScienceDirect

Surface & Coatings echnology

journal homepage: www.elsevier.com/locate/surfcoat

Spatial ALD of Al O_3 and ZnO using heavy water

Sami Kinnunen *, Timo Sajavaara

Accelerator aboratory, Department of Physics, University of J vaskyla, P. O. Box 35, FI-40014 University of J vaskyla, Finland
Nanoscience Center, Department of Physics, University of J vask la, P. O. Box 35, FI-40014 University of J vaskyla, Finland

A R T I C L E I N F O

Keywords:
SALD
Al O_3
ZnO
 oF-ERDA
Heavy water

A B S T R A C T

Al O_3 and ZnO thin films were deposited from trimethylaluminium (TMA) and diethylzinc (DEZ) in combination with water using cylindrical rotating substrate spatial atomic layer deposition (SALD). The depositions were done between 67 and 140 °C. he growth per cycle for Al O_3 varied between 0.75 and .0 × 10^{15} at./cm per cycle and for ZnO between 0.52 and 1.07 × 10^{15} at./cm per cycle. he hydrogen incorporation was studied by varying the deposition temperature and substrate rotation speed. The rotation speed affects the precursor exposure time (46–458 ms) and inert gas purging time (111–1120 ms). he results show that Al O_3 films can contain up to 25 at.% of hydrogen when the deposition temperature is 67 °C or the deposition exposure/purging times are short. The deposition of ZnO in similar conditions produces films with hydrogen concentrations up to 15 at.%. The source f impurity hydrogen was investigated by using heavy water, H O, as an xygen s urce. he main hydrogen isotope in the Al O_3 films at low temperatures and fast deposition speed was found t be ^{1}H, while at higher temperatures and lower deposition speeds H isotope was dominant. For ZnO, ^{1}H was the majority hydrogen isotope in the films in all the studied deposition conditions except at the lowest rotation speed.

1. Introduction

Conventional pulsed atomic layer deposition (ALD) c nsists f two r more precursor pulses separated in time with inert gas purging in between. Atomic layer deposition is a widely studied and used method to deposit pinhole ree films with sub-nanometer thickness control, and it enables precise deposition on complex 3D-structures and high-aspect-ratio substrates [1–3]. While the conventional ALD can be considered as a temporal ALD, spatial atomic layer deposition (SALD) separates the precursor pulses in space rather than in time. his enables aster deposition, or example, or solar cell passivation [4–7] and the construction of roll-to-roll (R2R) reactors or flexible substrates [8,9]. Fast large area deposition is also desired, or example, on packaging materials [10,11], n organic electronics like memristors [12] r n organic light emitting diode (OLED) displays where thin and transparent gas and moisture permeation barriers are required [9,10,13,14]. Spatial ALD also enables completely new substrates such as large area abrics to be coated effectively with ALD [15]. Spatial ALD has great potential also in i-ion battery [16–18] applications and printed electronics [19].

Temporal ALD is ten performed at low pressure c nditions enabling efficient gas transfer and purging of the by-products [2], while SALD can be operated even at atmospheric pressure [20,21]. This can further increase the throughput since there is no need or pumping down to a low deposition pressure. With SALD the coating head is in close proximity to the substrate so that air cannot infiltrate to the reaction space between the coating head and substrate surface. Therefore, the deposition space and all the unreacted precursor molecules can be pumped without escaping. his removes the requirement or vacuum in the reactor space, making deposition with roll to roll and on large surface area substrates much more attractive.

The benefit of SALD is ften believed to be that long purging times between the precursor pulses are not needed [22]. With temporal ALD at low deposition temperatures the purging times can be rather minutes than seconds [23,24]. The close proximity f precursor head to substrate significantly decreases the adsorption of precursor molecules n reactor walls, present in the temporal ALD. Therefore, much shorter purging time is required, and high speed SALD has realised deposition rates as high as 1 nm/s [25,26]. However, the picture is more complicated when the deposition temperature is low and the reaction and by-product desorption rates are slow. Understanding the non-ideal ALD-conditions is important especially when flexible organic substrates are used. hese often start to deteriorate at higher temperatures required for the deposition of high quality thin films.

On the downside, spatial ALD does not enable easy and independent

* Corresponding author.
E-mail address: samantki@jyu.fi (S. Kinnunen).

https://doi.org/10.1016/j.surfcoat.2022.128456
Received 4 March 2022; Received in revised form 12 April 2022; Accepted 18 April 022
Available online 28 April 2022

control of purging and precursor exposure time, characteristic to temporal ALD. As the precursor inlets inject the precursors continuously, also the consumption of precursors requires optimisation in rder t minimise the waste of the often expensive precursors [27]. In SALD, either the substrate is moved at constant speed in close proximity to the precursor inlets r regions, or the coating head containing the exposure/purge sequence is moved while the substrate remains stationary [28]. Therefore, the whole reactor configuration must be changed if the precursor exposure and purging time ratio is tuned. In rder to address this challenge Yersak et al. used modular SALD-reactor where varying the exposure/purge ratio was realised through removable spacers [18]. However, in most cases with SALD it is possible to play only with purging and precursor flows and the control of process parameters is usually more limited compared to the temporal ALD.

ALD thin films deposited at low temperatures often contain significant amounts of hydrogen and other impurities riginating from the precursors [23,24,29–33]. In this study we used heavy water, H O, instead of normal water in two common ALD processes: Al O_3 rom trimethylaluminium (TMA) and water, and ZnO rom diethylzinc (EZ) and water. ALD Al O_3 is an amorphous dielectric and can be used as a high-k layer in several applications, but it also has been studied as a moisture barrier or OLEDs and packaging [10,13,34]. ALD ZnO is a polycrystalline wide band gap semiconductor with wurtzite crystal structure [30,35]. The electrical properties f ZnO are tunable through doping and, or example, aluminum doped ZnO (AZO) have been studied as a transparent conducting xide [36]. In addition, Al O_3/ZnO nanolaminates are studied as barrier layers [37] as well as in biosensing applications due to their tunable ptical properties [38–41].

Earlier we studied these two processes using heavy water with temporal ALD [24,33] and we und out that, in addition to the deposition temperature, the purging time has a significant effect on impurity incorporation. Precursors containing rare isotopes have been used t study reaction mechanisms f the temporal ALD [29,31,42,43] but to our knowledge this is the first time isotopic precursors are used to study SALD films. By varying the temperature and substrate velocity (precursor exposure/purge time) we und out that hydrogen/deuterium incorporation follows mostly similar trend as the deposition with temporal ALD in ur previous studies [24,33]. However, the temperature in which the majority hydrogen isotope shifts from ^{1}H to H was und to be higher than with temporal ALD. We also und ut that the gr wth-per-cycle (GPC) of the ZnO decreases more with increasing substrate rotation speed compared to Al O_3.

. Experimental methods

A modified spatial ALD reactor, Beneq FS 200R (Fig. 1), was used to deposit Al O_3 and ZnO films on a flexible Ti-coated polyethylene terephthalate (PET) (Rowo Coatings). Trimethylaluminium (Strem Chemicals, min. 98%) and diethylzinc (Volatec, min. 99%) were used as metal precursors and both normal (^{1}H O) and heavy water (H O, Medical Isotopes Inc., Pelham, NH, USA, 99.9%) were used as oxygen precursors. Nitrogen (Linde AG, 99.999% purity) was used as carrier gas and purging gas. All precursors were heated to 35 °C in rder to increase their vapor pressure. The substrate was attached to a cylinder with a diameter f 10 cm and there is a 500 µm gap between the precursor nozzle and the substrate. During the deposition the cylinder is rotated so that the substrate passes through stationary precursor and purging zones. he reactor consisted of 4 MA/DEZ and 4 water inlets divided by N barrier fl ws. Due to the modification of the reactor, one r tati n the substrate cylinder effectively c nsists nly f three ALD cycles as two of the TMA/DEZ and two of the H O inlets are successively as seen in Fig. 1. All Al O_3 samples and ZnO samples deposited using normal water were grown with 333 rotations. Due to the lower GPC, ZnO samples grown with heavy water were deposited with 500 rotations. Total nitrogen barrier flow during the deposition was 4600 sccm and both metal precursor and water were delivered using N carrier gas fl w f 100 sccm. During the deposition the base pressure in the reactor was 17– 3 mbar depending on the deposition temperature.

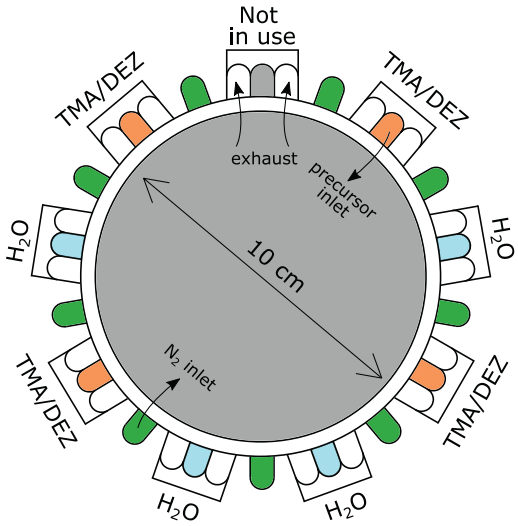

Fig. 1. Schematics f the modified SALD reactor used in the study.

Temperature series was carried ut for both materials at deposition temperatures between 67 °C and 140 °C with substrate rotation speed 10 rpm. In addition, the rotation speed e.g. the precursor exposure/purge time was varied by changing the substrate rotation speed between 5 and 50 rpm at the deposition temperature 100 °C.

The elemental compositions and film thicknesses were measured with time-of-flight elastic recoil detection analysis (ToF-ERDA) [44] using 13.615 MeV $^{63}Cu^{6+}$ incident i ns or the Al O_3 samples and 13.615 MeV $^{127}I^{7+}$ for the ZnO samples. Elemental depth profiles were analysed with Potku software [45]. All the samples deposited with H O were measured immediately after the deposition. his was done t ensure that the H concentration does not change due to hydrogen exchange reactions with ambient moisture or hydrogen gas [24,33].

3. Results and discussion

The thicknesses and the elemental c mposition of the films were determined by means ToF-ERDA depth profiles. In a oF-ERDA measurement incident ions are accelerated in the energy range rom few MeV to a few tens f MeVs towards the sample. Incident beam recoils sample atoms through elastic collisions towards a detector, in which the velocity (ToF) and the energy f these recoils are measured in coincidence. From ToF-energy histogram (Fig. 2a) different masses can be separated. his enables differentiating not only the elements but also the isotopes if there are no overlapping masses. The stopping power e.g. the energy loss of ions in medium as well as the scattering cross sections are well known. herefore, quantitative elemental composition and a depth profile can be calculated without any reference samples [44,46].

The determination of absolute values for film thicknesses suffers from the substrate roughness and multiple scattering effects in ion beam analysis, especially with ZnO oxide films [47]. However, the relative trends in GPC can be observed and analysed. All the films (apart rom Al O_3 films deposited at 67 °C with ^{1}H O) were conformal by visual inspection. In addition, depositing Al O_3 at 67 °C with H O did not produce a proper film at all with the rotation speed f 10 rpm.

As an example, Fig. a presents the coincidence time-of-flight and energy histogram f a Al O_3 film deposited with TMA and H O at 100 °C using 5 rpm rotation speed. In Fig. b is shown a depth profile the same sample. he elemental c mposition of all the samples is determined from the center f the film excluding both surface and interface regions.

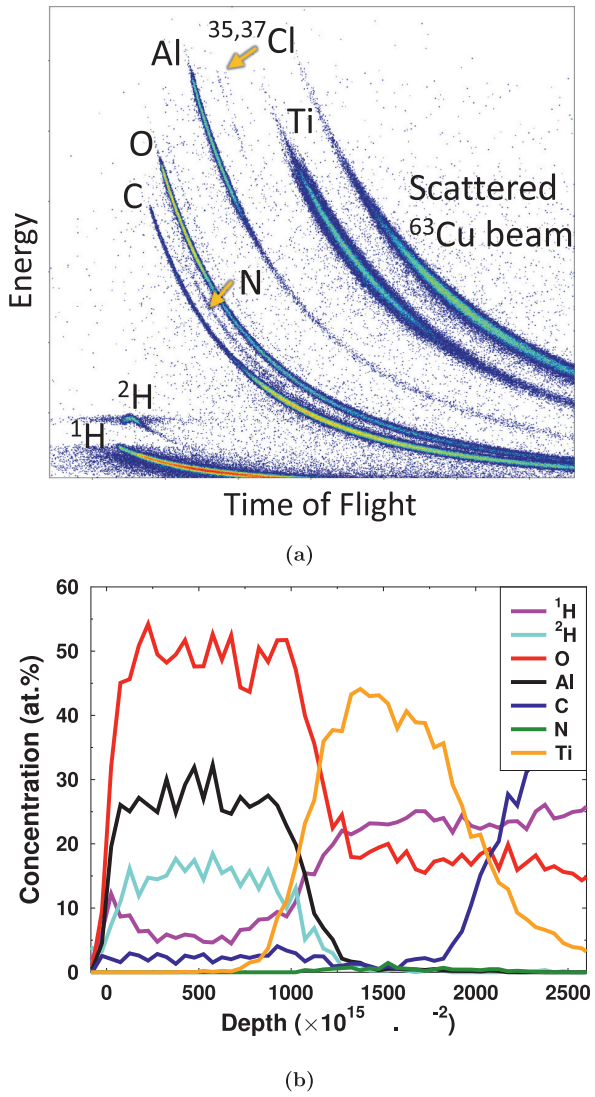

Fig. . a) Coincidence time-of-flight and energy histogram f Al O_3 film deposited with TMA and H O at 100 °C with 5 rpm. he film contains trace Cl at the surface and interface but it is mitted from the analysis for clarity. Minor amount f nitrogen from the Ti layer is also visible. b) Depth profile f the same sample where Ti film on top of PET substrate can be seen.

The growth-per-cycle for Al O_3 films deposited with normal water is relatively independent on the deposition temperature between 85 and 140 °C when normal water is used, as seen in (Fig. 3a) and it is in line with our previous study with the temporal ALD [24]. However, the GPC is somewhat lower than often reported in the literature [23,29,48]. Ion beam techniques can measure the thicknesses in atoms/cm rather than in nanometers. he thickness of 1×10^{15} at./cm corresponds roughly t 1 Å if the density of Al O_3 is assumed to be the bulk value f 3.5 g/cm^3. However, it must be noted that ALD films deposited at low temperatures tend to be less dense than their bulk counterparts or even the nes deposited at higher temperatures [23]. Fig. 3a shows also that the use heavy water decreases the GPC slightly. This is most probably due to the kinetic isotope effect (KIE) which lowers the reaction rate by increasing the activation energy [49]. Similar effect has been detected for the temporal ALD [24,33,50]. It has also been previously shown with temporal ALD that water has a temperature dependent sticking probability and therefore the water pulse is the limiting factor at low temperatures [51,52]. The lower GPC, when heavy water is used, is further evidence of water being the growth limiting precursor.

When the deposition temperature of Al O_3 was decreased to 67 °C the GPC increased rapidly due to the CVD-like growth. This is attributed in most studies to the adsorption of multiple layers f water at low deposition temperatures [23,53,54]. This will lead to excess water n the substrate surface which will in turn react with the next precursor leading to a more CVD-like growth if the purging time is not long enough for water to desorb. Maydannik et al. studied anomalous growth of SALD Al O_3 with similar reactor design as urs. hey first suspected that mixing of the precursors is due to a boundary layer formed above the rotating substrate and this caused the high GPC [55]. Later they concluded that the higher than expected GPC cannot be due to the boundary layer but must be due to the adsorpted excess water and insufficient purging at low deposition temperature [53]. Even though the CVD-growth can be a problem as shown above, the deposition Al O_3 has been successfully demonstrated even near room temperature by both temporal [23] and spatial [48] ALD.

Interestingly, the excess growth does not seem to apply to EZ + H O process. As seen in Fig. 3b, the anomalous CVD-growth is not bserved even at 67 °C. he same bservation was done in our previous article with temporal ALD [33]. In that study we could not find CVD-growth neither at low temperature (40 °C) nor with very short purging times (3 s) at 60 °C, b th of which should lead to more than a m nolayer water based on the conclusions drawn rom the Al O_3 depositions [24]. As EZ is highly reactive towards water, it should also react with the excess water if it is available. herefore, there are two possible intuitive explanations: 1) Adsorption of excess TMA contributes to the CV -like growth which is absent with DEZ due to its faster desorption or 2) it is also possible, that the desorption rate of the excess water molecules on ZnO surface is much higher than on the Al O_3 surface and therefore CVD-growth is not detected on the ZnO surface.

The effect of heavy water on ZnO GPC is similar to Al O_3 but somewhat greater. No CVD-growth was detected even at low temperatures with heavy water, as seen in Fig. 3b. he GPC of the ZnO films seems also to be somewhat lower compared to reported values rom temporal ALD studies [30,33,56,57]. Low values of GPC or ZnO deposited with SALD around 100 °C compared to temporal ALD have also been reported by thers [26,35,58]. In the case of ZnO, 1×10^{15} at./cm corresponds to 1.2 Å if the bulk density 5.6 g/cm^3 is used. H wever, also ZnO films deposited at low temperature probably have lower density [57,59] and therefore the GPC in Å/cycle is higher than expected from the bulk density. The GPC of ZnO increases with temperature which is also in line with temporal ALD. With ^{1}H O, the GPC starts t decrease at temperatures higher than 120 °C. he decrease in GPC at high deposition temperatures is characteristic to DEZ + H O process as the desorption of the OH-groups and physisorpted EZ starts to limit the GPC [51,60], although the maximum GPC is ten bserved around 150 °C [33,56,57,61]. The temperature where the maximum GPC is achieved can depend on the process parameters as demonstrated by Nelson et al. [62]. They showed that the temperature f maximum GPC of SALD ZnO films depend on the pulse/purge time.

Both Al O_3 and ZnO films were deposited at 100 °C with varying rotation speed. In ur previous work [24] we und out that the purging time did not change the GPC MA + H O deposition at 100 °C when all the other parameters were kept constant. From Fig. 3c can be concluded that the rotation speed has an effect on the GPC of Al O_3, but the reduction with increased rotation speed is much more pronounced with ZnO as seen in Fig. 3d. here is earlier evidence EZ soft saturation [18,19,62–64] and the increase in GPC towards slower speed could be because f the longer precursor exposure time. However, in ur study with temporal ALD we showed that just by increasing the purging times increased the GPC of ZnO deposition at 60 °C [33]. Therefore, in the case of ZnO, it is possible that the increasing GPC at slower substrate rotation speeds is not only due to the increasing exposure time but also a result f longer purging. On the other hand, at higher deposition temperatures than used in this study, increasing the purging time has been

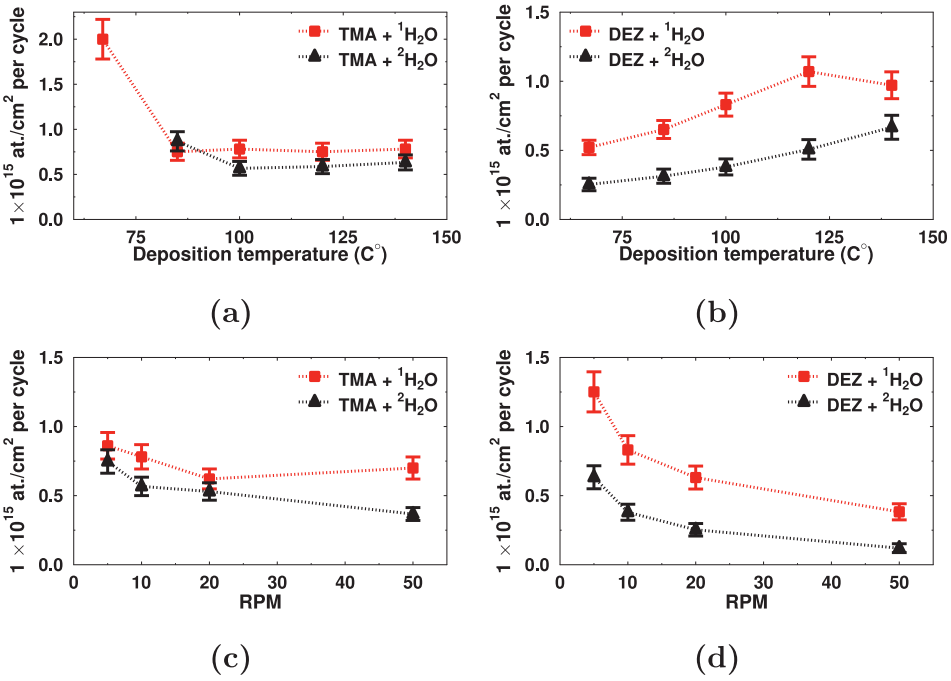

Fig. 3. Growth per cycle determined from the ToF-ERDA depth profiles. GPC of a) Al O_3 and b) ZnO as a unction of deposition temperature. he sample rotation speed was held at 10 rpm for all the samples. The GPC as a unction of the substrate rotation speed at 100 °C for c) Al O_3 and d) ZnO.

found to decrease the GPC due to desorption of reaction sites [62,65]. The precursor exposure and purging times with different rotation speeds are shown in Table 1. However, due to the modification of the reactor (Fig. 1), there is ne MA/DEZ and one H O double pulse in every rotation. he rotation speed f 10 rpm used in temperature series with exposure time 229 ms should be more than sufficient. While the precursor exposure times vary significantly from study to study, exp - sure times f even as short as 8 ms have been reported for ZnO [58]. However, exposure times in range few tens of milliseconds are often reported or SALD processes [19,25,26,36,62,66].

In ur previous study we found signs f transient steric hindrance when depositing ZnO [33] proposed by [67]. In ur study we separated the precursor pulses into three shorter pulses at 40 °C while keeping the precursor exposure unchanged. his increased the GPC by 33%. This transient steric hindrance can be due to the slow reactions and slowly desorbing by-products that block the reaction sites temporarily. Similar approach was also utilised by Muneshwar and Cadien [68] and they found that bulkier ligands emphasise the effect. As ethyl-ligands in EZ are bulkier than methyls in MA, the effect should be more pron unced with the ZnO process and this is supported by the experiment. herefore, it is possible that the reaction rate and the desorption of by-products can inhibit the growth f ZnO if the purging is too short. It is also p ssible that the soft-saturation of ZnO is not a separate phenomenon but just a consequence of the transient steric hindrance.

The elemental c mposition of the films was determined with oF-ERDA and all the results are presented in Tables –5. The stoichiom- etry f the main c mponents of the films changes considerably with b th the deposition temperature (Fig. 4a and b) and rotation speed (Fig. 4c and d). Both Al O_3 and ZnO films were oxygen rich which seems to be typical r low temperature deposition these processes [23,24,29,30,33,69]. Increasing both the temperature and the expo- sure/purge time improves the film quality and produces films closer to the stoichiometric O/Al ratio (1.5) and O/Zn ratio (1). Again, the films deposited with heavy water tend to be somewhat less optimal due to the lower reactivity H O. Especially ZnO deposited with high substrate velocity and heavy water is very ar from stoichiometric ZnO. Measuring the O/Zn ratio with ToF-ERDA using ^{127}I ion beam suffers from the multiple scattering and as a result the concentration of Zn is somewhat underestimated [47]. However, the results presented in Fig. 4b and d show that the O/Zn ratio approaches the ideal ratio of 1 as the tem- perature is increased r the rotation speed is slowed. The high xygen concentration for both Al O_3 and ZnO at low temperatures would imply that many unreacted OH-groups are buried in the film leading to higher than expected oxygen c ncentration. he hydrogen concentrations in these films point towards the same explanation.

The hydrogen impurities in the Al O_3 and ZnO films can riginate from two sources: 1) From the metal precursor, TMA r EZ, which both contain alkyl groups r) from unreacted OH-groups originating rom water. he simplified reaction mechanism MA/DEZ with water leading to methane/ethane by-products has been somewhat challenged in recent years. Gurre-Nuñez et al. ound a relation between the high O/ Al ratio and deuterium c ncentration [29] in Al O_3 films deposited with temporal ALD. They concluded that most f the hydrogen, in the rm deuterium, is left in the films due rehydroxylation xygen atoms in subsequent cycles. On the other hand, there are evidence f persistent methyl-groups in the case of Al O_3 [43,51] that do not react with water at low deposition temperatures even with excessive pulsing of water. Sperling et al. concluded that the presence of persistent CH_3 is due to the coverage dependent activation energy [70]. Towards the end of the water pulse, when CH_3 coverage is low, the reaction barrier increases making the reaction of isolated CH_3-groups unlikely. These groups could get buried in the film in subsequent pulses. However, the films have often very low carbon concentration [24,29,30,33,43] which implies

Table 1
Precursor residence and purge times with different substrate rotation speeds r each individual precursor nozzle and inert gas purging.

RPM	Residence time (ms)	Purge time (ms)
5	458	1120
10	9	559
0	115	80
50	46	111

Table
The elemental composition of Al O_3 films deposited at different temperatures with both normal (^{1}H O) and heavy water (H O).

	T (°C)	Al	O	C	^{1}H	H	tot H	GPC (1 × 10^{15} at/cm)	eposition rate (1 × 10^{15}at/cm per s)
^{1}H O	67		50	1.7	6.5	–	6.5	.0	1.0
	85	8	50	3	19.5	–	19.5	0.75	0.38
	100	30	53	1.9	15.6	–	15.6	0.78	0.39
	120	30	52	3.3	14.1	–	14.1	0.75	0.38
	140	33	54	1.6	10.7	–	10.7	0.78	0.39
H O	67	–	–	–	–	–	–	–	–
	85	4	51	1.1	3.7	0.6	4.3	0.87	0.43
	100	5	48	.7	1.9	.9	4.8	0.57	0.28
	120	9	51	1.9	4.6	14.2	18.8	0.59	0.29
	140	31	53	1.9	3.7	9.8	13.5	0.63	0.32

Table 3
The elemental composition of ZnO films deposited at different temperatures with both normal (^{1}H O) and heavy water (H O).

	T (°C)	Zn	O	C	^{1}H	H	tot H	GPC (1 × 10^{15} at/cm)	eposition rate (1 × 10^{15}at/cm per s)
^{1}H O	67	41	50	0.7	8.6	–	8.6	0.52	0.26
	85	43	50	0.4	6.2	–	6.2	0.65	0.33
	100	45	51	0.4	4.3	–	4.3	0.83	0.42
	120	47	50	0.3	.6	–	.6	1.07	0.54
	140	47	50	0.4	.6	–	.6	0.97	0.49
H O	67	37	49	0.7	8.2	4.9	13.1	0.25	0.13
	85	39	50	0.9	6	4	10.0	0.31	0.16
	100	39	49	1.5	6.6	3.1	9.7	0.38	0.19
	120	43	49	1.8	4.5	1.7	6.2	0.51	0.25
	140	45	50	1.1	.4	1.2	3.6	0.67	0.33

Table 4
The elemental composition of Al O_3 films deposited at with different rotation speeds at 100 °C with both normal (^{1}H O) and heavy water H O.

	RPM	Al	O	C	^{1}H	H	tot H	GPC (1 × 10^{15} at/cm)	eposition rate (1 × 10^{15}at/cm per s)
^{1}H O	5	31	53	1.6	14.0	–	14.0	0.86	0.22
	10	30	53	1.9	15.6	–	15.6	0.78	0.39
	0	8	51	.0	19.0	–	19.0	0.62	0.62
	50	3	49	1.4	7	–	7	0.70	1.75
H O	5	8	49	.2	5.6	15.2	0.8	0.75	0.19
	10	5	48	.7	1.9	.9	4.8	0.57	0.28
	0	4	51	1.7	.4	0.5	.9	0.53	0.53
	50	4	48	.9	3.9	0.2	4.1	0.37	0.92

Table 5
The elemental composition of ZnO films deposited at with different rotation speeds at 100 °C with both normal (^{1}H O) and heavy water (H O).

	RPM	Zn	O	C	+H	H	tot H	GPC (1 × 10^{15} at/cm)	eposition rate (1 × 10^{15} at/cm per s)
^{1}H O	5	47	51	0.3	.1	–	.1	1.25	0.31
	10	45	51	0.4	4.3	–	4.3	0.83	0.42
	0	44	49	0.6	5.8	–	5.8	0.63	0.63
	50	38	50	1.0	10.7	–	10.7	0.38	0.96
H O	5	45	50	0.3	1.5	.9	4.4	0.63	0.16
	10	39	49	1.5	6.6	3.1	9.7	0.38	0.19
	0	37	51	1.2	7.8	3.5	11.3	0.25	0.25
	50	5	55	.8	14.6	.0	16.6	0.12	0.3

that these persistent groups are not incorporated into the film. Persistent methyl groups probably react with water in subsequent cycles but definitive explanation is not yet given. In addition, Werbrouck et al. [71] und out that there is potentially a secondary reaction pathway causing etching of the already reacted species during the H O pulse. Similarly t TMA-process, persistent ethyl ligands have been bserved to stay unreacted at the surface f the ZnO films deposited rom EZ and water at low deposition temperatures. These persistent ethyls have been both experimentally bserved [72] and computationally predicted [60].

The hydrogen concentration of the Al O_3 and ZnO deposited with ^{1}H O process follows an expected trend of decreasing concentration with increasing deposition temperature, reported in many studies before with temporal ALD for both Al O_3 [23,24,29,51] and ZnO [30,31,33] as seen in Fig. 5a and c. Compared to temporal ALD, the hydrogen concentration of SALD films is somewhat higher.

When heavy water is used, the total hydrogen and deuterium concentrations are slightly higher than with the normal water, which is in agreement with isotopic effect discussed earlier. These results are also in agreement with previous work with temporal ALD [24,33]. In the case Al O_3 with heavy water, we see a change in majority hydrogen isotope (Fig. 5a) similar t our previous work with Al O_3 films deposited with temporal ALD [24]. As the deposition temperature is decreased below 120 °C, the main hydrogen source changes from deuterium to hydrogen. With temporal ALD the same shift was bserved between 70 and 80 °C. In addition to the temperature, this phenomenon is related to the purging times, which can explain the difference in the temperature.

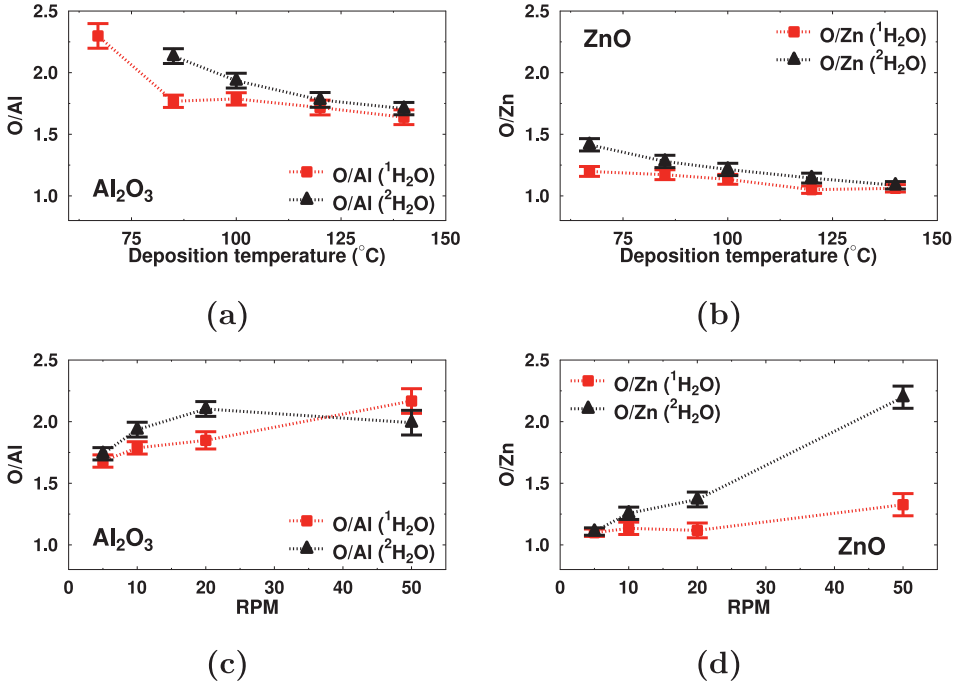

Fig. 4. Ratio of a) O/Al and b) O/Zn as a unction of the deposition temperature. he rotation speed was kept at 10 rpm. Ratio of c) O/Al and d) O/Zn as a unction the rotation speed. The deposition temperature was kept at 100 °C.

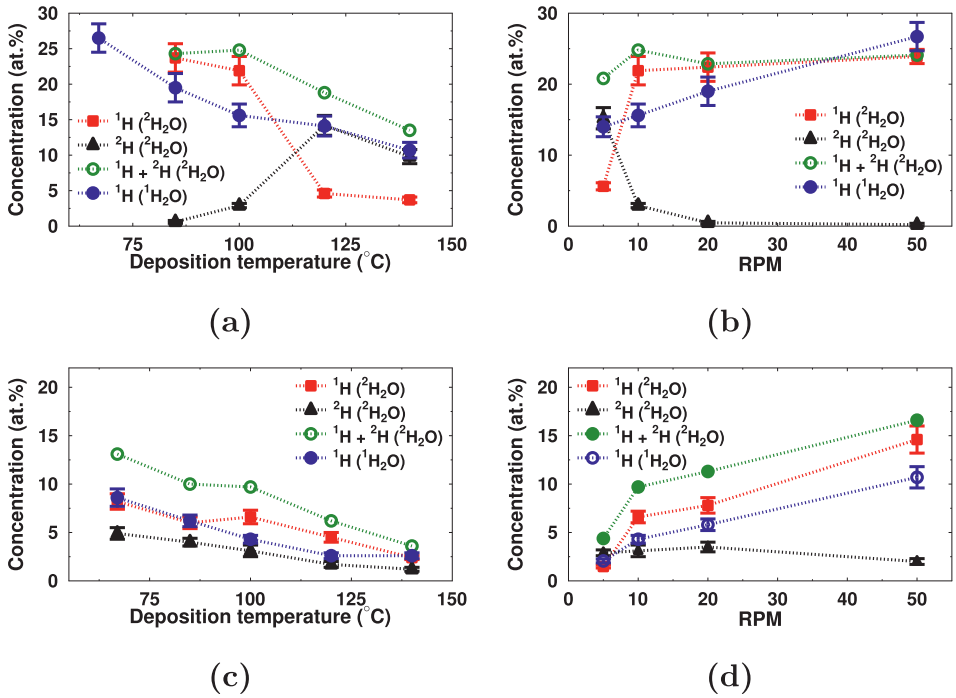

Fig. 5. ^{1}H and H concentrations of the films as a unction of the deposition temperature or a) Al O_3 and b) ZnO. The substrate rotation speed was kept at 10 rpm. ^{1}H and H concentrations f the films as a unction of the rotation speed deposited at 100 °C for c) Al O_3 and d) ZnO.

With temporal ALD, a similar change of the main impurity isotope was observed also at 100 °C, when purging times were decreased to 3 s. This can be due to the slowly reacting CH_3-groups discussed earlier, some which do not react with water even with very long precursor exp sure and purging times [51] if the deposition temperature is low. With too short reaction and purging times there might not be enough time t remove these methyl groups and many f them are buried in the film. Increasing the temperature increases the energy available for the reaction to vercome the barrier and more and more f these methyl groups react leaving less ^{1}H in the film.

As mentioned above, the effect of the purging time to majority hydrogen isotope concentration is evident when the rotation speed is

varied as seen in Fig. 5b. With 5 rpm (longest exposure/purge) the main hydrogen isotope is H, but as the rotation speed is increased and the time or the reaction to go to the completion is too short, the main hydrogen isotope changes to ^{1}H. his effect of changing majority hydrogen isotopes is visible when short purging times are used in temporal ALD, so it is not related only to the too short exposure times in itself. The results with SALD are in good agreement with our previous studies with temporal ALD [24,33] where we showed that purging time has a big effect on hydrogen/deuterium incorporation even though the GPC does not change significantly.

With temporal ALD, a similar change f the majority hydrogen isotope incorporation was und also for the DEZ + H O process [33]. However, in ur SALD process, ^{1}H remained as the main hydrogen isotope regardless of the deposition temperature (Fig. 5c). A likely explanation for the high ^{1}H concentration is t fast rotation speed (10 rpm) or the given temperature (100 °C). his conclusion is supported by the change f the GPC in Fig. 3d, as the GPC was found to increase significantly as the rotation speed was decreased to 5 rpm at 100 °C. More evidence of this is the hydrogen/deuterium concentration when rotation speed f 5 rpm is used (Fig. 5d). As the rotation speed is decreased to 5 rpm, the ^{1}H concentration goes just below the H concentration, similar to when long purging times are used in temporal ALD [33].

The high oxygen concentration at low deposition temperatures does not seem to lead to a high deuterium concentration as would be expected if the excess oxygen is in the rm of buried O H-groups suggested by Guerra-Nuñez et al. [29]. However, the situation is quite the pposite: the higher the ^{1}H concentration is the higher the O/Al and O/Zn ratios are. From the previous studies we know that both Al O_3 and ZnO films deposited with ALD have very low carbon concentration even at l w deposition temperatures [24,29,30,33,43]. As seen in the Tables –5, the carbon concentration is not strongly dependent on the process parameters or Al O_3 and the carbon concentration was between 1.4 and 3.3 at.%. For the ZnO films the carbon concentration varied between 0.3 and 2.8 at.% and there is a clear dependency on rotation speed but the maximum concentration stays rather low. These numbers are low i we consider the ^{1}H concentration of the films deposited with low deposition temperature r ast rotation speeds. If the ^{1}H would riginate purely from the embedded methyl/ethyl groups, the carbon concentration should be significantly higher. From previous studies [24,33] we know that H migrates within the film and can be replaced by ^{1}H from ambient gasses. his effect was minimized by measuring all the films containing H immediately after the deposition exposing the film or ambient condition nly or c uple of minutes. However, it is not impossible that the ^{1}H/ H exchange reactions take place already during the deposition leading to higher than expected ^{1}H concentration.

In ur previous studies the higher ^{1}H concentration compared to the H concentration was found to be related to too short purging times r the given temperature. The films deposited at “ideal” conditions (high enough temperature, long purging times) had always higher H concentration than ^{1}H concentration for both Al O_3 and ZnO. For example, Guerra-Nuñez et al. [29] and Guziewicz et al. [31] reported H to be the majority hydrogen isotope at similar deposition temperatures in Al O_3 and ZnO films, respectively. Both f them used long purging times which explains why they did not ound films with ^{1}H as a majority hydrogen isotope. However, results obtained by Hiraiwa et al. [50] n ^{1}H/ H concentration of Al O_3 are somewhat mixed. Similar to us, they reported ^{1}H to be the majority isotope at 100 °C, and at higher temperature (450 °C) the H concentration was higher than the ^{1}H concentration. However, they reported that the total hydrogen concentration at 450 °C was higher when normal water was used. In a recent study Xia et al. reported quite contradictory results on ZnO films [57] compared to ur results in this and in our previous study [33]. According to them the ^{1}H concentration is higher than H concentration in all deposition temperatures between 100 and 300 °C even though they have used long (60 s) purging times. his emphasises the need or precise description and consideration of the process parameters since they will impact the film composition and other properties, and the conclusions drawn rom them. This question has earlier been addressed, or example, by Sønsteby et al. [73].

As seen rom Tables –5, the actual deposition rate in 10^{15} at./cm /s increases with increasing substrate rotation speed even if the GPC decreases. his is true or both Al O_3 and ZnO but the GPC of ZnO decreases more rapidly with increasing rotation speed. Therefore, the actual increase in throughput of ZnO is significantly lower than with Al O_3. On the other hand, a high deposition speed also leads to lower quality films with higher impurity concentrations. This can, for example, have an effect on the electrical properties of the film [74,75]. Also, the barrier properties f the film can be affected by the high impurity concentrations. For example, hydrogen incorporation impacts indirectly the performance of ALD films in moisture and gas barrier applications. Films with high hydrogen concentration are known to be less dense [23,29,76], leading often to a poor barrier quality when low deposition temperature r ast deposition speed is used [9,13,34]. However, the deposition rate achieved by the SALD at low temperatures can be an rder of magnitude higher than with temporal ALD making it an attractive ption if satisfactory film quality can be reached.

4. Conclusions

Both Al O_3 and ZnO films contain ^{1}H and H when deposited with heavy water. he main hydrogen isotope in the films depends on the deposition conditions so that more ideal conditions (high temperature r long exposure/purge times) seem to favour incorporation of H ver ^{1}H. For low deposition temperature and short exposure/purge times the results are quite the pposite. This is in line with the results btained from temporal ALD studies [24,33]. After the deposition at non-ideal conditions both films are also highly oxygen rich. euterium gets incorporated presumably in the films as OH-groups, which should lead to high O and H concentrations. On the other hand, high ^{1}H concentration does not lead to as high carbon concentration as would be expected if methyl/ethyl groups are buried into the films. hese assumptions are in contradiction with each ther. Our results show that the mechanism behind the simultaneous high oxygen and ^{1}H concentrations at non-ideal deposition conditions is related to inadequate purging at given temperature, but requires further studies to be understood c mpletely.

eposition of thin films with spatial ALD requires precise consideration in rder to produce high quality and low impurity films. he throughput i.e. the growth rate (Å/s) of the ALD deposition can be sped up considerably by shortening the exposure/purging time. Even though the growth-per-cycle decreases, the throughput can increase due t shorter cycle times. he throughput f the Al O_3 increases significantly with increasing rotation speed while the GPC of the ZnO suffers m re rom shorter exposure/purging times. H wever, the increase in throughput does not come without a cost and leads to higher impurity concentration. In addition, the precursor exposure and purge times cannot be as easily or independently changed as in temporal ALD. This makes the design and construction of a SALD-reactor that is suitable r multitude of processes much more challenging.

CRediT a thorship contribution statement

Sami Kinnunen: Writing – original draft, Investigation, Visualization. **Timo ajavaara:** Conceptualization, Writing – review & editing, Supervision.

Declaration of ompeting nterest

The authors declare that they have no known competing financial interests or personal relationships that could have appeared t influence the work reported in this paper.

References

[1] R.L. Puurunen, Surface chemistry of atomic layer deposition: a case study for the trimethylaluminum/water process, J. Appl. Phys. 97 (2005), 121301.
[2] S.M. George, Atomic layer deposition: an overview, Chem. Rev. 110 (2010) 111–131. PMID: 19947596.
[3] V. Miikkulainen, M. eskelä, M. Ritala, R. Puurunen, Crystallinity of inorganic films grown by atomic layer deposition: verview and general trends, J. Appl. Phys. 113 (2013), 021301.
[4] P. Poodt, V. iba, F. Werner, J. Schmidt, A. Vermeer, F. Roozeboom, Ultrafast atomic layer deposition of alumina layers or solar cell passivation, J. Electrochem. Soc. 158 (2011) H937.
[5] C. Frijters, P. Poodt, A. Illiberi, Atmospheric spatial atomic layer deposition of Zn (O, S) buffer layer for Cu(In, Ga)Se2 solar cells, Sol. Energy Mater. Sol. Cells 155 (2016) 356–361.
[6] Z. Xing, J. Xiao, T. Hu, X. Meng, . Li, X. Hu, Y. Chen, Atomic layer deposition metal xides in perovskite solar cells: present and uture, Small Methods 4 (2020) 000588, https://doi.org/10.1002/smtd.202000588.
[7] B. Vermang, A. Rothschild, A. Racz, J. John, J. Poortmans, R. Mertens, P. P dt, V. iba, F. Roozeboom, Spatially separated atomic layer deposition of Al2O3, a new ption for high-throughput si solar cell passivation, Prog. Photovolt. Res. Appl. 19 (2011) 733–739.
[8] D. Muñoz-Rojas, V.H. Nguyen, C. Masse de la Huerta, S. Aghazadehchors, C. Jiménez, D. Bellet, Spatial atomic layer deposition (SALD), an emerging tool r energy materials. Application to new-generation photovoltaic devices and transparent conductive materials, C.R.Phys. 18 (2017) 391–400. emain l'énergie.
[9] P.S. Maydannik, .O. Kääriäinen, K. ahtinen, D.C. Cameron, M. S¨derlund, P. Soininen, P. Johansson, J. Kuusipalo, L. Moro, X. Zeng, Roll-to-roll atomic layer deposition process for flexible electronics encapsulation applications, J. Vac. Sci. Technol. A 32 (2014), 051603.
[10] T.O. Kääriäinen, P. Maydannik, D.C. Cameron, K. Lahtinen, P. Johansson, J. Kuusipalo, Atomic layer deposition on polymer based flexible packaging materials: growth characteristics and diffusion barrier properties, Thin Solid Films 519 (2011) 3146–3154.
[11] K. Lahtinen, . Kääriäinen, P. Johansson, S. Kotkamo, P. Maydannik, T. Seppänen, J. Kuusipalo, D.C. Cameron, UV protective zinc oxide coating r biaxially riented polypropylene packaging film by atomic layer deposition, hin S lid Films 570 (2014) 33–37.
[12] K. Ali, J. Ali, S.M. Mehdi, K.-H. Choi, Y.J. An, Rapid abrication of Al2O3 encapsulations r rganic electronic devices, Appl. Surf. Sci. 353 (2015) 1186–1194.
[13] K.L. Jarvis, P.J. Evans, Growth of thin barrier films on flexible polymer substrates by atomic layer deposition, hin Solid Films 624 (2017) 111–135.
[14] M. Aghaee, P.S. Maydannik, P. Johansson, J. Kuusipalo, M. Creat re, . Homola, . C. Cameron, ow temperature temporal and spatial atomic layer deposition iO2 films, J. Vac. Sci. echnol. A 33 (2015), 041512.
[15] M.B.M. Mousa, J.S. Ovental, A.H. Brozena, C.J. Oldham, G.N. Parsons, Modeling and experimental demonstration of high-throughput flow-through spatial atomic layer deposition of Al2O3 coatings on textiles at atmospheric pressure, J. Vac. Sci. Technol. A 36 (2018), 031517.
[16] C.-H. Chao, C.-T. Hsieh, W.-J. Ke, .-W. Lee, Y.-F. Lin, H.-W. Liu, S. Gu, C.-C. Fu, R.-S. Juang, B.C. Mallick, Y.A. Gandomi, C.-Y. Su, Roll-to-roll atomic layer deposition of titania c ating on polymeric separators or lithium ion batteries, J. P wer Sources 482 (2021), 8896 .
[17] S. Moitzheim, J.E. Balder, P. Poodt, S. Unnikrishnan, S. e Gendt, P.M. Vereecken, Chlorine doping of amorphous TiO2 for increased capacity and faster i+-ion storage, Chem. Mater. 29 (2017) 10007–10018.
[18] A.S. Yersak, K. Sharma, J.M. Wallas, A.A. Dameron, X. Li, Y. Yang, K.E. Hurst, C. Ban, R.C. enent, S.M. George, Spatial atomic layer depositi n for coating flexible porous i-ion battery electrodes, J. Vac. Sci. echnol. A 36 (2018) 01A123.
[19] C.R. Ellinger, S.F. Nelson, Selective area spatial atomic layer deposition of ZnO, Al2O3, and aluminum-doped ZnO using poly(vinyl pyrrolidone), Chem. Mater. 6 (2014) 1514–1522.
[20] D. Muñoz-Rojas, T. Maindron, A. Esteve, F. Piallat, J. Kools, J.-M. ecams, Speeding up the unique assets f atomic layer deposition, materials t day, Chemistry 12 (2019) 96–120.
[21] K.P. Musselman, C.F. Uzoma, M.S. Miller, Nanomanufacturing: high-throughput, cost-effective deposition of atomic scale thin films via atmospheric pressure spatial atomic layer deposition, Chem. Mater. 28 (2016) 8443–8452.
[22] P. P dt, D.C. Cameron, E. Dickey, S.M. George, V. Kuznetsov, G.N. Parsons, F. Roozeboom, G. Sundaram, A. Vermeer, Spatial atomic layer deposition: a r ute towards further industrialization of atomic layer deposition, J. Vac. Sci. echnol. A 30 (2012), 010802.
[23] M.D. Groner, F.H. Fabreguette, J.W. Elam, S.M. George, Low-temperature Al2O3 atomic layer deposition, Chem. Mater. 16 (2004) 639–645.
[24] S. Kinnunen, K. Arstila, T. Sajavaara, Al2O3 ALD films grown using TMA + rare isotope 2H and 1O precursors, Appl. Surf. Sci. 148909 (2021).
[25] P. Poodt, A. Lankhorst, F. Roozeboom, K. Spee, D. Maas, A. Vermeer, High-speed spatial atomic-layer deposition of aluminum oxide layers or s lar cell passivation, Adv. Mater. 22 (2010) 3564–3567.
[26] A. Illiberi, F. Roozeboom, P. Poodt, Spatial atomic layer deposition of zinc xide thin films, ACS Appl. Mater. Interfaces 4 (2012) 68 –272. PMID: 171693 .
[27] V.H. Nguyen, A. Sekkat, C. Jiménez, D. Muñoz, D. Bellet, D. Muñoz-Rojas, Impact of precursor exposure on process efficiency and film properties in spatial atomic layer deposition, Chem. Eng. J. 403 (2021), 126234.
[28] David Muñoz-Rojas, Viet Huong Nguyen, César Masse de la Huerta, Carmen Jiménez, Daniel Bellet, Spatial Atomic ayer Deposition, Chemical Vapor eposition for Nanotechnology, IntechOpen, 019, https://doi.org/10.5772/intechopen.82439.
[29] C. Guerra-Nuñez, M. Döbeli, J. Michler, I. Utke, Reaction and growth mechanisms in Al2O3 deposited via atomic layer deposition: elucidating the hydrogen source, Chem. Mater. 29 (2017) 8690–8703.
[30] J. Malm, E. Sahramo, J. Perälä, T. Sajavaara, M. Karppinen, w-temperature atomic layer deposition of ZnO thin films: c ntrol of crystallinity and rientation, Thin Solid Films 519 (2011) 5319–5322.
[31] E. Guziewicz, W. Wozniak, S. Mishra, R. Jakiela, M. Guziewicz, V.Y. Ivanov, E. usakowska, R. Schifano, Hydrogen in As-grown and annealed ZnO films grown by atomic layer deposition, Phys. Status Solidi A 218 (2021), 000318.
[32] M. Napari, J. Malm, R. ehto, J. Julin, K. Arstila, T. Sajavaara, M. ahtinen, Nucleation and growth f ZnO on PMMA by low-temperature atomic layer deposition, J. Vac. Sci. echnol. A 33 (2015) 01A128.
[33] S. Kinnunen, M. Lahtinen, K. Arstila, T. Sajavaara, Hydrogen and deuterium incorporation in ZnO films grown by atomic layer deposition, Coatings 11 (2021).
[34] H.G. Kim, S.S. Kim, Aluminum xide barrier c ating on polyethersulfone substrate by atomic layer deposition for barrier property enhancement, Thin Solid Films 520 (2011) 481–485.
[35] M.-J. Zhao, Z.-T. Sun, C.-H. Hsu, P.-H. Huang, X.-Y. Zhang, W.-Y. Wu, P. Gao, Y. Qiu, S.-Y. Lien, W.-Z. Zhu, Zinc oxide films with high transparency and crystallinity prepared by a low temperature spatial atomic layer deposition process, Nanomaterials 10 (2020).
[36] D.B. Fullager, G.D. Boreman, C.D. Ellinger, . Hofmann, Broadband ptical properties f aluminium zinc xide thin films prepared by spatial atomic layer deposition, hin Solid Films 653 (2018) 67 – 73 .
[37] D.won Choi, S.-J. Kim, J.H. ee, K.-B. Chung, J.-S. Park, A study f thin film encapsulation on polymer substrate using low temperature hybrid ZnO/Al2O3 layers atomic layer deposition, in: Current Applied Physics, Pr ceedings f the Second International Symposium on Hybrid Materials and Processing Busan, Korea, 27-29 October 2011, 12, 2012, pp. S19–S23.
[38] A.A. Chaaya, R. Viter, I. Baleviciute, M. Bechelany, A. Ramanavicius, Z. Gertnere, D. Erts, V. Smyntyna, P. Miele, uning optical properties f Al O3/ZnO nanolaminates synthesized by atomic layer deposition, J. Phys. Chem. C 118 (2014) 3811–3819.
[39] J. ópez, J. Martínez, N. Abundiz, . Domínguez, E. Murillo, F. Castill´n, R. Machorro, M. Farías, H. Tiznado, Thickness effect on the optical and morphological properties in Al2O3/ZnO nanolaminate thin films prepared by atomic layer deposition, Superlattice. Microstruct. 90 (2016) 65– 73 .
[40] R. Viter, I. Iatsunskyi, V. Fedorenko, S. umenas, Z. Balevicius, A. Ramanavicius, S. Balme, M. Kempiński, G. Nowaczyk, S. Jurga, M. Bechelany, Enhancement electronic and optical properties f ZnO/Al2O3 nanolaminate coated electrospun nanofibers, J. Phys. Chem. C 120 (2016) 5124–5132.
[41] Z. Balevicius, A. Paulauskas, I. Plikusiene, L. Mikoliunaite, M. Bechelany, A. Popov, A. Ramanavicius, A. Ramanaviciene, owards the application of Al2O3/ZnO nanolaminates in immunosensors: total internal reflection spectr scopic ellipsometry based evaluation of BSA immobilization, J. Mater. Chem. C 6 (2018) 8778–8783.
[42] M. Juppo, A. Rahtu, M. Ritala, M. eskelä, In situ mass spectrometry study n surface reactions in atomic layer deposition of Al2O3 thin films rom trimethylaluminum and water, Langmuir 16 (2000) 4034–4039. Cited By 94.
[43] V. Vandalon, W.M.M.E. Kessels, Revisiting the growth mechanism of atomic layer deposition of Al2O3: a vibrational sum-frequency generation study, J. Vac. Sci. Technol. A 35 (2017) 05C313.
[44] M. Laitinen, M. Rossi, J. Julin, . Sajavaara, Time-of-flight – energy spectrometer for elemental depth profiling – Jyväskylä design, Nucl. Instrum. Methods Phys. Res., Sect. B 337 (2014) 55–61.
[45] K. Arstila, J. Julin, M. Laitinen, J. Aalto, T. Konu, S. Kärkkäinen, S. Rahkonen, M. Raunio, J. Itkonen, J.-P. Santanen, . Tuovinen, T. Sajavaara, in: Nuclear Instruments and Methods in Physics Research Section B: Beam Interactions with Materials and Atoms, 11th European C nference on Accelerators in Applied Research and echnology, 331, P tku – new analysis s tware for heavy ion elastic recoil detection analysis, 2014, pp. 34–41.
[46] K. Yasuda, Time-of-flight ERDA for depth profiling of light elements, Quantum Beam Sci. 4 (2020), 40, https://doi.org/10.3390/qubs4040040.
[47] K. Arstila, T. Sajavaara, J. Keinonen, Monte Carlo simulation f multiple and plural scattering in elastic recoil detection, Nucl. Instrum. Methods Phys. Res., Sect. B 174 (2001) 163–172.
[48] K. Ali, K.-H. Choi, Low-temperature roll-to-roll atmospheric atomic layer deposition of Al2O3 thin films, Langmuir 30 (2014) 14195–14203. PMID: 5407477 .
[49] M. Gómez-Gallego, M. Sierra, Kinetic isotope effects in the study rganometallic reaction mechanisms, Chem. Rev. 111 (2011) 4857–4963. PMID: 1545118 .
[50] A. Hiraiwa, T. Saito, D. Matsumura, H. Kawarada, Isotope analysis f diamond-surface passivation effect of high-temperature H2O-grown atomic layer deposition-Al2O3 films, J. Appl. Phys. 117 (2015), 15304 .
[51] V. Vandalon, W.M.M. Kessels, What is limiting low-temperature atomic layer deposition of Al2O3?A vibrational sum-frequency generation study, Appl. Phys. Lett. 108 (2016), 011607.
[52] K. Arts, V. Vandalon, R.L. Puurunen, M. Utriainen, F. Gao, W.M.M.E. Kessels, H.C. M. Knoops, Sticking probabilities f H2O and Al(CH3)3 during atomic layer deposition of Al2O3 extracted from their impact on film conformality, J. Vac. Sci. Technol. A 37 (2019), 030908.

[53] P.S. Maydannik, .O. Kääriäinen, D.C. Cameron, Continuous atomic layer deposition: explanation for anomalous growth rate effects, J. Vac. Sci. echnol. A 30 (2012) 01A122.
[54] P. Poodt, A. Illiberi, F. Roozeboom, The kinetics of low-temperature spatial atomic layer deposition of aluminum oxide, thin solid films 532, in: The 9th International Conference on Coatings on Glass and Plastics, 2013, pp. – 5 .
[55] P. Maydannik, . Kääriäinen, D. Cameron, An atomic layer deposition process r moving flexible substrates, Chem. Eng. J. 171 (2011) 345–349.
[56] J. Cai, Z. Ma, U. Wejinya, M. Zou, Y. iu, H. Zhou, X. Meng, A revisit to atomic layer deposition of zinc oxide using diethylzinc and water as precursors, J. Mater. Sci. 54 (2019) 5236–5248.
[57] B. Xia, J. Ganem, E. Briand, S. Steydli, H. Tancrez, I. Vickridge, The carbon and hydrogen contents in ALD-grown ZnO films define a narrow ALD temperature window, Vacuum 190 (2021), 110289.
[58] N. Nandakumar, B. ielissen, D. Garcia-Alonso, Z. Liu, R. Görtzen, W.M.M. Kessels, A.G. Aberle, B. Hoex, Resistive intrinsic ZnO films deposited by ultrafast spatial ALD for PV applications, IEEE J.Photovoltaics 5 (2015) 1462–1469.
[59] M. Vähä-Nissi, M. Pitkänen, E. Salo, E. Kenttä, A. Tanskanen, . Sajavaara, M. Putkonen, J. Sievänen, A. Sneck, M. Rättö, M. Karppinen, A. Harlin, Antibacterial and barrier properties oriented polymer films with ZnO thin films applied with atomic layer deposition at low temperatures, Thin Solid Films 562 (2014) 331–337.
[60] T. Weckman, K. Laasonen, Atomic layer deposition of zinc oxide: study on the water pulse reactions rom first-principles, J. Phys. Chem. C 122 (2018) 7685–7694.
[61] S. Kim, S. ee, S.-Y. Ham, D.-H. Ko, S. Shin, Z. Jin, Y.-S. Min, A kinetic study f ZnO atomic layer deposition: effects f surface hydroxyl concentration and steric hindrance, Appl. Surf. Sci. 469 (2019) 804–810.
[62] S.F. Nelson, .H. evy, .W. Tutt, M. Burberry, Cycle time effects on growth and transistor characteristics of spatial atomic layer deposition f zinc xide, J. Vac. Sci. echnol. A 30 (2012) 01A154.
[63] E.B. Yousfi, J. F uache, . Lincot, Study of atomic layer epitaxy of zinc oxide by in-situ quartz crystal microgravimetry, Appl. Surf. Sci. 153 (2000) 3 – 34 .
[64] K. Sharma, D. Routkevitch, N. Varaksa, S.M. George, Spatial atomic layer deposition on flexible porous substrates: ZnO on anodic aluminum xide films and Al2O3 on li ion battery electrodes, J. Vac. Sci. echnol. A 34 (2016) 01A146.
[65] H.K. Park, B.S. Yang, S. Park, M.S. Kim, J.C. Shin, J. Heo, Purge-time-dependent growth of ZnO thin films by atomic layer deposition, J. Alloys C mpd. 605 (2014) 124–130.
[66] D. Pan, .-C. Jen, C. Yuan, Effects f gap size, temperature and pumping pressure on the fluid dynamics and chemical kinetics of in-line spatial atomic layer deposition of Al2O3, Int. J. Heat Mass Transf. 96 (2016) 189–198.
[67] H. Wang, Z. Wang, X. Xu, Y. iu, C. Chen, P. Chen, W. Hu, Y. uan, Multiple short pulse process for low-temperature atomic layer deposition and its transient steric hindrance, Appl. Phys. Lett. 114 (2019), 01902 .
[68] T. Muneshwar, K. Cadien, AxBAxB… pulsed atomic layer deposition: numerical growth model and experiments, J. Appl. Phys. 119 (2016), 085306.
[69] E. Guziewicz, .A. Krajewski, E. Przezdziecka, K.P. Korona, N. Czechowski, L. Klopotowski, P. Terziyska, Zinc oxide grown by atomic layer deposition: rom heavily n-Type to p-type material, Phys. Status Solidi B 257 (2020), 1900472.
[70] B.A. Sperling, B. Kalanyan, J.E. Maslar, Atomic layer deposition of Al2O3 using trimethylaluminum and H2O: the kinetics of the H2O half-cycle, J. Phys. Chem. C 124 (2020) 3410–3420.
[71] A. Werbrouck, M. Shirazi, F. Mattelaer, S.D. Elliott, J. endooven, C. etavernier, A secondary reaction pathway for the alumina atomic layer deposition process with trimethylaluminum and water, revealed by ull-range, time-resolved in situ mass spectrometry, J. Phys. Chem. C 124 (2020) 6443 – 6454 .
[72] A.J.M. Mackus, C. MacIsaac, W.-H. Kim, S.F. Bent, Incomplete elimination precursor ligands during atomic layer deposition of zinc-oxide, tin-oxide, and zinc-tin-oxide, J. Chem. Phys. 146 (2017), 052802.
[73] H.H. Sønsteby, A. Yanguas-Gil, J.W. Elam, Consistency and reproducibility in atomic layer deposition, J. Vac. Sci. echnol. A 38 (2020), 020804.
[74] E. Przezdziecka, E. Guziewicz, D. Jarosz, D. Snigurenko, A. Sulich, P. Sybilski, R. Jakiela, W. Paszkowicz, Influence xygen-rich and zinc-rich conditions n donor and acceptor states and conductivity mechanism of ZnO films grown by ALD—experimental studies, J. Appl. Phys. 127 (2020), 075104.
[75] A.C. Kozen, M.A. Schroeder, K.D. Osborn, C.J. Lobb, G.W. Rubloff, Examining the role f hydrogen in the electrical performance of in situ fabricated metal-insulator-metal trilayers using an atomic layer deposited Al2O3 dielectric, Appl. Phys. ett. 102 (2013), 173501.
[76] S.E. Potts, G. Dingemans, C. Lachaud, W.M.M. Kessels, Plasma-enhanced and thermal atomic layer deposition of Al2O3 using dimethylaluminum isopropoxide, [Al(CH3)2(-OiPr)]2, as an alternative aluminum precursor, J. Vac. Sci. echnol. A 30 (2012), 021505.